MEDNARODNA PODIPLOMSKA ŠOLA JOŽEFA STEFANA
JOŽEF STEFAN INTERNATIONAL POSTGRADUATE SCHOOL

MARKO JAMŠEK

PREDICTIVE EXOSKELETON CONTROL BASED ON PROBABILISTIC MODELS

DOCTORAL DISSERTATION

LJUBLJANA, DECEMBER 2022

PREDICTIVE EXOSKELETON CONTROL BASED ON PROBABILISTIC MODELS

Marko Jamšek

Doctoral Dissertation
Jožef Stefan International Postgraduate School
Ljubljana, Slovenia

Supervisor: Prof. Dr. Jan Babič, IPS and Jožef Stefan Institute, Ljubljana, Slovenia

Evaluation Board:
Prof. Dr. Bojan Nemec, Chair, IPS and Jožef Stefan Institute, Ljubljana, Slovenia
Prof. Dr. Juš Kocijan, Member, IPS and Jožef Stefan Institute, Ljubljana, Slovenia
Prof. Dr. Elmar Rueckert, Member, Montanuniversität Leoben, Austria

MEDNARODNA PODIPLOMSKA ŠOLA JOŽEFA STEFANA
JOŽEF STEFAN INTERNATIONAL POSTGRADUATE SCHOOL

Marko Jamšek

PREDICTIVE EXOSKELETON CONTROL BASED ON PROBABILISTIC MODELS

Doctoral Dissertation

PREDIKTIVNO VODENJE EKSOSKELETOV NA PODLAGI VERJETNOSTNIH MODELOV

Doktorska disertacija

Supervisor: Prof. Dr. Jan Babič

Ljubljana, Slovenia, December 2022

Acknowledgments

I would like to express my gratitude to everyone who helped me during the time I spent working on this dissertation. First, I thank my supervisor prof. dr. Jan Babič for his invaluable guidance and feedback given to me over the years. I am sincerely grateful also to all of the friends and colleagues that supported me and created a fun and inspiring working environment. I am deeply grateful to my family who inspired and supported me throughout my studies. Finally, I would like to thank Emanuela, who stood by my side and supported me throughout all of the ups and downs during this time.

The research in this thesis was funded by the Slovenian Research Agency (PR-08345); the European Union's Horizon 2020 through the SPEXOR project (contract no. 687662); and by AnDy project (contract no. 731540).

Abstract

Research and development of exoskeletons for injury prevention and assistance with everyday living has steadily increased in the last decade. With some products already available on the market, a widespread adoption of exoskeletons appears to be within close reach. However, many challenges still remain to be overcome, one of which is the development of high level control strategies that would allow for a seamless human-robot integration. The purpose of this thesis is to explore novel control architectures suitable for high-level exoskeleton control and expand the current state of the art with an emphasis on the effects of human-robot interactions on human movements.

First, we explored the effectiveness of using probabilistic models to facilitate the decision making in a high-level controller for use with a quasi-passive spinal exoskeleton. The controller consisted of Gaussian mixture models in combination with a state machine that identified and classified the movement of the user in real time and provided a timely control output for the quasi-passive spinal exoskeleton. The results of this study showed that our approach is a useful tool for the control of quasi-passive exoskeletons. Second, we evaluated the use of probabilistic movement primitives (ProMP) for predicting user movement intentions during walking and arm reaching. In the walking scenario we showed that we can accurately predict some crucial gait parameters in real-time during the stride cycle. In combination with other systems monitoring the environment our method can be used to predict collisions of the feet with the surrounding environment. For the arm reaching scenario, we present an exoskeleton control method that utilizes ProMP to generate predictions of user movements in real-time which are then combined with a velocity-field-based controller to provide assistance to the user in a predictive way. We evaluated our approach with a haptic robot, where participants had to perform movements towards different target locations. We showed that we accurately predicted user movement intentions while at the same time significantly decreasing the overall physical effort exerted by the participants to achieve the task, without affecting their movement kinematics.

For any device assisting healthy individuals, it is crucial that it does not significantly modify their movements, as this could have negative health implications. However, sometimes the modifications of user kinematics with exoskeletons is desired. For example when we want to recreate artificial environments such as microgravity. We investigated whether local gravity simulation of altered gravitational conditions on the arm would lead to changes in kinematic parameters comparable to a full-body experience of microgravity and hypergravity. We developed a robotic device that applied forces at the wrist to simulate micro- or hypergravity conditions for the arm while subjects performed pointing movements on a touch screen. We analysed and compared the results of several kinematic parameters and muscle activity using this system with data of the same subjects being fully exposed to altered gravitational conditions onboard a parabolic flight. Our results suggest, that simulated altered gravity can elicit similar changes in some movement characteristics for arm reaching movements. This forms the basis for developing devices such as exoskeletons to aid in training individuals prior to undertaking tasks in varying gravitational conditions.

Povzetek

Razvoj eksoskeletov za preprečevanje poškodb posameznikov in pomoč pri vsakdanjem življenju se je v zadnjem desetletju vztrajno povečeval. Zdi se, da so eksoskeleti že na dosegu roke, saj je na trgu na voljo že več različnih izdelkov. Kljub temu je potrebno rešiti še veliko izzivov, med katerimi je tudi razvoj strategij nadzora na visoki ravni, ki bi omogočile brezhibno integracijo človek-robot. Namen doktorske disertacije je raziskati nove arhitekture vodenja, primerne za vodenje eksoskeletov na visoki ravni in razširitev trenutnega stanja tehnike s poudarkom na vplivu interakcij med človekom in robotom na človeško gibanje.

Najprej smo raziskali učinkovitost uporabe verjetnostnih modelov za izboljšanje odločitev regulatorja na visoki ravni za uporabo s kvazipasivnim eksoskeletom. Regulator je bil sestavljen iz modela Gaussovih mešanic v kombinaciji z regulatorjem končnih stanj (state-machine), ki je v realnem času ugotavljal in klasificiral gibanje uporabnika ter zagotavljal pravočasen ukaz za kvazipasivni eksoskelet hrbtenice. Rezultati te študije so pokazali, da je naš pristop uporabno orodje za vodenje kvazipasivnih eksoskeletov. Za tem smo ocenili uporabo verjetnostnih elementarnih gibov (ang. probabilistic movement primitives - ProMP) za napovedovanje gibanja uporabnika med hojo in gibanjem rok. V primeru hoje smo pokazali, da lahko v realnem času natančno napovemo nekatere ključne parametre hoje v vsakem koraku. V kombinaciji z drugimi sistemi za spremljanje okolja bi se naša metoda lahko uporabila za napovedovanje trkov stopal z okolico. Za primer gibanja roke predstavljamo metodo, ki s pomočjo predvidevanja gibov nudi pomoč uporabniku. Z uporabo ProMP ustvarjamo napovedi premikov uporabnikov v realnem času, ki jih nato kombiniramo z regulatorjem na osnovi hitrostnih polj. Predlagano metodo smo ocenili z eksperimentom s haptičnim robotom, kjer so udeleženci izvajali gibe proti različnim ciljnim lokacijam. Pokazali smo, da smo natančno predvideli želeno gibanje uporabnikov, hkrati pa se je občutno zmanjšal celoten fizični napor udeležencev, potreben za doseg naloge, brez da bi pri tem znatno vplivali na njihovo kinematiko.

Za vsako napravo, ki pomaga zdravim posameznikom, je ključnega pomena, da ne povzroči bistvene spremembe v njihovem gibanju, saj bi to lahko negativno vplivalo na njihovo zdravje. Kljub temu pa so spremembe kinematike gibanja včasih lahko tudi zaželene. Na primer, ko želimo poustvariti umetna okolja, kot je mikrogravitacija. Raziskali smo, ali lokalna sprememba gravitacijskih pogojev na roki privede do sprememb v kinematičnih parametrih, primerljivih z izkušnjo mikrogravitacije in hipergravitacije na nivoju celega telesa. Razvili smo robotsko napravo, ki je aplicirala sile na zapestju za simulacijo spremenjenih gravitacijskih razmer na roko, medtem ko so subjekti izvajali gibe na zaslonu na dotik. Z uporabo tega sistema smo analizirali in primerjali rezultate več kinematičnih parametrov in mišične aktivnosti s podatki istih subjektov, ko so le-ti bili izpostavljeni spremenjenim gravitacijskim pogojem na paraboličnem letu. Naši rezultati kažejo, da simulirano spremenjena gravitacija lahko povzroči podobne spremembe v nekaterih značilnostih gibanja roke. To je osnova za razvoj naprav, kot so eksoskeleti, za pomoč pri usposabljanju posameznikov pred opravljanjem nalog v spremenjenih gravitacijskih razmerah.

Contents

List of Figures

List of Tables

Abbreviations

ANN	...	Artificial Neural Networks
ANOVA	...	analysis of variance
BIC	...	Bayesian information criterion
CAE	...	clutched elastic actuator
CAN	...	controller area network
CNES	...	Centre national d'études spatiales
CPDMP	...	compliant parametric movement primitives
DMP	...	dynamic movement primitive
EEG	...	electroencephalography
EMG	...	electromyography
FN	...	false negative
FP	...	false positive
GMM	...	Gaussian Mixture Models
GMR	...	Gaussian mixture regression
HMM	...	Hidden Markov Models
HS	...	heel strike
IMU	...	inertial measurement unit
kNN	...	k-Nearest Neighbours
LbD	...	learning by demonstration
LDA	...	Linear discriminant analysis
MP	...	movement primitive
NASA	...	National Aeronautics and Space Administration
PEA	...	parallel elastic actuator
ProMP	...	probabilistic movement primitive
PWS	...	preferred walking speed
QDA	...	Quadratic discriminant analysis
RMSE	...	root mean squared error
SEA	...	series elastic actuator
SVM	...	Support Vector Maachines
TN	...	true negative
TO	...	toe-off
TP	...	true positive
TPV	...	time to peak velocity

Chapter 1

Introduction

1.1 Introduction and Description of the Problem

1.1.1 General overview of exoskeleton devices

Robotic exoskeletons are promising tools to assist humans in various real-life tasks [1]. They are robotic devices that are designed to be worn on the body and to provide direct motion assistance to the user. They can be either full body exoskeletons, for upper or lower extremities, or only for supporting specific joints of the human body. The common applications of exoskeletons are physical rehabilitation for impaired patients [2], assistance of frail individuals [3] and motion augmentation of able-bodied workers [4]. These robotic devices are predominantly categorized in two categories, active or passive. Active exoskeletons use actuators that can inject energy into the movement of the human. The actuators can be either electric, hydraulic, pneumatic or a combination of these [5]–[7]. On the other hand, passive exoskeleton systems only use passive viscoelastic elements such as springs and dampers to provide assistance to the user. Even though these devices do not add energy to the human, they have been proven to effectively reduce muscular activity and fatigue, which can alleviate injuries or lower the risk of musculoskeletal disorders [8]–[11]. Additionally to the active and passive systems, several combinations of active and passive elements were proposed in literature, including clutched elastic actuators (CAEs) [12], series or parallel elastic actuators (SEAs, PEAs) [13] and variable stiffness actuators [14].

1.1.2 From low-level to high-level control of exoskeletons

The common denominator to all the previously described exoskeleton systems, apart from purely passive devices, is the need for suitable control algorithms. This is perhaps one of the most significant issues that needs to be addressed in order to maximize the potential of these robotic devices and enable a truly seamless human-robot interaction. The control of robotic devices is always either explicitly or implicitly structured in a hierarchy as was proposed in several generalized control frameworks [15], [16]. At the lowest level the actuators of the devices need precise control of the torques and forces they exert which is typically achieved with fast feedback loops that control the electrical current or pressure in the actuator itself. The input to these low-level control loops are desired output states of the device which can either be positions, velocities, accelerations or directly torques and forces, depending on the type of device and control architecture. Apart from some cases such as admittance or impedance control [17], these desired output states are generally only part of a mid-level controller that translates the user intentions or commands that originate from a high-level controller. The high-level controller is responsible for correctly identifying the intentions of the user of the robotic device. Some intentions of the

user can be explicitly specified via controls such as joysticks or buttons [18], but ideally to achieve a truly seamless human-robot interaction while wearing an exoskeleton, the device itself should automatically detect user movement intentions and act accordingly [16]. In human-robot interaction literature there are several keywords that are associated with detecting or predicting human movement intention such as anticipation, intention recognition, activity recognition, legibility, goal estimation and inference [19]. All these keywords were considered during the review of the current state of the art. However, regardless of the terminology, the detection of user movement intent can be performed as a separate step and complemented with predefined actions, or it can be intrinsically performed such that the output can be directly exploited to drive the exoskeletal device in the form of movement primitives. The following paragraphs will be split by first presenting the various techniques used for recognizing human movement states and intentions, followed by a description of path guidance algorithms that can be used in combination with the intention recognition, and by presenting various techniques of encoding and predicting movements in the form of movement primitives. Finally we also present an overview of the important effects of human-robot interaction on the human body and identify the major considerations when using such devices.

1.1.3 Human activity recognition

The prediction or inference of user movement intentions can be sensed through various channels, such as cortical and neuro-muscular activity, myoelectric signals, the posture or state of the user or device and through the interaction of the user with the device and the surrounding environment. Each of these input modalities differ in the amount of invasiveness and amount of information that is available [20]. Although there is some overlap between algorithms used to process all these different input modalities, we primarily focus on presenting methods designed for use with the least invasive sensors, such as those embedded in the device itself or additional inertial measurement units (IMUs) for monitoring the user kinematics. State machines are a powerful tool to implement different controllers for different situations, such as an impedance-based controller in stance and a kinematic controller for swing phase [21]. Usually in such state machines the rules for transitions are hand tuned and fixed which is a very simplistic method but can be fairly effective in many scenarios, such as detecting mode transitions between different gait events [22] or lifting events [23]. Unfortunately, this type of control architecture is unsuitable for more general purposes, as it is impossible to predict in advance all possible states and the transitions between them. However, state machines can be used to complement automated pattern recognition techniques as they can include hard coded safety limitations that are of paramount importance when designing human-robot interfaces. A more sensible approach for human intent recognition is the use of automated pattern recognition techniques. The advantages over using manually set rules is that a multitude of inputs can be used simultaneously for generating the classification decision boundaries. Several classification algorithms have been exploited for human intention recognition including k-Nearest Neighbours (kNN), Linear Discriminant Analysis (LDA), Quadratic Discriminant Analysis (QDA), Gaussian Mixture models (GMM), Support Vector Machines (SVM), Hidden Markov Models (HMM) and Artificial Neural Networks (ANN) as presented in several review papers concerning human activity recognition in general [24], [25] or classification of activities in the scope of control of wearable robots [16], [26]. The choice of an appropriate classifier heavily depends on a multitude of factors. For less complex input data, simpler algorithms such as kNN, LDA or QDA may perform sufficiently, however with increased sensor inputs and modalities they could struggle. For more complex systems, approaches with GMM, HMM or ANN could be more suitable, the latter especially for complex sig-

nals such as EMG or EEG. However, safety is of paramount importance when it concerns human-robot interaction and relying solely on the classification algorithms for generating control outputs is inappropriate. As previously mentioned, this can be accomplished by combining these machine learning classification algorithms with state machines. One example of such a combination was successfully used to detect various states of the user while wearing a spinal exoskeletal device, by combining a state machine with a QDA classifier [27]. However, in this study, the main algorithm for detecting the various states was still a hand tuned threshold-based state machine and the trained QDA classifier was used only for differentiating from a falsely identified lift versus a true lift event. A more general and useful approach would be to primarily focus on the classifier to classify the input data and complement the outputs with a state machine in order to satisfy hardware limitations and safety aspects of the human-robot interaction. For some applications it is necessary to estimate certain parameters instead of the specific activity, such as different gait parameters during walking. Approaches of using kinematic data for estimating gait parameters such as toe-off and heel-strike are fairly accurate and can be used to a great extent in laboratory and in rehabilitation scenarios [28]–[31]. Concerning robotic devices, it is also possible to easily distinguish between swing and stance phases with simple threshold-based algorithms [32]. However,the limitation of these methods is that it is difficult to infer future events and as such these types of controllers merely act in a reactive and non-predictive manner.

Classification of activity and simple control can be effective and can even be used to control active exoskeleton devices by selecting appropriate assistive profiles based on the classified activity of the user as presented in [33], [34] for use with spinal exoskeletons. For use cases regarding upper or lower limb exoskeletons another option is more suitable, where the classified activity is used to select a predetermined reference trajectory. These trajectories can then be used with various path control algorithms as we present in the following subsection.

1.1.4 Guidance along predefined paths

In an effort to make physical therapy more accessible (in the sense of reducing costs and increasing dosages) there has been a lot of development of robotic devices for either the upper limbs [17] or lower limbs, especially gait training of post stroke patients [3], [35]. Most of these devices use some sort of reference trajectory either in task [36] or in joint space [37] to compliantly guide the user. A viable method to provide assistance along such reference trajectories is to use potential-field-based controllers [38]–[40]. However, such control algorithms generate high forces in the event of larger errors with respect to the specified path [38]. To overcome this problem, a velocity-field-based controller was proposed by Martinez et al. [38], which applies corrective torques based on a viscous flow field control law. They showed that this approach could effectively guide movements of the user's leg along a reference path while being less resistive to large path deviations and thus making the controller inherently safer. All of the aforementioned methods for guidance along a predefined path could benefit greatly from a reference trajectory that is predicted from the user movement. This could then enable the expansion of the application of these methods from uses in physiotherapy to wearable devices for the prevention of musculoskeletal disorders in able-bodied individuals. Therefore, we have explored the possibilities of estimating user movement intention with methods that are capable of predicting future evolution of the movement trajectory which we present in the following subsection.

A well-established approach for trajectory representation in robotics is by encoding the trajectory using movement primitives (MPs) in a process often referred to as learning by demonstration (LbD). There are a number of different versions of MPs such as dynamic movement primitives (DMPs) [41], [42], compliant parametric dynamic movement prim-

itives (CPDMP) [43], Gaussian Mixture Regression (GMR) [44], and probabilistic movement primitives (ProMPs) [45]. These algorithms have been extensively used especially for controlling robots in a multitude of tasks ranging from assembly [46] to surgical applications [47]. Many use cases also incorporate human-robot interaction. In these scenarios some of these same algorithms were exploited for human movement prediction in the form of inferring trajectories and end goals of the humans such as GMR [48]–[50] and ProMPs [51], [52], with very promising results. Additionally ProMPs were successfully used for real-time prediction of human movement outside the scope of robotics [53]. However, most of these algorithms were rarely applied in the scope of exoskeleton control [54], despite having many advantageous properties. ProMPs specifically have a high potential for use in exoskeleton control, due to their representation of trajectories together with their variance. This could allow the controller to modulate the feedback gains based on the variance of movement and provide high precision only in certain parts of the movement, which was shown to be important for successful human-robot interaction [55], [56].

1.1.5 Effects on human movements in human-robot interaction

When considering any interaction between humans and robots we strive to minimise the negative effects on the human body. Depending on the application and circumstances, this can mean low interaction forces, maintaining the full range of motion, and no significant effect on the kinematics of the movements. Low interaction forces are desirable primarily in human robot collaboration, where we wish to minimize the effort of users to perform a given task [57]–[59]. We also strive towards more ergonomic postures for the human when using robotic assistance [60]. However, when we assist able-bodied individuals in various tasks there is one more aspect that we need to be aware of: movement kinematics. While reducing forces and generally assisting individuals, it is very important that we do not modify their movements significantly. Imperfect implementations of robot control can cause humans to make compensatory changes to their movement patterns. This can lead to increased loading of other joints which can cause other musculoskeletal disorders or injuries [9], [61]–[65]. Sometimes however, the opposite is true. For example patients that have neuromuscular disorders and have trouble controlling their movements, have to be trained to correct their movement patterns [54], [59]. This implies that significant modifications of their kinematics is a desirable outcome. This can be achieved through various exercises with simulated haptic environments etc. Additionally, changing of user kinematics can be desirable when we want to simulate artificial environments. Similar to how we train movement-impaired individuals to execute more healthy trajectories, we can implement the use of robots with healthy individuals and modify their movements or muscle activations in order to train them to adapt to new environments. One area which is still largely unexplored is the use of exoskeletons for training individuals prior to undertaking tasks in changed gravitational environments i.e. space travel.

1.2 Thesis Purpose, Goals and Hypothesis

1.2.1 Purpose of the dissertation

The main purpose of this dissertation is to explore novel control architectures suitable for high-level exoskeleton control and expand upon the current state of the art with a strong emphasis on the effects of human-robot interactions on human movements. One area that is currently largely unexplored is the high-level control of newer types of exoskeleton systems that combine passive and active elements. This thesis addresses this deficiency with the development and evaluation of a high-level control algorithm for a quasi-passive spinal

exoskeleton based on probabilistic models of user data. Another area worth exploring is repetitive tasks such as manual object manipulation on assembly lines or walking, where there is an opportunity to exploit the repetitiveness of movements and apply modern probabilistic models to predict user movement intentions and design a high-level controller that will improve the overall human-robot interaction experience. In the scope of this thesis, we explored the possibilities of using probabilistic movement primitives (ProMPs) in exoskeleton control applications, primarily as a form of human movement prediction to create control schemes that can better adapt to users of exoskeletal devices. Additionally we explored the effects of using a simple human-robot interaction to simulate microgravity and hypergravity conditions for arm movements on Earth.

1.2.2 Goals of the dissertation

To realize the purposes of this dissertation four main goals are set.

G1. Develop a high-level controller for a quasi-passive spinal exoskeleton device based on probabilistic models of user data. To successfully classify user movement intent and control an exoskeleton device accordingly, it is crucial to utilize probabilistic models of user data. This should form the basis for the decision making inside the controller while hard coded safety limits should be used to complement this information in order to assure safe operation of the device.

G2. Evaluate the use of ProMPs as a method for predicting gait kinematic parameters for use in predictive control schemes for lower limb exoskeleton devices. The use of ProMPs could provide more valuable real-time prediction of step length than conventional methods for estimating these parameters. This could in turn be used to predict collisions of the user with the environment which could be used as an input for an exoskeleton. Additionally, the use of ProMPs would enable a control algorithm to condition the predicted trajectory towards a different end goal and control the exoskeleton towards that goal (i.e. to prevent the collision from occurring).

G3. Exploit state of the art probabilistic methods for human movement prediction to develop a high-level controller for use in upper limb exoskeleton devices. With this goal we aim to expand the use cases of already developed path guidance algorithms beyond physical rehabilitation of movement impaired individuals towards assistive exoskeletal devices intended for prevention of musculoskeletal disorders in various working scenarios with repetitive tasks.

G4. Evaluate the effects of human-robot interaction for simulating microgravity and hypergravity conditions for arm movements on Earth. The use of robotic devices for simulating alternate gravitational conditions for limbs could prove useful in the research field of neuromechanics as well as for training individuals prior to undertaking tasks in changed gravitational conditions.

1.2.3 Hypothesis

In line with the purpose and goals of the dissertation we formulated the following hypothesis:

- H1. Gaussian mixture models can be successfully used to encode different movements and used to provide control outputs for a quasi-passive spinal exoskeleton.
- H2. Using probabilistic movement primitives, we can predict crucial gait parameters in real time during the swing phase of the foot.
- H3. Using probabilistic movement primitives, we can accurately predict user movement intention also for new never seen end target locations.

- H4. Employing user movement prediction enables assistance also for new never seen end goals.
- H5. The combination of movement prediction with a path guidance algorithm enables a seamless human-robot interaction.
- H6. Exploiting human-robot interaction to simulate microgravity and hypergravity conditions for arm movements in normogravity can recreate similar changes in the parameters of motion.

1.3 Thesis Structure

This thesis is structured in the following way.

Chapter 2 presents our work of developing a new control scheme consisting of GMM in combination with a state machine controller to identify and classify the movement of humans as early as possible and provide a timely control output for a quasi-passive spinal exoskeleton.

Chapter 3 describes the use of probabilistic movement primitives for predicting user foot placement in real-time where we have shown that we can accurately predict user step length after observing only the initial part of the trajectory during the swing phase.

Chapter 4 presents the answers to hypothesis H3-H5 where we evaluated a novel control approach using ProMPs to generate predictions of user movements in real-time and utilizing them to generate an assistive controller.

Chapter 5 describes our work of simulating micro and hypergravity conditions for arm reaching on ground with a robotic device and comparing the results with data obtained from subjects fully exposed to micro and hypergravity conditions.

The thesis conclusions are presented in Chapter 6.

Chapter 2

Gaussian Mixture Models for Control of Quasi-Passive Spinal Exoskeletons

2.1 Introduction

Exoskeletons are recently being developed to solve issues of worker injuries and prevent musculoskeletal disorders [1], [4]. In particular, there has been a lot of development of spinal exoskeletons to help alleviate the problems of low-back pain, and shoulder exoskeletons to assist users in overhead working scenarios [66]–[68]. These exoskeletons exist predominantly in two categories: passive and active. Active exoskeletons can add energy to the human motion using various types of actuators, ranging from hydraulic, electric, pneumatic or a combination of these [5]–[7]. However, active exoskeletons usually require a substantial energy storage that increases the weight of the system, and have a limited amount of operational time. The additional weight of the exoskeleton increases the inertia of the system which is difficult to compensate [69]. On the other hand there are passive exoskeleton systems that only use passive viscoelastic elements such as springs and dampers to provide assistance to the user. Even though these devices do not add energy to the human, they have been proven to effectively reduce muscular activity and fatigue, which can alleviate injuries or lower the risk of muscoloskeletal disorders [8]–[11]. Nevertheless, they usually suffer from a limited versatility as they can restrict some of the user movement for tasks that do not require support, such as walking, for spinal exoskeletons [70] and arm motion for shoulder exoskeletons.

One way of solving this issue is by using passive elements to provide the supporting torque and small actuators to engage or disengage this support making these devices quasi-passive. Actuators used for such purposes are called Clutched Elastic Actuators (CEA) [71]. By means of having the possibility to engage or disengage the passive support of the exoskeleton, unobtrusive movement of the user can be achieved for tasks that do not require assistance. For all other tasks the support is engaged. One of the problems with such devices is the need for a controller that has to determine when to turn the support on and off.

Work regarding the control of devices implementing CEA's is sparse as it is usually limited to the low level control of forces and stiffness [71]–[73]. Most papers regarding control of exoskeletons deal with active devices [27], [74], [75]. Some studies were dealing specifically with controllers for active spinal exoskeletons, where various techniques of lifting were being classified and based on this, appropriate support was given to the user [23], [27]. These studies focused on the detection and classification of the upward lifting motion and neglected the initial part, when the body bends down towards the load. This is appropriate only if the exoskeleton can actively generate mechanical power. For

a quasi-passive exoskeleton this is not a feasible approach, since the energy to assist the upward motion needs to be stored in the viscoelastic elements already when performing the downward motion. This is a more difficult task as some movements start similarly and only become different in later stages (e.g. sitting down on a chair vs. bending down to lift an object from the ground). Arguably this would imply that the initial part of the motion should be considered the same for both tasks (e.g. bending down is common to both sitting down and lifting an object). This would, however, require a more complex acquisition of the ground truth information, such as video analysis of the performed movements. In the scope of this work, we used clean and elementary ground truth information about the performed movements in combination with a probabilistic classification algorithm, to develop a controller that is able to handle the similarities between the movements and provide a control output for the quasi-passive spinal exoskeleton.

A variety of classification techniques exist that were used for human movement classification from body mounted sensors. These range from simple algorithms like threshold based classification, k-nearest neighbours or decision trees, to probabilistic approaches such as Gaussian mixture models, Hidden Markov models, or Support vector machines, Fuzzy logic and artificial neural networks [25]. Regarding exoskeleton control, Gaussian mixture models (GMM) have already been implemented for EMG and EEG signal classification for the purpose of controlling an exoskeleton [76]–[78]. GMM are also an effective tool for probabilistic classification of user movements [79], [80]. The main advantage of GMM is that they provide a probability estimate for classification rather that assigning new input data to one specific class. As such, the classification of the model is not discrete, which allows us to use this information to condition the transitions of a state machine in order to modulate the control output for the quasi-passive spinal exoskeleton. In this chapter, we present an exploitation of the GMM probabilistic classification expanded with a state machine to control the quasi-passive exoskeleton in such a way that it supports the user when needed and is unobtrusive when the support is not necessary.

2.2 Materials and Methods

2.2.1 Experimental setup

We used a quasi-passive spinal exoskeleton [81] (Figure 2.1) that can provide support to the subject by unloading the spine when performing lifting movements. It is comprised of two main components: the upper spinal module and the bottom spring mechanism. The upper part is a spinal elastic module with carbon fibre beams that transfers the extension torque generated by the passive spring mechanism at the hip to the trunk of the subject. Additionally it provides passive support when the subject is performing trunk flexion. In the bottom part of the exoskeleton there is a spring mechanism that is compressed during hip flexion which generates an extension torque at the hip. The mechanical design is presented in greater detail in the work of Näf et. al. [81]. The spring mechanism can be engaged or disengaged via a clutch located at both hip joints. If the clutch is disengaged, the springs do not provide any support as the mechanism freely rotates around the hip joint. This means that the exoskeleton does not hinder the subject when performing movements like walking or sitting down. It is important to note that the mechanical design of the clutch enables a transition from engaged to disengaged or vice versa only when the forward rotation around the hip joint of the exoskeleton is lower than 25°. The rotation around the hip joint of the exoskeleton is directly correlated with the subject's hip angle.

To automatically engage or disengage the clutch, one small servo motor (KST X15-908, KST Digital Technology Limited, Meihzou, Guangdong, China) is used on each side of the

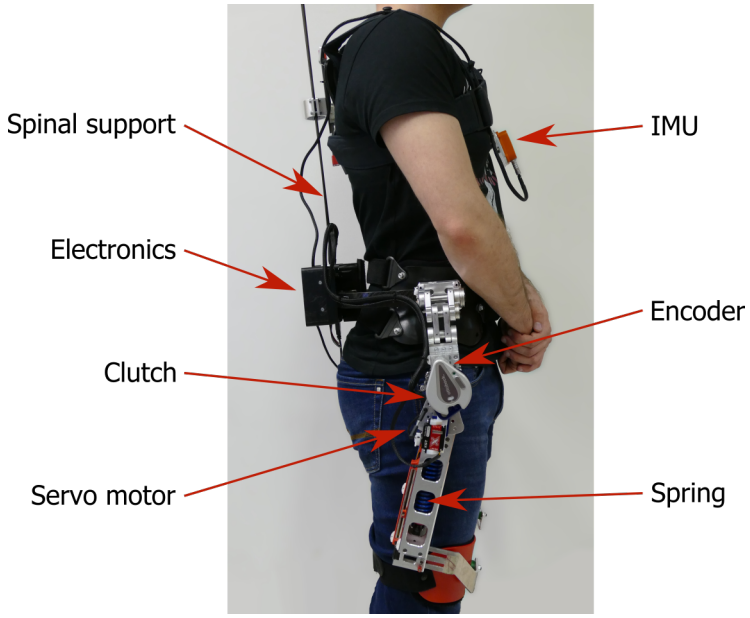

Figure 2.1: Lateral view of a subject wearing the exoskeleton. Red arrows indicate the locations of key components of the device.

exoskeleton. Each servo motor is attached to the lever arm of the clutch and can engage or disengage the clutch in 0.05 s. For a regular motion of the user, the expected rotational velocity of hip flexion is around 100 °/s. Based on the servo actuation timing, the subject can move 5° during the activation of the clutch. This limits the actual engagement window of the clutch to 20° of hip flexion.

The exoskeleton is equipped with sensors to monitor the configuration of the exoskeleton and therefore the pose of the subject wearing it. It has built-in rotational encoders in both hip joints to monitor the hip flexion or extension (AS5048A, ams AG, Premstaetten, Austria). In addition to the encoders, an IMU (Xsens, Enschede, Netherlands) is attached on the chest straps of the exoskeleton. The IMU provides information of the orientation of the subject's trunk in space. For the experiment performed in this study, we recorded the orientation of the subject's trunk in the sagittal plane.

The exoskeleton includes on-board electronics to read sensor data and send commands to the servo motors. The main computing module consists of a Raspberry Pi Model 3B+ (Raspberry Pi Foundation, Cambridge, United Kingdom). It allows a controller to be programmed in Matlab Simulink (Mathworks, Natick, MA, United States) and deploy the compiled code on the target hardware. The power supply for the raspberry Pi is an off-the-shelf product PiJuice HAT (Pi Supply, East Sussex, United Kingdom). It provides uninterrupted power supply for the Raspberry Pi from a 4.2 V, 1820 mAh battery. The servo motors are powered from a separate 7.4 V, 1000 mAh Li-Poly battery.

2.2.2 Experimental protocol

Seven healthy subjects participated in the study (age: 27.14 ± 2.12 years, height: 172.00 ± 9.27 cm, weight: 69.86 ± 12.69 kg). The experiment was conducted at Jožef Stefan Institute in accordance with the principles stated in the Declaration of Helsinki and approved by the Slovenian National Medical Ethics Committee (No. 339/2017/7).

Subjects performed a sequence of tasks while wearing the exoskeleton, representative of a typical working environment, shown in Figure 2.2. The task sequence was predetermined

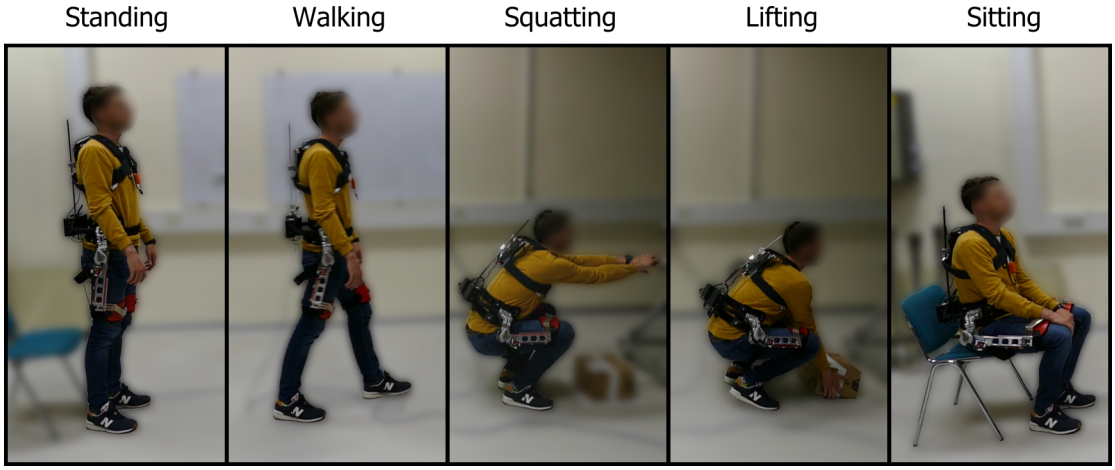

Figure 2.2: Example of performed tasks during the experiment.

and consisted of a random number of repetitions of the following movements: walking, sitting, squatting and lifting a 3 kg box from the floor. In between every movement, the subjects came back to a normal upright stance and awaited instructions for the next movement. The sequence of tasks was unknown to the subjects and the instructions were given verbally, only after every completed movement. Each subject performed in total 20 walks, 20 squats, 20 box lifts and 20 chair sits. The subjects were not instructed to perform any specific lifting technique such as stoop or squat lifting. They were free to use their preferred lifting technique as well as perform all movements at their preferred speed. Data from the sensors was recorded using the Raspberry Pi at a frequency of 100 Hz. For reference, the average duration of the performed movements was 1.38 s $\pm$ 0.73 s, 4.64 s $\pm$ 0.86 s, 2.67 s $\pm$ 0.47 s, 2.98 s $\pm$ 0.39 s and 5.61 s $\pm$ 1.57 s for the tasks of standing, walking, squatting, lifting and sitting, which corresponds to an average of 138, 464, 267, 298 and 561 data samples. The total length of the experiment was on average 460.5 $\pm$ 52.3 s. Prior to the start of each recording session, we recorded the orientation of the IMU for 1 second. The mean value of this recording was used as a reference for normal upright standing (0° of trunk inclination). During the experiment, the exoskeleton clutch was disengaged at all times.

To have a ground truth label to train and validate our classification method, the recorded dataset was segmented and hand-labelled. The set of possible labels was: 1 - standing, 2 - walking, 3 - squatting, 4 - lifting, 5 - sitting. Labelling was based on the set of instructions given to the subjects during the experiment. For example, the whole motion of performing the instruction "Sit", "Stand up", was labelled as sitting. The start and end of the task were determined by the standing phase.

2.2.3 Classification algorithm with GMM

The foundation of our control algorithm is based on GMM to discriminate between the various tasks performed by the subject. This is done in two steps: fitting and predicting.

First, data belonging to each task j was modelled using a superposition of K Gaussian densities (Gaussian mixtures) by

$$p_j(\boldsymbol{x}) = \sum_{k=1}^{K} \tau_k \phi_k(\boldsymbol{x}|\boldsymbol{\mu}_k, \boldsymbol{\Sigma}_k), \tag{2.1}$$

where $\boldsymbol{x}$ is a 6x1 vector of input data (right encoder angle, left encoder angle, IMU orientation in the sagittal plane, right encoder angular velocity, left encoder angular velocity, rate of change of IMU orientation in the sagittal plane). Every k-th Gaussian density denoted as $\phi_k(\boldsymbol{x}|\boldsymbol{\mu}_k, \boldsymbol{\Sigma}_k)$ is a component of the mixture and has its own mean $\boldsymbol{\mu}_k$ and covariance $\boldsymbol{\Sigma}_k$. τ_k are the mixing coefficients of the components. Both $p_j(\boldsymbol{x})$ and the individual Gaussian components are normalized such that:

$$\int_{-\infty}^{\infty} p_j(\boldsymbol{x}) = 1 \tag{2.2}$$

and

$$\sum_{k=1}^{K} \tau_k = 1. \tag{2.3}$$

To fit the Gaussian mixtures we used the Expectation Maximization algorithm for fitting a predefined number of mixtures to the selected data. The number of mixtures K used for fitting was set to 1 for the standing task. For each of the tasks of walking, squatting, lifting and sitting, the value K was determined in an iterative process [82] separately, as follows. For each model with K Gaussians used, the Bayesian information criterion (BIC) was calculated and compared to the value of the previous model $(K-1)$. If the new value of BIC was lower, the new model was kept and the iteration continued until the value did not lower anymore or the set maximum value ($K = 5$) was reached. In Figure 2.3 we present an example of the trained GMM in a reduced feature space for the lifting and sitting task.

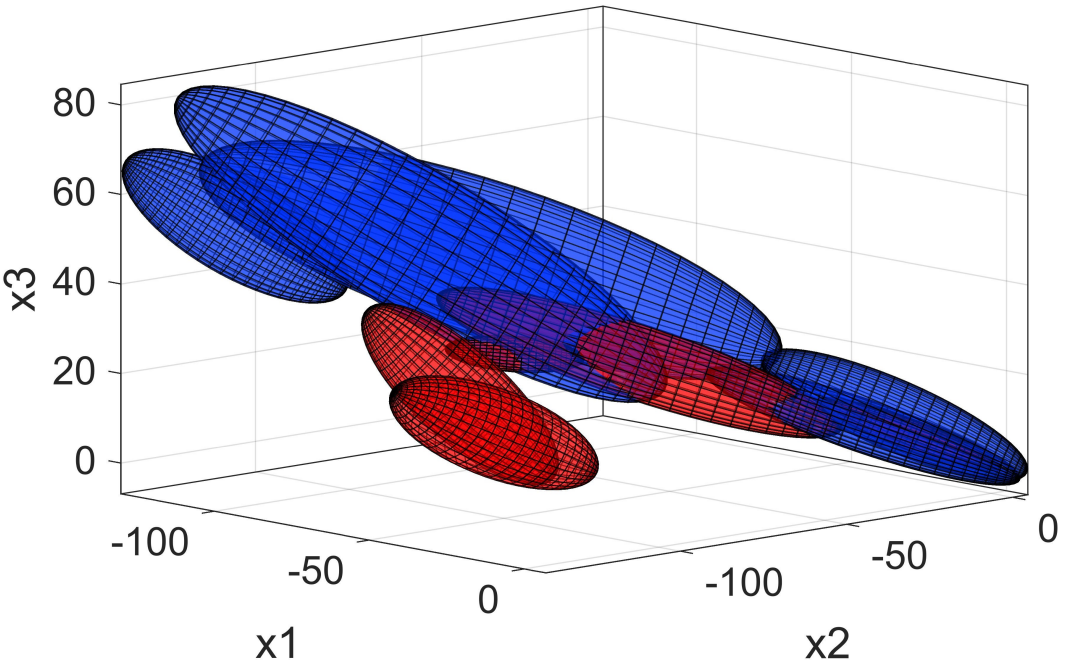

Figure 2.3: GMM representation in a reduced feature space for the lifting (Blue) and sitting task (Red); $K_{lift} = 5$, $K_{sit} = 5$. The axis $\boldsymbol{x}_1$, $\boldsymbol{x}_2$ and $\boldsymbol{x}_3$ represent right hip angle, left hip angle and trunk inclination respectively. For reference, all movements start in the bottom right corner, continue towards the left side of the graph and return to the starting position.

To use the Gaussian mixture models for classification of new input data we calculate the posterior probability of the new input data $\boldsymbol{x}$ belonging to each task j:

$$p_j(\boldsymbol{x}) = \sum_{k=1}^{K} \tau_k \Big(\frac{e^{-\frac{1}{2}(\boldsymbol{x}-\boldsymbol{\mu_k})^T \boldsymbol{\Sigma_k}^{-1}(\boldsymbol{x}-\boldsymbol{\mu_k})}}{\sqrt{(2\pi)^D |\boldsymbol{\Sigma_k}|}} \Big), \tag{2.4}$$

where D is the dimensionality of the model (6 in our case). We can combine these values in a vector $\boldsymbol{p}(\boldsymbol{x})$ that contains the posterior probabilities for each task. At this point it is possible to compare all of the probability values with each other and select the task with the highest probability. To do this, we define a function $imax(\boldsymbol{p})$ that selects the index j in the vector $\boldsymbol{p}$ that has the maximum probability,

$$imax(\boldsymbol{p}) = \big\{ j \mid p_j = max(\boldsymbol{p}) \big\}, \tag{2.5}$$

which gives us the prediction to which state the new input data $\boldsymbol{x}$ belongs to. This approach already provides valid and useful information about any new input data into the model. However, this can be problematic when GMM of different tasks overlap. Such an overlap can be observed in the bottom right corner of Figure 2.3. This is an outcome of the protocol used for acquiring the ground truth that was used for training the model. In this case the prediction using $imax(\boldsymbol{p})$ is not stable as it can change from one task to another for every new data sample acquired. To overcome this limitation and preserve the clean acquisition of ground truth, we developed a state machine controller that is presented in subsection 2.2.4.

2.2.4 Integration of GMM with a state machine

To complement the GMM probability outputs we developed a state machine controller which is schematically presented in Figure 2.4. The states of the controller are the five tasks performed during the experiment (standing, walking, squatting, lifting and sitting) along with a *pre-lift* state. We added a *pre-lift* state, because of the similarity of the models in the early stages of performing the tasks of squatting, lifting and sitting. By using this state we conditioned the output of the state machine to classify a *pre-lift* until the probability of squatting, lifting or sitting reaches a high enough value. This limits the amount of transitions between states in the initial part of the downward movement when the subject starts bending down. The transitions between the states are conditioned by probabilities of $\boldsymbol{p}(\boldsymbol{x})$, normalized based on the sum of probabilities of all tasks ($J = 5$) for the current input $\boldsymbol{x}$,

$$\boldsymbol{p}^n(\boldsymbol{x}) = \frac{\boldsymbol{p}(\boldsymbol{x})}{\sum_{j=1}^{J} p_j(\boldsymbol{x})}. \tag{2.6}$$

With this normalization, we simplify the comparison of probabilities for the current input $\boldsymbol{x}$. However, the normalized probabilities do not include information about the actual value of the posterior probability of $\boldsymbol{x}$ belonging to a task j. This is important, as it defines whether the current input data is similar to the data used for training the model or not. To account for this, we compare the current probability value of each state $p_j(\boldsymbol{x})$ with the maximum probability of the model for that state:

$$m_j(\boldsymbol{x}) = \frac{p_j(\boldsymbol{x})}{max(p_j(\boldsymbol{x}))}. \tag{2.7}$$

If the current probabilities for all states are lower than 0.005 of their respective maximum, the transitions between the states in the state machine are disabled. The initial state of the state machine is denoted by the circle and arrow leading to the state standing. The

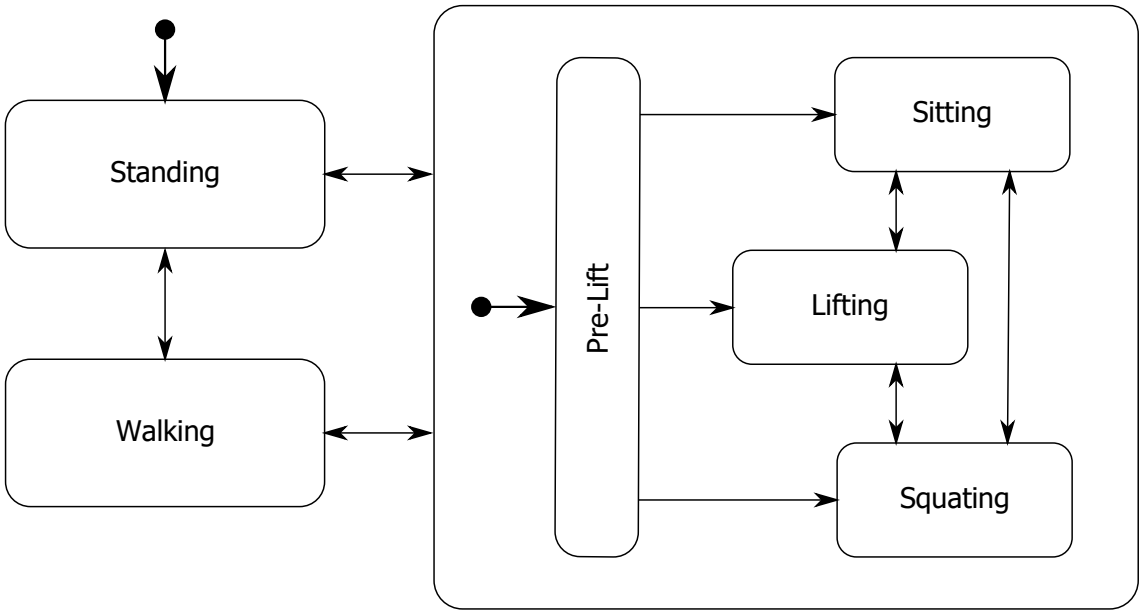

Figure 2.4: Structure of the state machine controller with all possible transitions between states. The states of pre-lift, squating, lifting and sitting are grouped inside a superstate which allows transitions back to the walking or standing state. Arrows with circles denote initial transitions.

transition to standing occurs when the sensors are calibrated in a normal standing pose of the user. After this, the state machine controller can switch between all the different states based on the following transition rules. The transition rule from standing or walking to the *pre-lift* state is defined as:

$$p_3^n(\boldsymbol{x}) + p_4^n(\boldsymbol{x}) + p_5^n(\boldsymbol{x}) > h_1. \tag{2.8}$$

All other transitions in the state machine from a current state i to the next state $i+1$ are defined as

$$p_{i+1}^n(\boldsymbol{x}) > h_1, \tag{2.9}$$

where h_1 is a fixed threshold value set to 0.8. Additionally, we add a hold condition, that holds the current state of the state machine when the subject is in the middle of a sit, squat or lift. The rule for the hold condition is $abs(v_T) < v_1$ AND ($p_3^n(\boldsymbol{x}) > h_2$ OR $p_4^n(\boldsymbol{x}) > h_2$ OR $p_5^n(\boldsymbol{x}) > h_2$), where h_2 and v_1 are fixed threshold values of 0.5 and 5 $^\circ/s$ respectively and v_T denotes the rate of change of orientation of the subject's trunk. The hold condition ends when the probability of standing or walking satisfies equation 2.9.

2.2.5 Performance evaluation of the controller

We evaluated the performance of our controller for task recognition and for the activation of support provided to the user. We split the collected data from the 7 subjects into 2 groups. The first 6 subjects were used to perform a leave-one-out cross validation of our proposed approach, while the final seventh subject was used separately as a testing subject. The methodology used to evaluate task recognition is presented in subsection 2.2.5.1. Activation of support provided to the user was evaluated based on the control signals generated for clutch actuation which is presented in subsection 2.2.5.2.

2.2.5.1 Evaluation of task recognition

To evaluate the performance of task recognition, we performed a leave-one-out cross validation procedure on the dataset due to a limited number of subjects that were recruited for the experiment. In the validation part, data of all except one subject was used to train the GMM and the remaining subject's data was used as the test dataset. This was repeated for each subject, using every subject once as the testing dataset, for a total of 6 times. After this procedure was carried out, the same metrics were calculated for the final testing subject, where the data of the first 6 subjects was used as the training dataset. To emphasize the importance of the state machine we calculated the performance metrics for the case of using only GMM and the combination of GMM with the state machine (GMM+S). First we looked at the overall accuracy, sensitivity and specificity of classification for GMM+S considering all input data samples collected during the experiment. We defined these classification metrics as:

$$Accuracy = \frac{TP + TN}{TP + TN + FP + FN} , \tag{2.10}$$

$$Sensitivity(k) = \frac{TP_k}{TP_k + FN_k} , \tag{2.11}$$

$$Specificity(k) = \frac{TN_k}{TN_k + FP_k} , \tag{2.12}$$

where, TP, TN, FP, FN denote the number of true positives, true negatives, false positives and false negatives. For the calculation of specificity for the 5 states, the TN and FP values were calculated for a one vs. all comparison.

More important in our case, are classification results for binary conditions of support ON and support OFF. In this case, we define a true positive result (TP) as a classification of support ON for lifting or squatting movements. A true negative result (TN) is considered a classification of support OFF for standing, walking and sitting movements. The definitions of the performance metrics of accuracy, sensitivity and specificity remain the same as defined in equations 2.10, 2.11 and 2.12. Since the calculation of these metrics across all input data is too general, we additionally calculated their values over the course of the performed movements. To do this, we normalized each individual repetition of a task over time. We then calculated the performance metrics for each 5 % of the normalized movement trajectories for each subject. The final results are presented with the mean and standard deviation of the performance metrics across all the test subjects.

2.2.5.2 Evaluation of support activation

To evaluate the efficacy of our controller for support activation we performed a simulation of the actuation of the exoskeleton's clutch. As stated in section 2.2.1, the clutch of the exoskeleton needs some time to actuate. We have taken into account this actuation time, by reducing the angle at which successful engaging of the clutch is deemed possible. For an average motion of the user, this angle corresponds to 20 °. The exoskeleton should support the lifting and squatting movements, therefore the clutch needs to successfully engage at the beginning of these movements. In contrast to this, the clutch should be disengaged for the standing, walking and sitting tasks to allow free movement to the user. The results of this evaluation are presented based on the binary state of the exoskeleton's clutch. A true positive result (TP) is considered a successfully engaged clutch for lifting and squatting movements. A true negative result (TN) is considered a disengaged clutch for standing, walking and sitting movements.

2.3 Results

The results sections is presented in two parts. First we present the results of the leave-one-out cross validation procedure with the first 6 subjects and then we present the results when testing the proposed approach with one subject.

2.3.1 Leave-one-out cross validation

2.3.1.1 Task recognition

The average size of the data samples for training the GMM model was 223056 ± 6068 samples, while the testing dataset on average consisted of 44611 ± 6068 samples. Using GMM+S, the overall recognition accuracy of all 5 tasks (standing, walking, squatting, lifting, sitting) for all input data samples was 79.32 ± 2.14 % (mean ± s.d.). The average sensitivities across 6 subjects for standing, walking, squatting, lifting and sitting were 92.50 ± 4.92 %, 90.63 ± 2.97 %, 60.07 ± 29.96 %, 88.45 ± 7.94 %, 64.16 ± 5.42 %, respectively. Whereas the specificities were: 76.33 ± 3.15 %, 75.37 ± 2.43 %, 83.88 ± 5.49 %, 86.69 ± 3.96 %, 74.47 ± 3.77 %. However, in our case, it is more important to look at results of support ON vs support OFF classification. For this binary case of support ON/OFF, the overall classification accuracy for all input data samples was 87.50 ± 0.95 % and the sensitivity and specificity were 95.77 ± 2.15 % and 84.77 ± 1.32 % respectively. The results of the performance metrics of accuracy over normalized trajectories are presented in Figure 2.5. We can observe that there is a very high accuracy for both cases (GMM and GMM+S) in the middle of the movement (at 0.5 of the normalized time). The GMM only (black error bars) shows a higher accuracy of recognition at an earlier stage of the movement (Accuracy $>$ 90 % at normalized time 0.3).

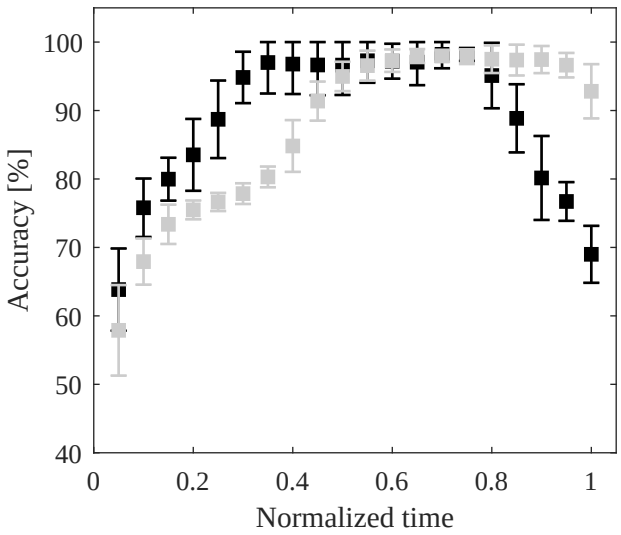

Figure 2.5: Mean and standard deviation of accuracy over the course of the performed movement for ON/OFF classification. Using only the maximum GMM probability (black) and using GMM+S (grey).

Sensitivity and specificity for ON/OFF classification are presented in Figure 2.6a and Figure 2.6b. Here we can observe, that using GMM only we obtain higher specificity of classification in the first half of the performed movements. This indicates a higher success rate of classifying support OFF when no support is required. However, the sensitivity

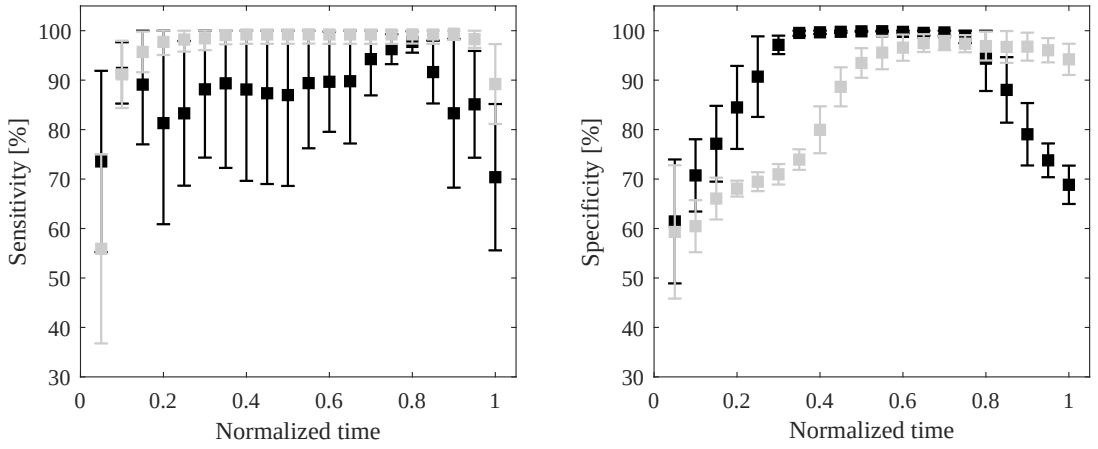

(a) Sensitivity (b) Specificity

Figure 2.6: Mean and standard deviation of sensitivity (a) and specificity (b) over the course of the performed movement for ON/OFF classification. Using only the maximum GMM probability (black) and using GMM+S (grey).

of classification using GMM only is lower, with a higher standard deviation, compared to using the combinations of GMM with the state machine (GMM+S). This means that, using the approach of GMM+S, we can reduce the number of misclassified movements when the support of the exoskeleton is required.

2.3.1.2 Support activation

An example of the control outputs of the controller is presented in Figure 2.7.

Lift and squat movements, when the support of the exoskeleton is required, are highlighted with shaded grey areas. The rest of the data represents sitting, standing and walking. In this example, all the movements requiring support were correctly classified and the support was provided successfully, which is denoted with a green highlight. Both sitting tasks are initially misclassified and are therefore highlighted in red. The results of support activation for all movements and for all subjects are presented in the form of a confusion matrix in Table 2.1. Accuracy of support activation was 86.35 ± 1.00 % (mean $\pm$ s.d.)). The sensitivity and specificity of support activation were 96.15 ± 3.89 % and 83.10 ± 0.92 % respectively. The specificity is reduced, due to the many sitting tasks being supported in the early part of the movement as can be seen in the example presented in Figure 2.7, highlighted in red. However, it is important to note that 93.05 ± 4.95 % of sitting tasks were correctly classified in the middle of the movement.

Table 2.1: Confusion matrix (mean $\pm$ s.d.) for support activation of exoskeleton.

		Required condition	
		Support ON	Support OFF
Output	Support ON	96.15 ± 3.89	16.90 ± 0.92
	Support OFF	3.85 ± 3.89	83.10 ± 0.92

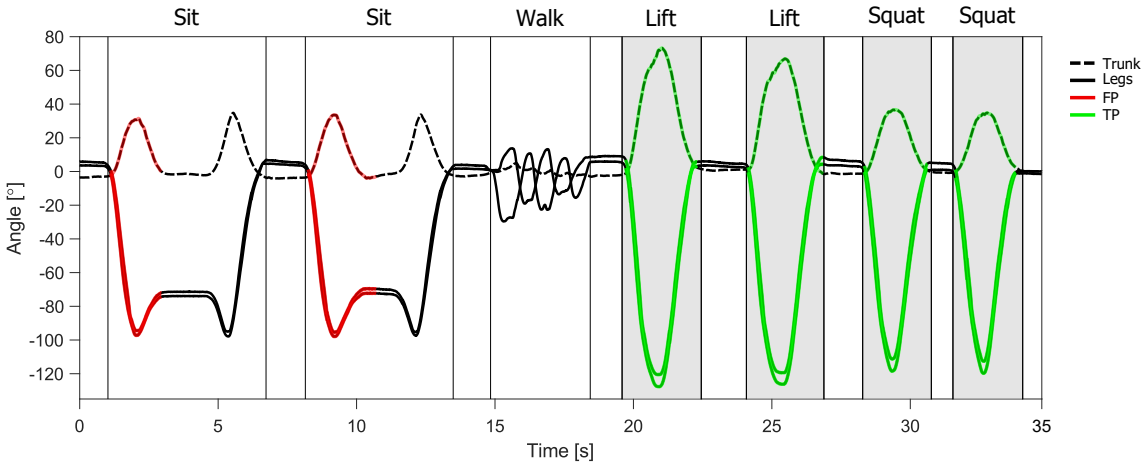

Figure 2.7: Example of control output for the support of the quasi-passive spinal exoskeleton. Shaded grey areas indicate when the support needs to be active. Highlighted trajectories represent the real-time output of the controller for support ON state. True positive (TP) activation of the support is denoted in green, False positive (FP) activation is denoted in red. Graph labels for the sections of standing are omitted for clarity.

2.3.2 Test subject

The training dataset for the test subject consisted of data from 6 subjects equating to 267668 samples of data. The testing dataset of subject 7 consisted in total of 46237 samples of data.

2.3.2.1 Task recognition

Using GMM+S, the overall recognition accuracy of all 5 tasks (standing, walking, squatting, lifting, sitting) for all input data samples was 84.49%. The sensitivity for standing, walking, squatting, lifting and sitting were 98.56 %, 93.90 %, 79.56 %, 90.49 %, 63.60 % respectively. Whereas the specificities were: 83.83 %, 81.40 %, 87.71 %, 88.15 %, 81.05 %. For the binary case of support ON/OFF, the overall classification accuracy for all input data samples of the test subject was 88.60 % and the sensitivity and specificity were 91.37 % and 87.69 % respectively. The results of the performance metrics of accuracy over normalized trajectories are presented in Figure 2.8. Sensitivity and specificity for ON/OFF classification are presented in Figure 2.9a and Figure 2.9b. Similar to the results during validation we can observe the slightly increased sensitivity while using the GMM+S versus using only the GMM probability outputs.

2.3.2.2 Support activation

The results of support activation for all movements for the test subject are presented in the form of a confusion matrix in Table 2.1. Accuracy of support activation for the test subject was 87.65 %. The sensitivity and specificity of support activation were 100 % and 83.47 % respectively. As during the validation we observe that the specificity is reduced, due to the many sitting tasks being supported in the early part of the movement just as in the example presented in Figure 2.7, highlighted in red. Likewise however, 90.00 % of sitting tasks were correctly classified in the middle of the movement for the test subject.

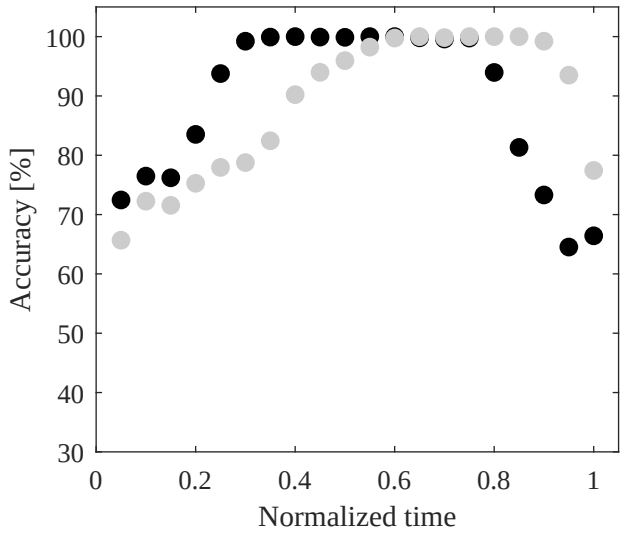

Figure 2.8: Accuracy over the course of the performed movement for ON/OFF classification for the test subject. Using only the maximum GMM probability (black) and using GMM+S (grey).

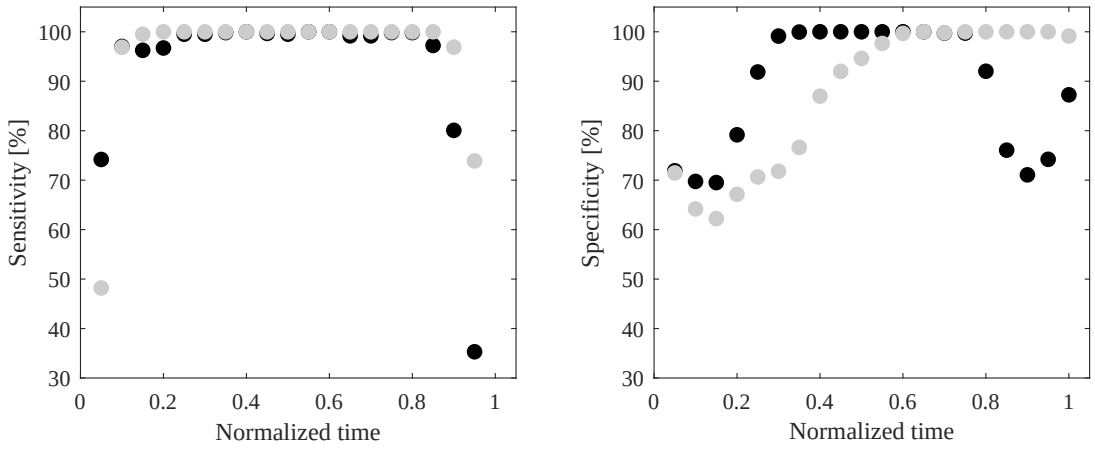

(a) Sensitivity

(b) Specificity

Figure 2.9: Sensitivity (a) and specificity (b) over the course of the performed movement for ON/OFF classification for the test subject. Using only the maximum GMM probability (black) and using GMM+S (grey).

2.4 Discussion

We described our approach of using probability outputs of a GMM in combination with a state machine to generate control signals in real-time for a quasi-passive spinal exoskeleton device. The inputs to the controller were limited only to the sensors embedded in the device. With this approach we achieved a very high accuracy of task recognition in the middle of the movement, when the support to the user is most critical for lifting movements. These results indicate that our approach would also be suitable for active exoskeletons, where

Table 2.2: Confusion matrix for support activation of exoskeleton for the test subject.

		Required condition	
		Support ON	Support OFF
Output	Support ON	100	16.53
	Support OFF	0	83.47

this method could be used to select different types of support profiles for various lifting techniques. Additionally, based on the type of lifting technique and an a priori knowledge of joint loading for each movement, the exoskeleton could prevent human joint overloading, while still enable a seamless execution of the task [83].

Using the state machine we complemented the versatility of GMM by controlling transitions between states during downward motion. With this, we achieved very good results during the leave-one-out cross validation with a sensitivity of support activation of 96.15 ± 3.89 %. The specificity of support activation was only 83.15 ± 0.85 %, which is mainly due to the many sitting tasks being initially misclassified. Similar results of support activation were also present for the test subject with a sensitivity for support activation of 100 % and specificity of 83.5%. Due to the similarity between a lifting and sitting movement at the beginning of the motion (Figure 2.3), it is difficult to disengage the support for sitting without compromising support for lifting. In this case, a more feasible solution would be the use of a different clutch mechanism that can be disengaged under load. Nevertheless, classification errors are inevitable and can greatly compromise the comfort or safety of the wearable device. Striving for reducing these errors is important, but equally so is the implementation of additional safety measures that prevent injuries or discomfort even in the unlikely event of misclassified user movements or intentions.

The protocol used for determining the ground truth required to learn the GMM, could be easily integrated in the wearable device itself, requiring user input for movement type along with the start and end of movement. In our approach, the absolute values of GMM probability were used only to limit transitions in case of uncertainty (low $m_j(x)$ values). However, this information could also be used to detect movements new to the model or give feedback to the user, prompting an update of the learned model. Another possible extension could be to look at the repetitions of the same movement in order to influence future predictions.

Even though much of the recent technological advances in spinal exoskeleton control are focused on active devices [84], we believe that the emerging passive and quasi-passive versions are equally important. The many benefits of passive devices are often limited by their poor versatility or the discomfort imparted to the users for performing some tasks [85]. Therefore the development of hybrid style devices along with adequate control is very important in order to advance the field of spinal wearable devices. Despite some limitations of this study, we believe our approach proved to be a promising tool for control of quasi-passive spinal exoskeletons and thus provides a meaningful contribution to the state of the art.

Chapter 3

Foot Placement Prediction in Real-Time Using Probabilistic Movement Primitives

3.1 Introduction

Falls and injuries associated with falls are very common among people, especially the elderly [86]. This is becoming an ever increasing problem, due to the continued population ageing in developed parts of the world [87]. To prevent these individuals from fall-related injuries there are already some systems which can protect the user after a fall is detected in the form of an airbag [88]. However, with the increase in development of exoskeleton systems for assisting users [89], another suitable approach would be to implement fall prevention strategies, that could reduce the probability of a fall even occurring. This may be ambitious, but for some scenarios it could certainly be implemented by predicting user foot placements in real-time and employing a warning or possibly some active manoeuvres with the exoskeleton e.g. shortening or lengthening the step length to reposition the foot.

The first prerequisite for such a system is the ability to gather positional data of the user. The gold standard for measuring human kinematics are camera-based systems that precisely track movement in 3D space. However, these systems are usually only limited to use in laboratories or rehabilitation facilities. Alternatively, there are other commercial systems which use inertial based sensors to reconstruct the kinematic data of human subjects. These systems have been extensively used and evaluated in a multitude of gait analysis studies. An extensive review based on 82 papers concluded that the validity and reliability of step and stride length using IMU systems were found to be good to excellent [90]. While these systems have some limitations, they are still very reliable and provide accurate kinematic data that can be gathered outside of the laboratory or even easily implemented in wearable robotic devices [91].

One of the most important aspects of the human gait is stability. This has been investigated in many studies which are nicely summarised in the work of Bruijn et.al [92]. In its essence however, the stability of the human gait is primarily a game between the location of the centre of mass (CoM) and the position of the feet i.e. the base of support (BoS). Many models to describe human gait were derived from the simple idea of the inverted pendulum [93]–[95]. While these models can be very accurate at predicting user foot placement, their underlying assumption is that the human is able to perform these movements. With elderly individuals however, these assumptions may not be valid and alternative models could be more appropriate for estimating future feet positions. Some studies have looked at the possibility of predicting user foot placement from the

subject's gaze [96] or using kinematic data of the foot in 3D space [97], [98]. However the research in this field is very sparse. We have previously successfully implemented probabilistic movement primitives (ProMPs), for predicting user movement intention for arm movements [99]. In this chapter, we present an alternative use case of ProMPs for predicting foot placement in real time at the beginning of the swing phase. We evaluate whether we can accurately predict the step length for steady state walking at a constant speed on a treadmill.

3.2 Methods

Twelve healthy young adults (4 women and 8 men, age 28.5 ± 4.8 years (mean ± SD); height 178.9 ± 11.2 cm; weight 71.8 ± 14.2 kg) participated in the study. The study was carried out in accordance with the recommendations of the Slovenian National Medical Ethics Committee (No. 0120- 339/2017/7) and all subjects gave written informed consent for participation.

3.2.1 Experimental setup

The experiment was caried out using a custom made wide belt treamill (dimensions of 2.00 x 1.2 m) driven by a servo motor (EMMS-AS-140-S-RM, Festo, Esslingen, Germany) controlled via CAN-bus network with an in house developed Simulink Real-Time control interface. The motor has a built in encoder which is used to precisely monitor the rotational velocity of the motor. By multiplying the motor speed on the output shaft of the motor with the gear reduction and the radius of the treadmill driving roller, we can calculate the velocity of the treadmill. This is however susceptible to measurement error. Therefore, to ensure the validity of the controlled speed of our treadmill, a standardised treadmill calibration procedure was carried out which is presented in detail in the work of Padulo et. al. [100]. The speed of our treadmill was calibrated by first measuring the length of the treadmill belt (4.19 m). After measuring the belt length, the treadmill was set to a speed of 1 $ms^{-}1$. We then proceeded to time 20 revolutions of the treadmill belt with a stopwatch and calculated the actual velocity of the treadmill belt. The difference in the calculated and measured treadmill velocity was used as a correction factor for the control input to the treadmill motor. We then proceeded to time 20 revolutions of the treadmill belt with a stopwatch to calculate the actual velocity. We determined the final accuracy of the treadmill velocity at 0.08 $ms^{-}1$. The speed of the treadmill was verified also with a subject (weight: 80 kg) walking on the treadmill with no significant deviation from the set velocity.

3.2.2 Protocol

To collect user kinematic data in this study we used the Xsens Awinda system (Xsens, Enschede, Netherlands). Before the start of the recording, the Xsens system was calibrated and aligned, so that the forward direction of the system (X direction) matched the forward direction of the treadmill. To compensate for any small misalignments between the model and the treadmill, the orientation of the pelvis segment was used to rotate all data points about the vertical axis. To determine their preferred walking speed (PWS) during the familiarization trial, the subjects used a keyboard to increase and decrease the speed of the treadmill until they found a setting they deemed suitable. This speed was then saved and used in the experimental trials. The subjects then walked on a treadmill at their preferred walking speed (PWS), 30% slower (SWS), and 30% faster (FWS) in the following sequence of trials (PWS → SWS → FWS → PWS → SWS → FWS). In the scope of this work, we

analysed only the first trial at the preferred walking speed (PWS). The first half of the data was used for training the ProMp model, whereas the second half of the data was used for testing.

3.2.3 Step segmentation

We used the inter-malleolar point located midway between the lateral and medial malleoli [101] for detecting heel strike events as in [31]. Heel-strikes (HS) were detected as the local maxima of the anterior-posterior (AP) position of the inter-malleolar point. Conversely, the toe-off (TO) events were detected as the local minima of the AP position of the inter-malleolar point. The general shape of the segmented trajectories is presented in figure 3.1 where we show an example set of trajectories for one leg of one subject.

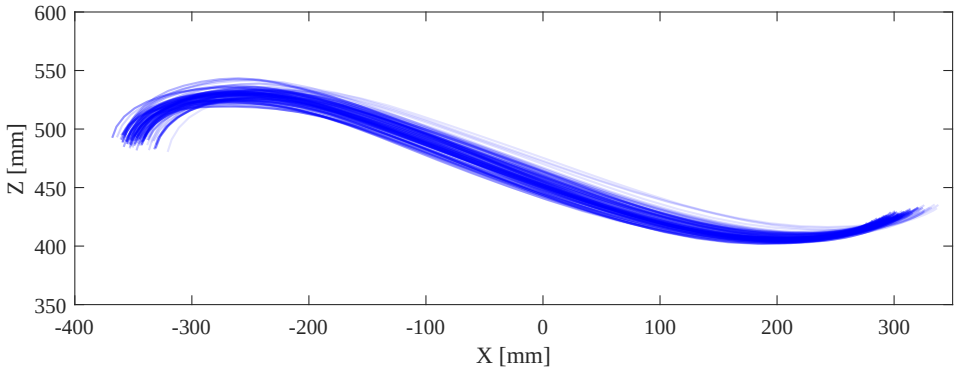

Figure 3.1: Example set of trajectories from one subject in the sagittal plane.

3.2.4 Probabilistic model for prediction

In this section we present the framework of the probabilistic movement primitives, i.e. how the trajectories are encoded, how the model is generated and how the future predictions are computed from the observed data points.

3.2.4.1 Encoding trajectories

Let $\boldsymbol{\phi}_t \in \mathbf{R}^{1\times J}$ denote a basis function vector containing values of J basis functions at time t: $\boldsymbol{\phi}_t = \begin{bmatrix}\phi_{1,t} & \phi_{2,t} & \cdots & \phi_{J,t}\end{bmatrix}$. The variable $\boldsymbol{w}' \in \mathbf{R}^{J\times 1}$ represents a J-dimensional feature vector that encodes weights for each of the J basis functions. We can extend this formulation and define a diagonal matrix $\boldsymbol{\Phi}_t$ as

$$\boldsymbol{\Phi}_t = diag(\boldsymbol{\phi}_t,\ \dot{\boldsymbol{\phi}}_t) = \begin{bmatrix}\boldsymbol{\phi}_t & 0\\ 0 & \dot{\boldsymbol{\phi}}_t\end{bmatrix} \tag{3.1}$$

that includes the basis functions and their derivatives. The weight vector gets extended to a vector $\boldsymbol{w} = [\boldsymbol{w}'_{pos}, \boldsymbol{w}'_{vel}]$ that includes the weights for the basis functions and for the derivatives of the basis functions. With this notation, an observation in time $\boldsymbol{y}_t = [x_t, \dot{x}_t]^T$ which represents the position and velocity in one dimension at time t, can be approximated as

$$\boldsymbol{y}_t = \begin{bmatrix}x_t\\ \dot{x}_t\end{bmatrix} = \boldsymbol{\Phi}_t \boldsymbol{w} \tag{3.2}$$

This can be further extended to multi-dimensional states. Assuming that our variable $\boldsymbol{y}_t$ now has D dimensions $\boldsymbol{y}_t = \begin{bmatrix} y_{1,t} & \cdots & y_{D,t} \end{bmatrix}^T$, the basis function matrix $\boldsymbol{\Phi}_t$ extends to a block diagonal matrix $\boldsymbol{\Psi}_t \in \mathbf{R}^{D \times JD}$ and the weight vector $\boldsymbol{w}$ becomes a concatenation of the weight vectors of each dimension $\boldsymbol{w} \in \mathbf{R}^{JD \times 1}$. Variable $\boldsymbol{y}_t$ is now approximated as

$$\boldsymbol{y}_t = \boldsymbol{\Psi}_t \boldsymbol{w} = \begin{bmatrix} \boldsymbol{\Phi}_t & \cdots & 0 \\ \vdots & \ddots & \vdots \\ 0 & \cdots & \boldsymbol{\Phi}_t \end{bmatrix} \begin{bmatrix} \boldsymbol{w}_1 & \cdots & \boldsymbol{w}_D \end{bmatrix}^T, \tag{3.3}$$

Using this formulation we can approximate a sequence of T states denoted by $\boldsymbol{\tau} = \boldsymbol{y}_{1:T}$, where

$$\boldsymbol{\tau} = \boldsymbol{\Psi}_{1:T} \boldsymbol{w} \tag{3.4}$$

with

$$\boldsymbol{\Psi}_{1:T} = \begin{bmatrix} \boldsymbol{\Psi}_1 & \cdots & \boldsymbol{\Psi}_t & \cdots & \boldsymbol{\Psi}_T \end{bmatrix}^T \in \mathbf{R}^{TD \times JD}. \tag{3.5}$$

The basis functions used in this work were Gaussian basis functions which are often used for point-to-point movements.

To approximate the trajectories in the previously described manner, the weights for each trajectory need to be calculated. For the i-th trajectory τ_i, the corresponding weight vector $\boldsymbol{w}_i$ can be estimated using a simple least squares estimate. In our case, we used the least squares method

$$\boldsymbol{w}_i = \left(\boldsymbol{\Psi}_{1:T}^T \boldsymbol{\Psi}_{1:T} + \lambda \boldsymbol{I} \right)^{-1} \boldsymbol{\Psi}_{1:t}^T \tau_i, \tag{3.6}$$

where λ represents a regularization parameter used to avoid numerical singularities. Its value should be small, in our case we used $\lambda = 10^{-12}$.

3.2.4.2 Creating the probabilistic model

When the weight vectors of all trajectories are calculated, we assume their values to be normally distributed, *i.e.*, $p(\boldsymbol{w}) = \mathcal{N}(\boldsymbol{w} | \boldsymbol{\mu}_w, \boldsymbol{\Sigma}_w)$. The mean $\boldsymbol{\mu}_w$ and the covariance matrix $\boldsymbol{\Sigma}_w$ can be estimated with sample mean and sample covariance of the $\boldsymbol{w}_i$ vectors.

With the function approximation (3.4) and the weight vectors $\boldsymbol{w}_i$ defined, we can define a probabilistic model for trajectories as

$$p(\tau | \boldsymbol{w}) = \prod_{t=1}^{T} \mathcal{N}(\boldsymbol{y}_t | \boldsymbol{\Psi}_t \boldsymbol{w}, \boldsymbol{\Sigma}_y) = \mathcal{N}(\boldsymbol{y}_{1:t} | \boldsymbol{\Psi}_{1:T} \boldsymbol{w}, \boldsymbol{\Sigma}_y). \tag{3.7}$$

This model describes the probability of observing a trajectory $\boldsymbol{\tau}$ given the weight vector $\boldsymbol{w}$, that is given as a linear basis function $\boldsymbol{y}_{1:t} = \boldsymbol{\Psi}_{1:T} \boldsymbol{w} + \epsilon_{y,1:T}$. The parameter $\boldsymbol{\Sigma}_y$ represents independent and identically distributed (*i.i.d.*) Gaussian noise in the trajectories $\boldsymbol{y}_t = \boldsymbol{\Psi}_t \boldsymbol{w} + \epsilon_y$, where $\epsilon_y \sim \mathcal{N}(\epsilon_y | 0, \boldsymbol{\Sigma}_y)$.

3.2.4.3 Computing Predictions from Observations

We can model predictions from observations by computing the conditional probability. First, we need to define the probability distribution over the trajectories τ, which can be computed by marginalizing out the weight vector w. In the case of a Gaussian distribution the marginal can be computed in closed form as

$$p(\boldsymbol{\tau}) = \int p(\boldsymbol{\tau} | \boldsymbol{w}) p(\boldsymbol{w}) d\boldsymbol{w} \tag{3.8}$$

$$= \int \mathcal{N}(\boldsymbol{y}_{1:T}|\boldsymbol{\Psi}_{1:T}\boldsymbol{w}, \boldsymbol{\Sigma}_y)\mathcal{N}(\boldsymbol{w}|\boldsymbol{\mu}_w, \boldsymbol{\Sigma}_w)d\boldsymbol{w} \tag{3.9}$$

$$= \mathcal{N}(\boldsymbol{y}_{1:t}|\boldsymbol{\Psi}_{1:T}\boldsymbol{w}, \boldsymbol{\Psi}_{1:T}\boldsymbol{\Sigma}_w\boldsymbol{\Psi}_{1:T}^T + \boldsymbol{\Sigma}_y). \tag{3.10}$$

What we get is a multivariate Gaussian distribution, the conditional probability of which we can compute in closed form.

When we receive a new point y^*, we can predict the most likely path of the foot (parametrized through $\overline{\boldsymbol{\mu}^*}$ and $\overline{\boldsymbol{\Sigma}^*}$) by conditioning the observed state over the weight vectors. Say that we observed a sequence of states y_{t1} to y_{tM} at m=1, 2,..., M-different time points. We declare $\boldsymbol{\nu}$ as a concatenation of the observed states $\boldsymbol{y}_{tm}$ and $\boldsymbol{\Psi}_\nu$ as the concatenation of the basis function matrices for the observed time points.

With the observed trajectories encoded as previously described, we can obtain a conditioned distribution $p(\boldsymbol{w}_\nu|\boldsymbol{\nu})$ over the weight vectors $\boldsymbol{w}$ as

$$p(\boldsymbol{w}_\nu|\boldsymbol{\nu}) \propto \mathcal{N}(\boldsymbol{\nu}|\boldsymbol{\Psi}_\nu\boldsymbol{w}_\nu, \boldsymbol{\Sigma}_0)p(\boldsymbol{w}) \tag{3.11}$$

$$:= \mathcal{N}(\boldsymbol{w}_\nu|\boldsymbol{\mu}_{w|\boldsymbol{\nu}}, \boldsymbol{\Sigma}_{w|\nu}). \tag{3.12}$$

We can compute the mean $\boldsymbol{\mu}_{w|\nu}$ and the covariance matrix $\boldsymbol{\Sigma}_{w|\nu}$ as

$$\boldsymbol{\mu}_{w|\boldsymbol{\nu}} = \boldsymbol{\mu}_w + \boldsymbol{\Sigma}_w\boldsymbol{\Psi}_\nu^T\boldsymbol{L}(\boldsymbol{\nu} - \boldsymbol{\Psi}_\nu\boldsymbol{\mu}_w) \tag{3.13}$$

and

$$\boldsymbol{\Sigma}_{w|\nu} = \boldsymbol{\Sigma}_w - \boldsymbol{\Sigma}_w\boldsymbol{\Psi}_{\boldsymbol{\nu}}^T\boldsymbol{L}\boldsymbol{\Psi}_\nu\boldsymbol{\Sigma}_w, \tag{3.14}$$

where

$$\boldsymbol{L} = \left(\boldsymbol{\Sigma}_0 + \boldsymbol{\Psi}_\nu\boldsymbol{\Sigma}_w\boldsymbol{\Psi}_\nu^T\right)^{-1}. \tag{3.15}$$

With the feature mean $\boldsymbol{\mu}_{w|\nu}$ and covariance matrix $\boldsymbol{\Sigma}_{w|\nu}$ obtained, we can now use this conditional distribution to calculate the distribution over the trajectories $p(\overline{\boldsymbol{\tau}})$ using (3.10)

$$p(\overline{\boldsymbol{\tau}}) = \mathcal{N}(\tilde{\boldsymbol{y}}_{1:T}|\boldsymbol{\Psi}_{1:T}\boldsymbol{\mu}_{w|\nu}, \boldsymbol{\Psi}_{1:T}\boldsymbol{\Sigma}_{w|\nu}\boldsymbol{\Psi}_{1:T}^T + \boldsymbol{\Sigma}_y), \tag{3.16}$$

where the predicted sequence of states $\tilde{\boldsymbol{y}}_{1:T}$ is represented by the product $\boldsymbol{\Psi}_{1:T}\boldsymbol{\mu}_{w|\nu}$.

3.2.5 Data acquisition and analysis

The encoding and model generation was performed based on the first half of the recorded data for each subject. The step segmentation, conditioning of new data, and generation of predictions was implemented in Simulink (Mathworks, Natick, MA, United States). New data about the foot positions was streamed over UDP in real time from the MVN Analyze (Xsens, Enschede, Netherlands) software to the Simulink model calculating the predictions. The analysis of data was performed in Matlab (Mathworks, Natick, MA, United States). We limited the analysis of the data to the sagittal plane, since this is the plane where the kinematic data from the Xsens system is the most accurate [102].

3.3 Results

The average number of steps during the PWS trial was 156.9 with a standard deviation of 13.4 steps. The mean and standard deviation of step lengths for each subject are presented in figure 3.2. We can observe different average step lengths for each subject as well as different levels of variations of steps during the trial. The average step length was 678.9 mm, while the average standard deviation of step length was 15.9 mm.

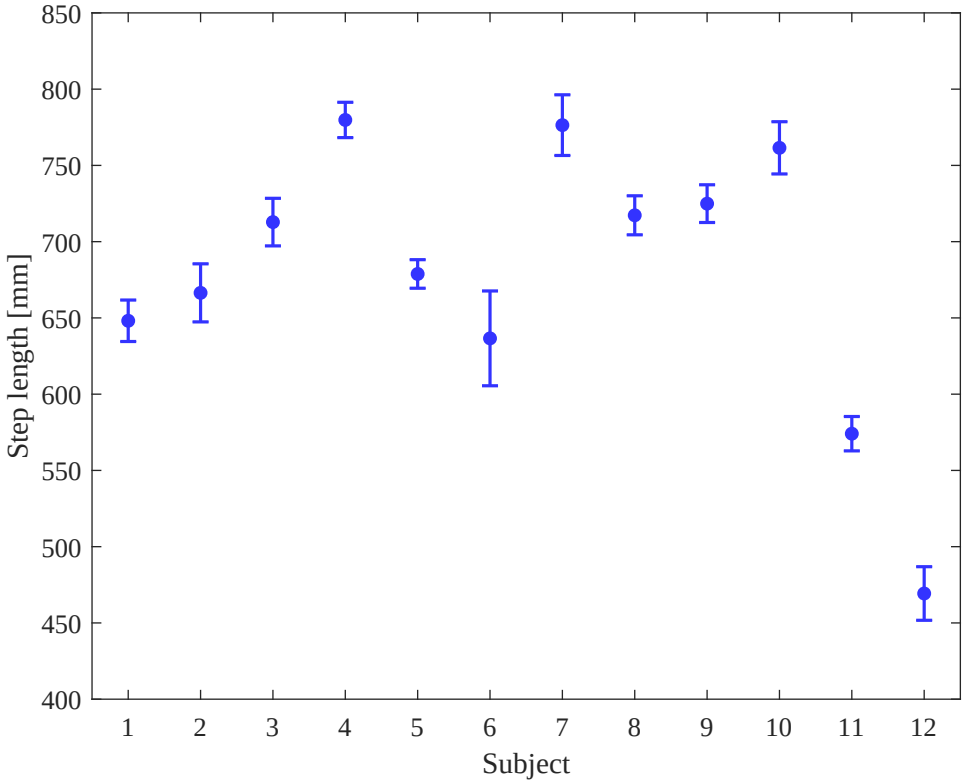

Figure 3.2: Mean and SD of step lengths for each subject.

Figure 3.3 shows an example prediction of the foot position in the AP direction at different times after movement onset.

The error of prediction of the step length for all subjects is presented in figure 3.4. The mean and standard deviation of the error of prediction was 7.9 ± 3.3, 8.6 ± 3.5 and 10.0 ± 3.7 mm for the 100, 150 and 200 ms observation windows respectively. The one sample t-test showed that the error of prediction is significantly lower than the standard deviation of the step length for all observation windows ($p < 0.001$). A paired t-test revealed that there is no significant difference between the three observation windows ($p < 0.001$).

To further evaluate the predictions of the model we looked at how the predicted trajectory differs from the actual trajectory over the whole movement. For each of the predicted trajectories we calculated the error from the actual trajectory (both normalized to the movement phase) for all data points and calculated the root mean squared error to have one single measure for each step. The root mean squared error of the predicted trajectories with the ProMps for all subjects is presented in Figure 3.5 in the form of boxplots of the mean RMSE of each subject. The mean and standard deviation of the RMSE was 14.8 ± 6.6, 14.5 ± 5.5 and 14.6 ± 6.0 mm for the 100, 150 and 200 ms observation windows respectively. A paired t-test revealed that there is no significant difference between the three observation windows ($p < 0.001$).

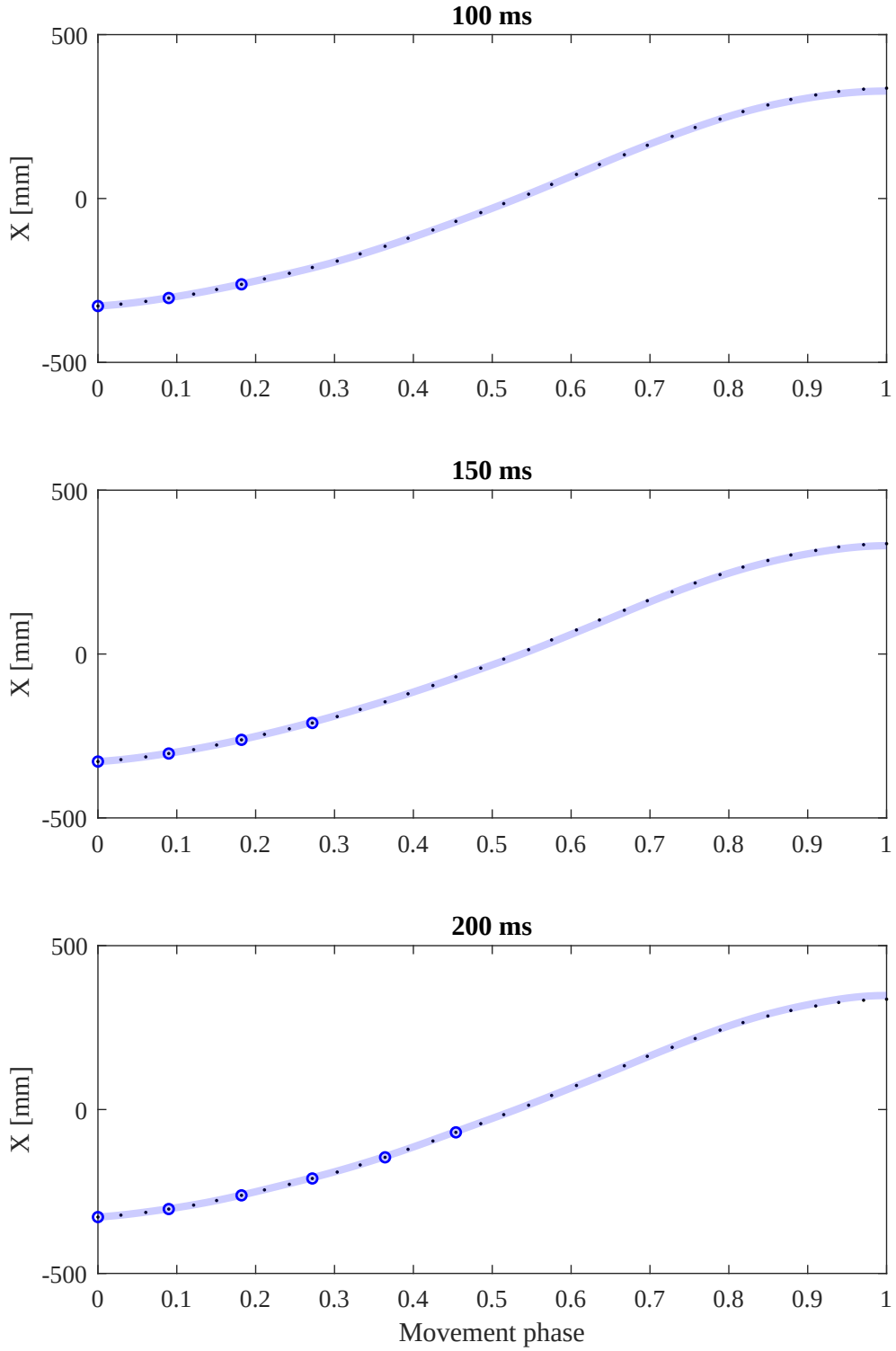

Figure 3.3: Example of a foot trajectory (black dots), observations used for making the prediction (blue circles), and the predicted trajectory (blue line) at 100, 150 and 200 ms after movement onset.

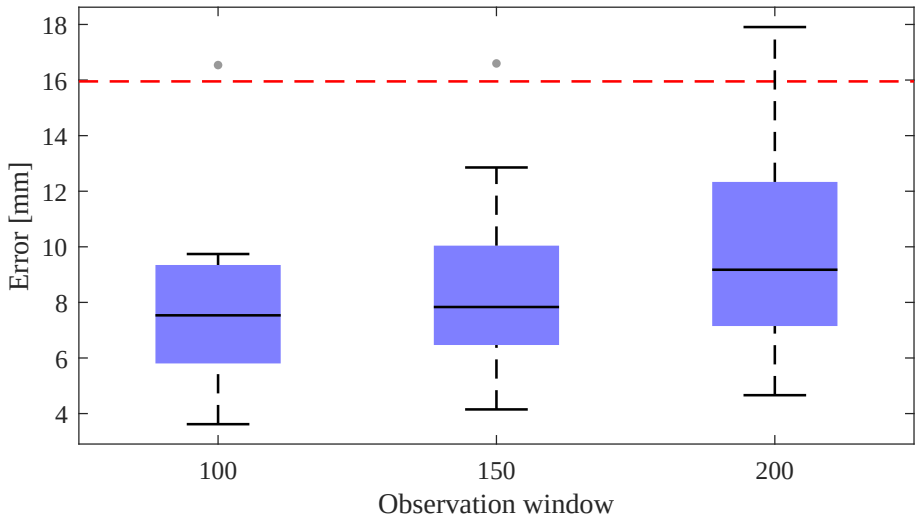

Figure 3.4: Boxplots of the mean error of all subjects of the predicted step length at different percentages of the swing phase. The red dashed line represents the average standard deviation of step length for all subjects.

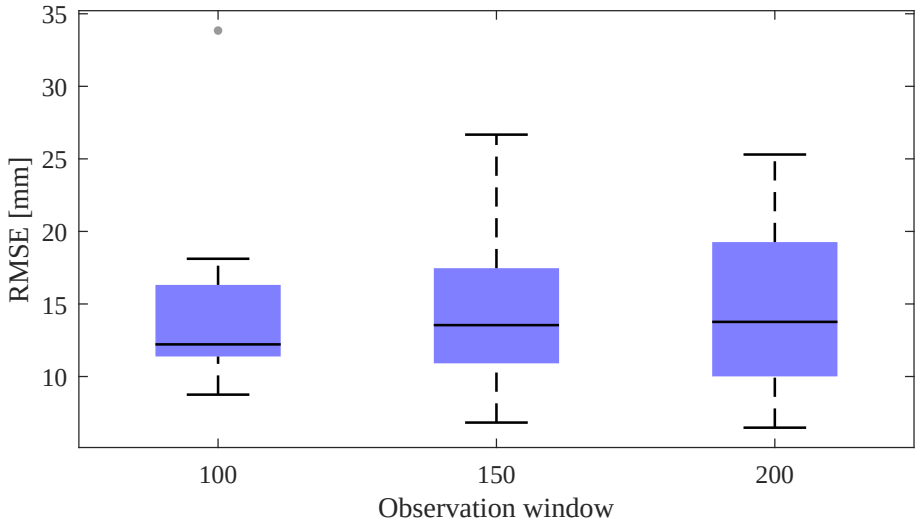

Figure 3.5: RMSE of the predicted trajectory at different percentages of the swing phase.

3.4 Discussion

Since the experiment consisted of steady state walking at a constant speed, the variation in step length is small for all subjects. Nevertheless, as we can observe from figure 3.4, the error of prediction was significantly lower than the standard deviation of the step lengths for the subjects. This is a very encouraging result for the use of ProMPs for predicting user foot placement. A similar study looked at the accuracy of prediction of foot placements with different machine learning regression algorithms [103] where they were able to predict the foot placement with an average error of 35 mm and a RMSE of 44 mm. In their experiment the protocol was slightly different where they had more variation in the step

length of the subjects.

In our case, the accuracy of prediction is very high already from the first few samples of observation (after 100 ms Figure 3.3). This was slightly unexpected as we did not anticipate such high accuracy until observing at least half of the trajectory. However, since the kinematic data of the foot position is relative to the pelvis location, the first data point is already somewhat dependent on the position of the COM of the subject. This is probably why there is already an inherent correlation between the initial foot position in the swing phase and the final leg position.

Another part of the reason for the error not decreasing over a prolonged observation window is due to not having a perfect alignment of the new data with the phase of the generated model. In order to improve our predictions over increased observations windows, we would need to implement a robust phase estimation algorithm such as that proposed by Ewerton et.al. [104] or possibly try to find additional features in the gait cycle that could help with the model alignment. This means that maybe we should also include data from the stance phase of the foot in order to have more data available for phase alignment during the early parts of the swing phase.

One of the limitations of our study was that we did not directly evaluate the global accuracy of the kinematic data of the Xsens system with an external optical system. However, due to the given complexity of aligning both system's kinematic models [102], [105], [106] such an evaluation is not a straightforward task. Therefore, this analysis was omitted from the study and we relied on the data from the Xsens system as our ground truth data which was shown to be very accurate especially in the sagittal plane [90].

3.5 Conclusion

Given constant technological advancements and the current state of art which already provides impressive results, we believe that inertial measurement based systems will provide even more accurate position estimations of foot placement in the near future. This would allow our proposed approach to be integrated to predict foot placement not only in the sagittal plane but also for media-lateral foot placement. In combination with systems monitoring the surrounding environment this could then be exploited to generate either warning signals for more able bodied individuals or initiate some gait correction strategies with an exoskeleton, e.g. lowering or lifting the foot prematurely, to prevent hitting an obstacle with the foot during swing phase. One of the limitations of this study is that we did not take into account more pronounced variations in the step length as well as analyse the predictions under different gait speeds. Based on the initial results presented in this study, we conclude that we would first need to implement a robust phase estimation algorithm to be able to better align the new observations of real data with the generated models. We will tackle this issue in future work.

Additionally we would like to further explore the possibilities of combining our approach for foot placement prediction with other foot placement estimation algorithms based on COM measurements and identifying the discrepancies between the prediction and estimation. This could then be used to determine mid swing whether the foot trajectory will be satisfactory or not.

Some additional use-cases of our proposed real-time foot placement prediction would be for rehabilitation and training procedures, where subjects are walking on a treadmill over virtual stepping stones. Such a system could integrate and predict the future placement of the foot and depending on the outcome, it could provide the user with an audio, visual, or haptic stimulus in the middle of the swing phase in order to promote correct/healthy foot placement.

Chapter 4

Predictive Exoskeleton Control for Arm-Motion Augmentation Based on Probabilistic Movement Primitives Combined with a Flow Controller

4.1 Introduction

Robotic exoskeletons are promising tools to assist humans in various real-life tasks [1]. They are designed to be worn on the body and to provide direct motion assistance to the user. The two common applications of exoskeletons are physical rehabilitation for impaired patients [2] and motion augmentation of able-bodied workers [4]. In physical rehabilitation, the exoskeleton is used to move the limbs of impaired individuals based on repetitive motion patterns defined by physiotherapists [107], while for able-bodied workers the exoskeleton rather amplifies the user's joint torques [66]. Popular control approaches for these exoskeletons are usually position or angle based for rehabilitation purposes or impedance/admittance based for movement augmentation [16], [17]. However, such control approaches lack the intention recognition needed for a successful human-robot interaction [108]. Since movement intention and prediction is a very complex problem, it is usually addressed by monitoring muscle or brain activity. Although they can be successful, such control architectures have greater complexity and are more invasive for the subject wearing the device [17].

Nevertheless, there are many work related repetitive tasks where an exoskeleton could significantly reduce the physical effort of users, such as manual object manipulation on assembly lines or in logistic centers [66]. In general, motion prediction is a very ambitious goal without the use of more invasive sensing technologies, but for the above mentioned repetitive tasks, prediction can be achieved using modern probabilistic trajectory representation.

Movement predictions using movement primitives: A well-established approach for trajectory representation in robotics is by encoding the trajectory using movement primitives (MPs). There are a number of different versions of MPs such as dynamic movement primitives (DMPs) [41], [42], compliant parametric dynamic movement primitives (CPDMP) [43], Gaussian Mixture Regression (GMR) [109], and probabilistic movement primitives (ProMPs) [110]. In this work, we focused on the use of ProMPs which offer a wide range of properties in one generalized framework [111]. They allow simple learning from demonstration with a low set of parameters needed to represent trajectories. Generalization to

new situations is possible by specifying different end-goals or specific via-points during the execution of the trajectory as well as temporal scaling of the movement. Another important property of ProMPs is the representation of trajectories together with their variance. This allows the controllers to modulate the feedback gains based on the variance of movement and provide high precision only in certain parts of the movement, which was shown to be important for successful human-robot interaction [55], [56]. Finally, ProMPs can be successfully used to make predictions of a trajectory based on the initial samples which was successfully used for real-time prediction of human movement [53].

Exoskeleton control strategies: A viable method to provide assistance along a specified path is to use potential-field-based controllers [39], [40]. However, such control algorithms generate high forces in the event of larger errors with respect to the specified path [38]. To overcome this problem, a velocity-field-based controller was proposed by Martinez et al. [38], which applies corrective torques based on a viscous flow field control law. They showed that this approach could effectively guide movements of the user's leg along a reference path while being less resistive to large path deviations and thus making the controller inherently safer.

In this chapter we investigate whether such a velocity-field-based controller could be adapted to other applications of exoskeletons involving able-bodied humans. Additionally, we explored whether this approach could be further improved by adapting to new movements in a predictive manner. We present the use of ProMPs to generate predictions of user movement in real-time in combination with a velocity-field-based controller to provide assistance to the user for performing an arm reaching task, hereby referred to as *Predictive Assistance*. With this combination we aimed to lower the physical effort of subjects while adapting to their movements. To evaluate our approach, we performed an experimental study where we measured a set of motion-related parameters for a group of 12 participants who had to perform reaching tasks to 4 different targets with and without assistance of a haptic robot. To emphasize the importance of user movement prediction, we additionally compared the *Predictive Assistance* to a *Fixed Assistance* that does not generalize to new unknown targets.

4.2 Methods

First in section 4.2.1 we describe the experimental setup, protocol and evaluation metrics used in this study. Then, in section 4.2.2 we present the methodology for generating a probabilistic model and using it to compute predictions of trajectories based on newly observed data. In 4.2.3 we present the methodology used for creating fixed reference trajectories. The predicted or fixed trajectories are the basis for generating the assistive flow field which we describe in section 4.2.4.

4.2.1 Experimental design

Twelve healthy young adults (4 women and 8 men, age 27.1 ± 4.0 years (mean ± SD); height 176.8 ± 10.1 cm; weight 70.5 ± 13.5 kg) participated in the study. The study was carried out in accordance with the recommendations of the Slovenian National Medical Ethics Committee (No. 0120-339/2017/7) and all subjects gave written informed consent for participation.

4.2.1.1 Setup

Subjects sat on a chair in front of a 50 inch TV screen that was located 2 m in front of the chair. Experiments were performed using a 3 axis haptic manipulator (Haptic master Mk2,

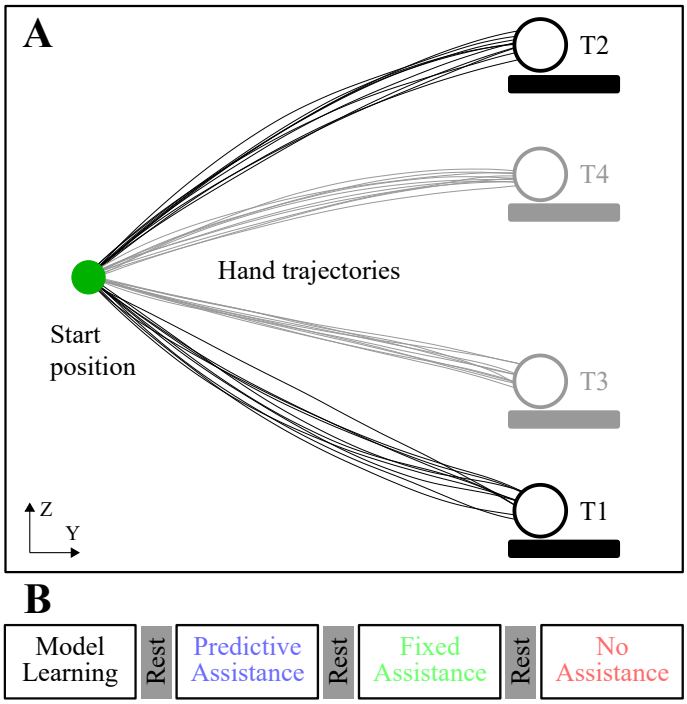

Figure 4.1: Experimental setup **A**. Subjects started their movement from the start position and had to reach one of the targets positioned on the screen while avoiding the obstacles shown as black and grey rectangles. Experimental protocol **B**. Following a series of familiarization trials, subjects performed 20 trials based on which the model was learned. Each subject then performed one block of 40 trials with *Predictive Assistance*, one block with *Fixed Assistance*, and one block with *No Assistance*. The order of blocks with different conditions was randomized. There was a rest period of three minutes in between each series of trials. During the *Familiarization* and *Model Learning* phase, the task included only targets T1 and T2. In all other phases, the task consisted of reaching to all four targets.

MOOG, Nieuw-Vennep, The Netherlands). The subjects were controlling the position of the cursor on screen by holding the end effector of the haptic manipulator. All reaching movements were performed in the frontal plane of the subject from left to right. Interaction force, velocity, and position of the end effector were acquired by the Haptic master with a sampling rate of 200 Hz.

The goal of the experiment was for subjects to successfully reach a target that was placed on a simulated shelf on the screen in front of them. Targets had a diameter of 4 cm and were placed in four different positions as can be seen in Fig. 4.1A. All the reaching movements were towards the right hand side either upward or downward. For reference, the average movement duration was 1.14 ± 0.29 s. Subjects started their movement from a circular (2.5 cm diameter) starting position in the left middle part of the screen. They were instructed to start their movement when the circle indicating the start position was coloured green and aim for the currently highlighted end target.

4.2.1.2 Protocol

The experiment consisted of 5 phases: *Familiarization*, *Model Learning*, *Predictive Assistance*, *Fixed assistance*, *No Assistance*. In the *Familiarization* and *Model Learning* phase, only 2 targets were part of the task (T1 and T2). The *Familiarization* phase consisted of 40 trials (20 per target) and gave the subjects time for adapting to the experimental setup.

After the *Familiarization*, the *Model Learning* phase followed, which consisted of a series of 20 trials (10 per target). Only the data collected in this phase was used for generating the probabilistic model for the *Predictive Assistance* phase as well as creating the reference trajectories for the *Fixed Assistance* phase.

The condition with *Predictive Assistance* is the main focus of this study. In this condition, data collected during the *Model Learning* phase was used to make a probabilistic model with ProMPs, which was later used to make predictions in real time for new arm reaching movements. It is important to note that the model was trained only on targets T1 and T2, but is then tested on all 4 targets. The predicted trajectories from the ProMPs are then fed into the flow controller in order to generate the assistive forces. As a comparison, we also implemented a simple model with fixed reference trajectories that was used in the *Fixed Assistance* condition. With this we aim to emphasize the shortcoming of pre-set reference trajectories and the need of movement prediction when the task changes to new target locations (i.e. T3 and T4). Such a change is often expected in a real world scenario where we never have full a priori knowledge of the task at hand. Finally a control condition (*No Assistance*) is necessary to establish a baseline for the execution of the task. Subjects were allocated a random sequence of blocks of conditions (*Predictive Assistance*, *Fixed Assistance*, *No Assistance*) in order to mitigate the effects of fatigue on the final results. All subjects performed 10 trials for each of the 4 targets (in total 40 trials per subject) in all three conditions. In between each phase of the experiment there was a rest period of three minutes. During the rest periods, subjects were given NASA TLX questionnaires [112] to record their perceived workload of the task in the current condition. The sequence of presented targets was randomized in all phases of the experiment. Subjects were informed whether they would receive assistance from the robot or not, but were not told about how the robot would try to assist them. The total length of the experiment was approximately 22 minutes per subject.

4.2.1.3 Evaluation and data analysis

To evaluate our proposed approach, we investigated the accuracy of our predicted trajectories, user effort, and potential changes in movement kinematics with the metrics presented in this section.

Prediction accuracy We analyzed the accuracy of the predicted trajectories by calculating the error of our movement predictions. We defined the error of prediction as the difference of the final point of the predicted trajectory from the centre of the target for each trial.

User effort To estimate physical effort for performing the task, we calculated the work exerted by the subjects from the start of the movement until the target was reached. The work was calculated as the integral of force $\boldsymbol{f}_h$ over the whole path of the movement $\boldsymbol{s}$

$$W = \int \boldsymbol{f_h} d\boldsymbol{s}. \tag{4.1}$$

The force of the subject $\boldsymbol{f}_h$ was measured with the force sensor located at the end effector of the haptic robot. Additionally, for six subjects we also measured muscle activity. Electrodes were placed on the skin following SENIAM recommendations [113] on the anterior and posterior deltoid, biceps brachii, and triceps brachii. EMG signals were recorded at 1250 Hz. After recording, EMG signals were band-pass filtered (zero lag, 2nd order Butterworth filter with cut-off frequencies of 20 and 450 Hz), full-wave rectified and low pass filtered (zero lag, 2nd order Butterworth algorithm, 10 Hz cut-off frequency). Finally,

the signal was normalized by the maximum value reached during the experiment for each subject and integrated over time (iEMG) for each trial to express the magnitude of muscle activity. From data collected with the NASA TLX questionnaires we calculated overall workload for each condition [112].

Movement kinematics To evaluate the impact of the assistive controllers on the subjects movements, we verified how the trajectories changed in the conditions with *Predictive Assistance* and *Fixed Assistance* as compared to when subjects had no assistance in the task. First, we normalized over time all trials for each target from the condition *No Assistance* and calculated the mean of these trajectories to serve as a reference. Then, for each trial and condition, we normalized the trajectory and calculated the error from the mean reference trajectory for all data points. Finally, we calculated the root-mean-square (rms) of this error to have a single value represent each trial.

Statistical analysis Two-Way repeated measures ANOVAs were performed to compare the calculated parameters across the different conditions. A 4 targets (T1, T2, T3, T4) $\times$ 3 conditions (*Predictive Assistance*, *Fixed Assistance*, *No Assistance*) statistical design was used to asses the effect of the different assistive scenarios on the computed variables. Prior to analysis, the data was tested for normality (Shapiro-Wilk test) and sphericity (Mauchly's tests). Post hoc t-tests with Bonferroni correction were conducted to determine significant differences between specific conditions relative to others. For the NASA TLX score, statistical significance between *Predictive Assistance*, *Fixed Assistance* and *No Assistance* was established using a One-Way Repeated measures ANOVA and post hoc tests with Bonferroni correction.

4.2.2 ProMPs and predicted reference trajectories

4.2.2.1 Encoding trajectories

To reduce the amount of parameters needed to represent trajectories, ProMPs use a basis function representation approach. To better understand the formulation, we present a simple example where we describe a point in time a_t (e.g. position of the end-effector) using this method. Let $\boldsymbol{\phi}_t \in \mathbf{R}^{1\times J}$ denote a basis function vector containing values of J basis functions at time t. The variable $\boldsymbol{w} \in \mathbf{R}^{J\times 1}$ represents a J-dimensional feature vector that encodes weights for each of the J basis functions. With $\boldsymbol{w}$ and $\boldsymbol{\phi}_t$ defined, a point at time t can be approximated as

$$a_t = \boldsymbol{\phi}_t \, \boldsymbol{w} = \begin{bmatrix}\phi_{1,t} & \cdots & \phi_{J,t}\end{bmatrix} \begin{bmatrix}w_1 & \cdots & w_J\end{bmatrix}^T. \tag{4.2}$$

This concept can be applied to multi-dimensional states by using block diagonal matrices. Assuming that our variable $\boldsymbol{a}_t$ now has D dimensions $\boldsymbol{a}_t = \begin{bmatrix}a_{1,t} & \cdots & a_{D,t}\end{bmatrix}^T$. In this case the basis function vector becomes a block diagonal matrix $\boldsymbol{\Phi}_t \in \mathbf{R}^{D\times JD}$ and the weight vector $\boldsymbol{w}$ becomes a concatenation of the weight vectors of each dimension $\boldsymbol{w} \in \mathbf{R}^{JD\times 1}$. Variable $\boldsymbol{a}_t$ is now approximated as

$$\boldsymbol{a}_t = \boldsymbol{\Phi}_t \, \boldsymbol{w} = \begin{bmatrix}\boldsymbol{\phi}_t & \cdots & 0 \\ \vdots & \ddots & \vdots \\ 0 & \cdots & \boldsymbol{\phi}_t\end{bmatrix} \begin{bmatrix}w_1 & \cdots & w_i & \cdots & w_D\end{bmatrix}^T, \tag{4.3}$$

where

$$\boldsymbol{\phi}_t = \begin{bmatrix}\phi_{1,t} & \phi_{2,t} & \cdots & \phi_{J,t}\end{bmatrix} \tag{4.4}$$

and

$$\boldsymbol{w}_i = \begin{bmatrix} w_{1,i} & w_{2,i} & \cdots & w_{J,i} \end{bmatrix}^T. \tag{4.5}$$

Using the same idea we can approximate a sequence of T states denoted by $\boldsymbol{\tau} = \boldsymbol{y}_{1:T}$, where

$$\boldsymbol{\tau} = \boldsymbol{\Phi}_{1:T}\boldsymbol{w} \tag{4.6}$$

with

$$\boldsymbol{\Phi}_{1:T} = \begin{bmatrix} \boldsymbol{\Phi}_1 & \cdots & \boldsymbol{\Phi}_t & \cdots & \boldsymbol{\Phi}_T \end{bmatrix}^T \in \mathbf{R}^{TD \times JD}, \tag{4.7}$$

where the vector $\boldsymbol{w}$ and the matrix $\boldsymbol{\Phi}_t$ are the same as before. In this work we used Gaussian basis functions which are often used for point-to-point movements.

To approximate the trajectories in the previously described manner, the weights for each trajectory need to be calculated. For the i-th trajectory $\boldsymbol{\tau}_i$, the corresponding weight vector $\boldsymbol{w}_i$ can be estimated using a simple least squares estimate. In our case, we used the least squares method

$$\boldsymbol{w}_i = \left(\boldsymbol{\Phi}_{1:T}^T\boldsymbol{\Phi}_{1:T} + \lambda\boldsymbol{I}\right)^{-1}\boldsymbol{\Phi}_{1:t}^T\boldsymbol{\tau}_i, \tag{4.8}$$

where λ represents a regularization parameter used to avoid numerical singularities. Its value should be small, in our case we used $\lambda = 10^{-2}$.

4.2.2.2 Creating the probabilistic model

When the weight vectors of all trajectories are calculated, we assume their values to be normally distributed, *i.e.*, $p(\boldsymbol{w}) = \mathcal{N}(\boldsymbol{w}|\boldsymbol{\mu}_w, \boldsymbol{\Sigma}_w)$. The mean $\boldsymbol{\mu}_w$ and the covariance matrix $\boldsymbol{\Sigma}_w$ can be estimated with sample mean and sample covariance of the $\boldsymbol{w}_i$ vectors.

With the function approximation (4.6) and the weight vectors $\boldsymbol{w}_i$ defined, we can define a probabilistic model for trajectories as

$$p(\boldsymbol{\tau}|\boldsymbol{w}) = \prod_{t=1}^{T}\mathcal{N}(\boldsymbol{y}_t|\boldsymbol{\Phi}_t\boldsymbol{w}, \boldsymbol{\Sigma}_y) = \mathcal{N}(\boldsymbol{y}_{1:t}|\boldsymbol{\Phi}_{1:T}\boldsymbol{w}, \boldsymbol{\Sigma}_y). \tag{4.9}$$

This model describes the probability of observing a trajectory $\boldsymbol{\tau}$ given the weight vector $\boldsymbol{w}$, that is given as a linear basis function $\boldsymbol{y}_{1:t} = \boldsymbol{\Phi}_{1:T}\boldsymbol{w} + \epsilon_{y,1:T}$. The parameter Σ_y represents independent and identically distributed (*i.i.d.*) Gaussian noise in the trajectories $\boldsymbol{y}_t = \boldsymbol{\Phi}_t\boldsymbol{w} + \epsilon_y$, where $\epsilon_y \sim \mathcal{N}(\epsilon_y|0, \boldsymbol{\Sigma}_y)$.

4.2.2.3 Computing Predictions from Observations

We can model predictions from observations by computing the conditional probability. First, we need to define the probability distribution over the trajectories $\boldsymbol{\tau}$, which can be computed by marginalizing out the weight vector $\boldsymbol{w}$. In the case of a Gaussian distribution the marginal can be computed in closed form as

$$p(\boldsymbol{\tau}) = \int p(\boldsymbol{\tau}|\boldsymbol{w})p(\boldsymbol{w})d\boldsymbol{w} \tag{4.10}$$

$$= \int \mathcal{N}(\boldsymbol{y}_{1:T}|\boldsymbol{\Phi}_{1:T}\boldsymbol{w}, \boldsymbol{\Sigma}_y)\mathcal{N}(\boldsymbol{w}|\boldsymbol{\mu}_w, \boldsymbol{\Sigma}_w)d\boldsymbol{w} \tag{4.11}$$

$$= \mathcal{N}(\boldsymbol{y}_{1:t}|\boldsymbol{\Phi}_{1:T}\boldsymbol{w}, \boldsymbol{\Phi}_{1:T}\boldsymbol{\Sigma}_w\boldsymbol{\Phi}_{1:T}^T + \boldsymbol{\Sigma}_y). \tag{4.12}$$

What we get is a multivariate Gaussian distribution, the conditional probability of which we can compute in closed form.

When we receive a previously unseen point $\boldsymbol{a}^*$, we can predict the most likely path of the end-effector (parametrized through $\overline{\boldsymbol{\mu}^*}$ and $\overline{\boldsymbol{\Sigma}^*}$) by conditioning the observed state over the weight vectors. Say that we observed a sequence of states $\boldsymbol{y}_{t1}$ to $\boldsymbol{y}_{tM}$ at m=1, 2,..., M-different time points. We declare ν as a concatenation of the observed states $\boldsymbol{y}_{tm}$ and $\boldsymbol{\Phi}_\nu$ as the concatenation of the basis function matrices for the observed time points.

With the observed trajectories encoded as previously described, we can obtain a conditioned distribution $p(\boldsymbol{w}_\nu|\boldsymbol{\nu})$ over the weight vectors $\boldsymbol{w}$ as

$$p(\boldsymbol{w}_\nu|\boldsymbol{\nu}) \propto \mathcal{N}(\boldsymbol{\nu}|\boldsymbol{\Phi}_\nu\boldsymbol{w}_\nu, \boldsymbol{\Sigma}_\nu)p(\boldsymbol{w}) \tag{4.13}$$

$$:= \mathcal{N}(\boldsymbol{w}_\nu|\boldsymbol{\mu}_{w|\nu}, \boldsymbol{\Sigma}_{w|\nu}). \tag{4.14}$$

We can compute the mean $\boldsymbol{\mu}_{w|\nu}$ and the covariance matrix $\boldsymbol{\Sigma}_{w|\nu}$ as

$$\boldsymbol{\mu}_{w|\nu} = \boldsymbol{\mu}_w + \boldsymbol{\Sigma}_w\boldsymbol{\Phi}_\nu^T\boldsymbol{L}(\boldsymbol{\nu} - \boldsymbol{\Phi}_\nu\boldsymbol{\mu}_w) \tag{4.15}$$

and

$$\boldsymbol{\Sigma}_{w|\nu} = \boldsymbol{\Sigma}_w - \boldsymbol{\Sigma}_w\boldsymbol{\Phi}_{\boldsymbol{\nu}}^T\boldsymbol{L}\boldsymbol{\Phi}_\nu\boldsymbol{\Sigma}_w, \tag{4.16}$$

where

$$\boldsymbol{L} = \left(\boldsymbol{\Sigma}_0 + \boldsymbol{\Phi}_\nu\boldsymbol{\Sigma}_w\boldsymbol{\Phi}_\nu^T\right)^{-1}. \tag{4.17}$$

With the feature mean $\boldsymbol{\mu}_{w|\nu}$ and covariance matrix $\boldsymbol{\Sigma}_{w|\nu}$ obtained, we can now use this conditional distribution to calculate the distribution over the trajectories $p(\overline{\boldsymbol{\tau}})$ using (4.12)

$$p(\overline{\boldsymbol{\tau}}) = \mathcal{N}(\tilde{\boldsymbol{y}}_{1:T}|\boldsymbol{\Phi}_{1:T}\boldsymbol{\mu}_{w|\nu}, \boldsymbol{\Phi}_{1:T}\boldsymbol{\Sigma}_{w|\nu}\boldsymbol{\Phi}_{1:T}^T + \boldsymbol{\Sigma}_y), \tag{4.18}$$

where the predicted sequence of states $\tilde{\boldsymbol{y}}_{1:T}$ is represented by the product $\boldsymbol{\Phi}_{1:T}\boldsymbol{\mu}_{w|\nu}$.

The encoding and model generation was performed based on data collected in the *Model Learning* phase of the experiment. Predictions for the subjects movement were calculated in real-time during each trial at a frequency of 20 Hz. The predictions were updating only for the first 400 ms, after which the predicted trajectory was fixed until the end of the trial. The predicted trajectories were used as a reference trajectory to generate the assistive force based on the control law specified by the flow controller. An example of the progression of the prediction during one trial is presented in Fig. 4.2 where we can observe how the variance of prediction decreases over time.

4.2.3 Assistance with fixed reference trajectories

To emphasize the importance of human movement prediction, we used an assistance with fixed reference trajectories as a comparison. The naming "*Fixed Assistance*" refers to the fact that this assistance does not adapt to new targets. In this case, we calculated the mean of the trajectories for each target during learning phase (T1 and T2). During the *Fixed Assistance* trial we continuously checked which of these 2 trajectories is closer to the current end effector position. The closest trajectory was selected as the reference trajectory that was passed through to the flow controller. An example is presented in Fig. 4.2 where the goal was to reach target T4. In this case, the fixed reference trajectory towards T2 is closer and is the one selected as the input for the flow controller.

4.2.4 Integration with the flow controller

The velocity-field-based controller as presented in [38], shortly referred to as flow controller, generates a flow field shaped according to a reference path. In our case, the reference path used to generate this flow field was either a predicted reference trajectory or a fixed

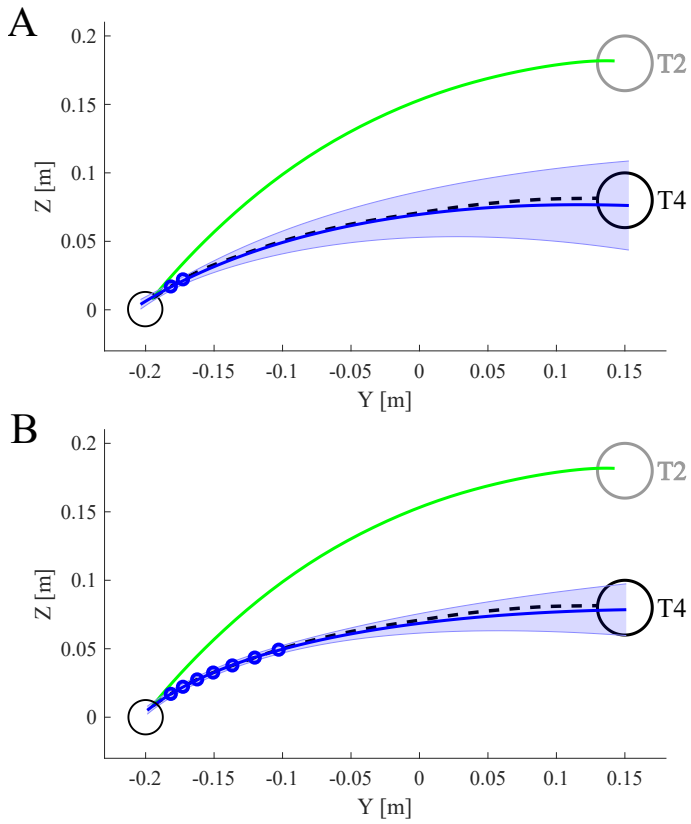

Figure 4.2: Example of the fixed reference (green) and predicted reference (blue) trajectory used as the input to the flow controller for one sample trial, at two time steps. **A** 150 ms after movement onset; **B** 400 ms after movement onset. The mean and SD of the predicted trajectory is marked in blue. The black dashed line represents the actual subject movement in the condition *Predictive Assistance*.

reference trajectory. We will now present the generation of the assistive flow field based on a reference trajectory.

For any given point in time, one point on the reference trajectory, denoted as $\boldsymbol{x}_c$, will be closest to the current end effector position $\boldsymbol{x}$. We can now define the expression for error $\boldsymbol{e}$

$$\boldsymbol{e} = \boldsymbol{x} - \boldsymbol{x}_c. \tag{4.19}$$

Additionally, we can calculate the gradient of the reference trajectory at the point $\boldsymbol{x}_c$, to define the tangent vector $\boldsymbol{t}$ which points in the direction of the prediction. We define the normalized tangent vector as:

$$\hat{\boldsymbol{t}} = \frac{\boldsymbol{t}}{|\boldsymbol{t}|}. \tag{4.20}$$

The normalized vector $\hat{\boldsymbol{n}}$ is orthogonal to the tangential vector and represents the normal to the reference path at the point $\boldsymbol{x}_c$. If we use θ to denote the angle between the error vector $\boldsymbol{e}$ and the normal to the curve $\hat{\boldsymbol{n}}$, we can define a new vector $\hat{\boldsymbol{n}}_i$ with the following condition:

$$\hat{\boldsymbol{n}}_i = \begin{cases} -\hat{\boldsymbol{n}}, & \text{if } \theta > 90 \\ \hat{\boldsymbol{n}}, & \text{otherwise} \end{cases}. \tag{4.21}$$

This ensures that the vector $\hat{\boldsymbol{n}}_i$ is always a normal vector pointing towards the reference trajectory.

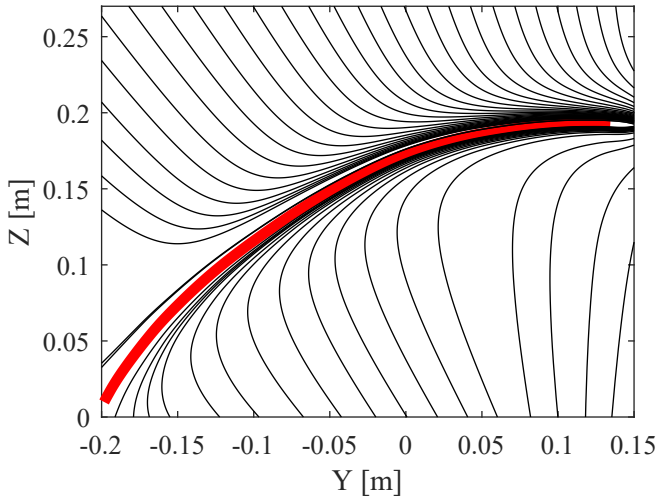

Figure 4.3: Example of a reference trajectory (red) with the flow field depicted as streamlines (black), $k_{sh} = 1000mm^2$. The streamlines show the shape of the flow field set by the reference velocity $\boldsymbol{v}_{ref}$. The flow field near the trajectory is tangent (flowing in the direction of the prediction), while further away it is normal to the trajectory. With the chosen parameter k_{sh}, the vector field has a 45 degree angle with respect to the reference trajectory at a distance of $e = 3cm$. The start of the movement trajectory is located at [-0.2, 0] whereas the target is located at [0.15, 0.18].

The equation of the flow field, written as a function of error and the tangential and normal components previously defined, is given by

$$\boldsymbol{v}_{ref} = \begin{cases} \Gamma(|\boldsymbol{e}|\hat{\boldsymbol{n}}_i + \frac{k_{sh}}{|\boldsymbol{e}|}\hat{\boldsymbol{t}}), & \text{for } |\boldsymbol{e}| > 1e^{-5} \\ \Gamma\hat{\boldsymbol{t}}, & \text{for } |\boldsymbol{e}| < 1e^{-5} \end{cases}, \tag{4.22}$$

where the scalar Γ determines the magnitude of the velocity reference. Here $|\boldsymbol{e}|\hat{\boldsymbol{n}}_i + \frac{k_{sh}}{|\boldsymbol{e}|}\hat{\boldsymbol{t}}$ is normalized such that $\boldsymbol{v}_{ref}$ is a unit vector multiplied by Γ.

The force generated by the flow controller describes a flow force on a symmetric body due to drag when immersed in a viscous fluid:

$$F_a = C_d(\boldsymbol{v}_{ref} - \boldsymbol{v}). \tag{4.23}$$

Here C_d is equivalent to a drag coefficient and $\boldsymbol{v}_{ref}$ is the velocity of the flow field defined in Equation 4.22. $\boldsymbol{v}$ represents the current velocity of the point $\boldsymbol{x}$ or in our case the velocity vector of the end effector of the haptic robot. A graphical representation of the flow field $\boldsymbol{v}_{ref}$ is presented in Fig. 4.3. The force F_a was calculated and updated at a frequency of 200 Hz. The values of the controller parameters used in the experiment were: $\Gamma = v_{s_{max}}$, $k_{sh} = 1000\ mm^2$ and $C_d = 20$ Ns/m. The magnitude of the reference velocity was calculated to match each subject's maximum velocity profile $v_{s_{max}}$ during the learning phase. This ensured that the subjects would not be forced to perform the movement faster than their preferred speed during the assisted trials. The magnitude of the reference velocity was the same for the *Predictive Assistance* and the *Fixed Assistance*. To prevent influencing the initial speed of the subject's movement, the controller was only activated 250 ms after movement onset. An example of the generated forces during one trial with *Predictive Assistance* and one trial using *Fixed Assistance* is presented in Fig. 4.4.

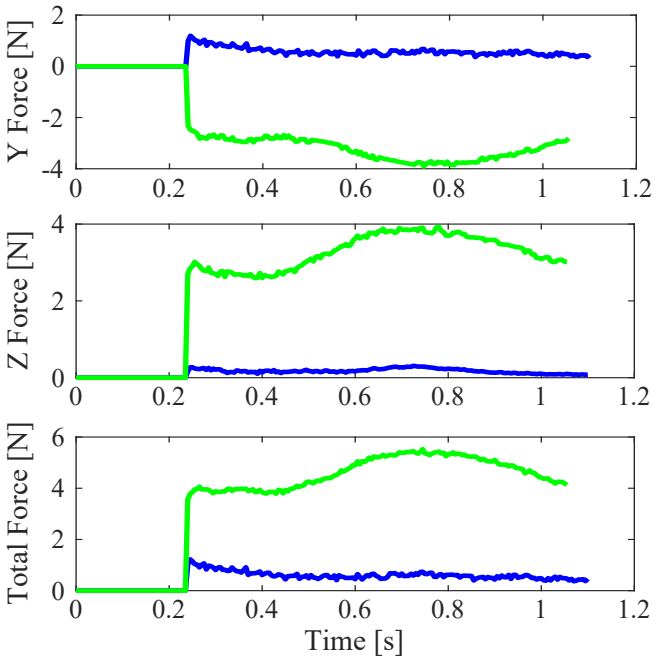

Figure 4.4: Example of the commanded force during an example trial while reaching towards target T4 with assistance. **Blue** with a predicted reference trajectory, **green** with a fixed reference trajectory.

4.3 Results

In this section we first present the accuracy of the movement predictions. We then present how the user effort was affected by analyzing the calculated exerted work, EMG muscle activity, and the NASA task load index. Finally, we present how movement kinematics are affected by the two different assistive strategies by analyzing the rms error of trajectories.

The error of the predicted trajectories was [2.3 ± 1.77 cm, 2.4 ± 1.83 cm, 2.3 ± 1.63 cm, 1.9 ± 1.24 cm] (mean $\pm$ SD) for targets T1, T2, T3, T4 respectively.

Does the predictive assistance lower user effort?: To evaluate the performance of our approach we calculated the work exerted by the subjects while performing the task. The results for each target and condition are presented in Fig. 4.5 in the form of boxplots. ANOVA revealed a significant main effect of controller condition on work required for task completion [$F(2, 22) = 14.13$, $p = 0.001$] as well as a significant target $\times$ controller condition interaction [$F(6, 66) = 65.05$, $p < 0.001$]. There was also a significant main effect of target position [$F(333) = 25.28$, $p < 0.001$], which was expected since the targets are at different distances away from the starting position. For targets T1 and T2, there was no difference between the different types of assistance. However, the work required for reaching the target T3 with the *Fixed Assistance* was significantly higher compared with *No Assistance* ($t(11) = 3.86$, $p = 0.008$) and *Predictive Assistance* ($t(11) = 8.72$, $p < 0.001$). The same is true for target T4, where the work during *Fixed Assistance* was significantly higher compared with *No Assistance* ($t(11) = 6.11$, $p = 0.002$) and *Predictive Assistance* ($t(11) = 11.91$, $p < 0.001$). Additionally, we show that the work required in *Predictive Assistance* was significantly lower than in the *No Assistance* condition for target T3 ($t(11) = 2.89$, $p = 0.04$) and T4 ($t(11) = 2.95$, $p = 0.04$).

As an additional measure of user effort we analyzed EMG muscle activity. For the posterior deltoid, ANOVA revealed a significant effect of condition $\times$ target interaction

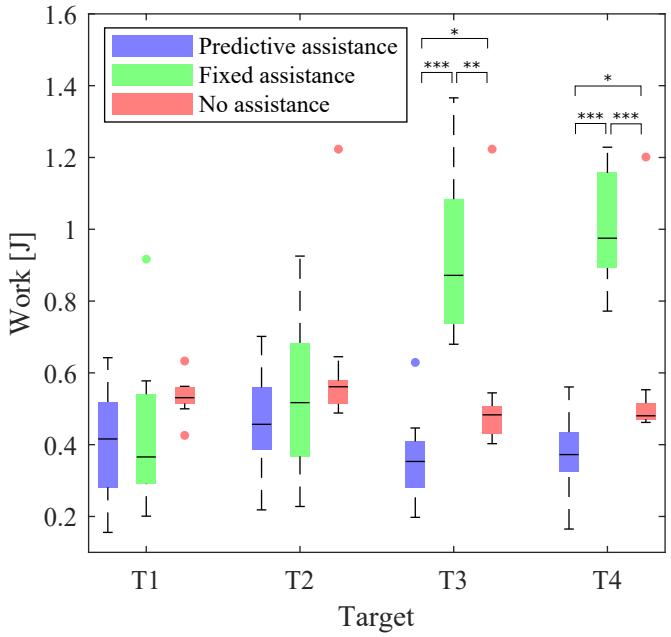

Figure 4.5: Boxplots of work performed by subjects for each of the four targets and three conditions. Boxplots for the *Predictive Assistance* are highlighted in blue, for *Fixed Assistance* in green and for *No Assistance* in red. *<0.05, **<0.01, ***<0.001.

$[F(6,30) = 12.59,\ p < 0.001]$. Post hoc tests showed that the increase in muscle activity during *Fixed Assistance* was significantly higher compared to *No Assistance* at target T3 ($t(5) = 3.82,\ p = 0.037$). For target T4 the muscle activity was significantly higher than with no assistance ($t(5) = 4.79,\ p = 0.015$) and *Predictive assistance* ($t(5) = 5.47,\ p = 0.008$). The results are also presented in graphical form in Fig. 4.6. The ANOVA also revealed a significant effect of condition × target interaction for the other muscles: anterior deltoid $[F(6,30) = 2.93,\ p = 0.023]$, biceps brachii $[F(6,30) = 3.26,\ p = 0.014]$ and triceps brachii $[F(6,30) = 7.282,\ p < 0.001]$. However, post hoc tests did not return any significant differences between conditions at each target. The overall workload calculated from the NASA TLX questionnaires was: 18.3 ± 13.1, 41.4 ± 18.9, 21.3 ± 11.1 (mean ± SD) for the *Predictive Assistance*, *Fixed Assistance* and *No Assistance* condition respectively. ANOVA revealed a significant main effect of controller condition $[F(2,22) = 15.27,\ p < 0.001]$. Post hoc tests revealed that the workload in condition *Fixed Assistance* was significantly higher than in the condition *No Assistance* ($t(11) = 4.18,\ p = 0.005$) and *Predictive assistance* ($t(11) = 4.41,\ p = 0.003$). There was no significant difference between *Predictive Assistance* and *No Assistance*.

Does the predictive assistance impact the overall kinematics of the movement?: While successfully lowering the effort for performing the task is important, the assistance should not impact the overall kinematics of the movement. In Fig. 4.7 we present the rms of the deviation from the mean trajectory calculated from the condition *No Assistance*, for each target and each condition. ANOVA revealed a significant main effect of controller condition on the rms $[F(2,22) = 27.25,\ p < 0.001]$ as well as a significant target × controller condition interaction $[F(6,66) = 5.95,\ p < 0.001]$. There was also a significant main effect of target position $[F(3,33) = 4.38,\ p = 0.011]$. Post hoc tests revealed that rms values in condition *Fixed Assistance* were significantly higher than in the condition *No Assistance* at targets T3 ($t(11) = 5.20,\ p < 0.001$) and T4 ($t(11) = 5.80,\ p < 0.001$) and also significantly

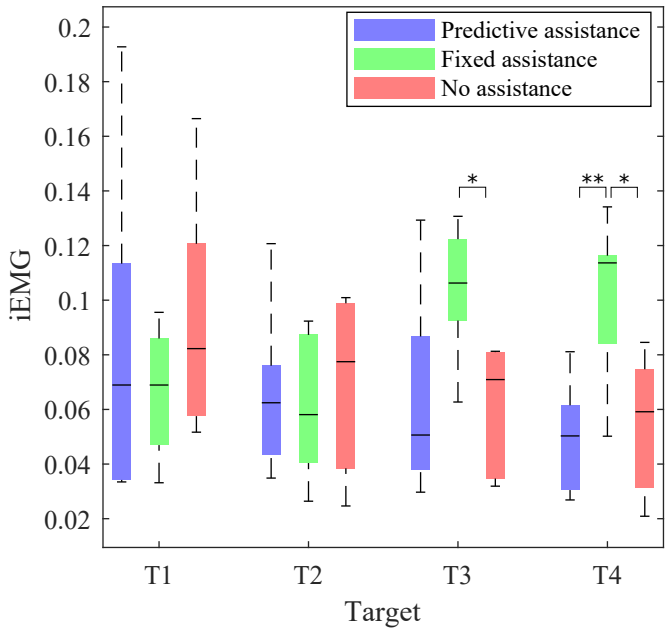

Figure 4.6: Boxplots of iEMG muscle activity of the posterior deltoid for each of the four targets and three conditions. Boxplots for the *Predictive Assistance* are highlighted in blue, for *Fixed Assistance* in green, and for *No Assistance* in red. *<0.05, **<0.01, ***<0.001.

higher than in the condition *Predictive Assistance* for targets T3 ($t(11) = 3.06$, $p = 0.011$) and T4 ($t(11) = 4.62$, $p = 0.002$). All other comparisons were not significantly different.

4.4 Discussion

In this study, we investigated the efficacy of a novel exoskeleton control approach combining movement predictions with a flow field controller. Our results showed that the probabilistic models used were able to accurately predict user movements and generalize to new target locations. This may be in part due to the fact that the initial movement was not altered by the assistive controller and therefore the speed of movement execution was similar to those performed in the *Model Learning* phase. However, as presented in [52] it would be possible to implement a phase estimation algorithm to take into account different speeds of movement execution while maintaining reliable predictions of movements.

The analysis of work required to perform the task had expected results. Overall, the work required for completing the task was lowered using our proposed predictive control. However, if the reference trajectory is not accurately predicted, this can still have an adverse effect on performance. This is shown by the fact that it was significantly more difficult for subjects to complete the task with the *Fixed Assistance* for targets T3 and T4. While the forces produced are not high (< 10 N) and subjects could still complete the task at hand, this had a negative effect on their performance. This was also reflected in the kinematics of the movement, the muscle activity as well as workload scores, which were all negatively affected in the *Fixed Assistance* condition.

The spread of data points for work in Fig. 4.5 is much lower for *No Assistance* than in the other conditions. This might indicate that the subjects started by using the same amount of work for the task, but they gradually learned how to exploit the assistance which lowered their effort for performing the task.

There was no strong indication that the *Predictive Assistance* lowered the perceived

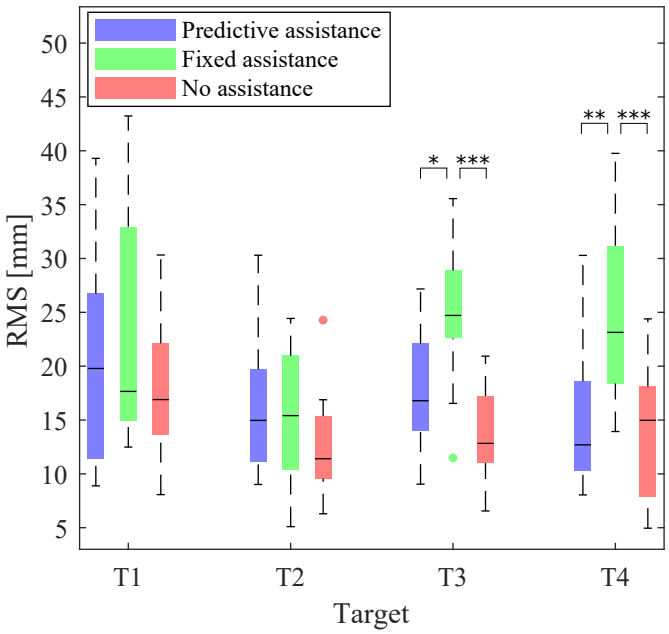

Figure 4.7: Boxplots of rms deviation from a mean reference for each of the four targets and three conditions. Boxplots for the *Predictive Assistance* are highlighted in blue, for *Fixed Assistance* in green, and for *No Assistance* in red. *<0.05, **<0.01, ***<0.001.

workload or muscle activity of subjects, which one might expect when considering the outcome of work analysis from the interaction force. However, this is probably because the task is not very demanding and it is therefore difficult to lower the workload even further.

4.5 Conclusion

In current exoskeleton control approaches, there exists a lack of human movement prediction without the use of invasive sensors, which is crucial for a seamless human-robot interaction. Additionally, it is very important to keep the system safe, as human safety is the single most important aspect for a successful human-robot interaction. Therefore, we proposed a novel control approach for assisting a human subject in performing a reaching task that combines movement predictions with a velocity-field-based controller.

Using ProMPs we were able to generate a model that accurately predicted user trajectories for all subsequent movements. The combination of user movement prediction with a flow controller resulted in an intuitive and safe assistance for the task. We validated our approach with an experiment emulating exoskeleton support for assisting in a reaching task, where we showed a significant reduction of effort required by the users to perform the task without affecting the user's kinematics.

For future progression of this work, we plan to further exploit the probabilistic nature of ProMPs and incorporate the predicted variance of movement in the flow controller. Meaning, we could modulate the parameter k_{sh} depending on the variance in order to provide a more restrictive flow where the movements need to be more determined whereas the flow could be more general in parts of the movement with higher variance. This would however require a different and more complex task setup with locally constrained movement trajectories (e.g. avoiding an obstacle mid trajectory) in order to properly evaluate such modulation of the flow field. Furthermore, the variance of the prediction could be used in order to determine when to "trust" the prediction more and therefore also increase the

level of assistance by increasing the value of the drag coefficient C_d.

One argument could be made for using only ProMPs to generate the assistance needed for the given task, as they inherently poses properties which would probably work well in the context of our simulated task. However, even though ProMPs can provide temporal scaling of movements and lower feedback gains in parts of trajectories with high variance, we believe that a flow field controller could be inherently safer for human-robot interaction as was argued in the work of Martinez et al. [38]. Additionally, one might argue that it would be possible to use the flow controller by itself to provide enough assistance for the task by using the average trajectories to all targets and increase the width of the flow field. However, we believe that such an approach would be too general as it would (in our case) approach a scenario with only a relatively constant force being applied in the direction of all targets.

While we showed that the proposed assistive control is capable of providing adequate assistance, future work with a direct comparison with other assistive controllers would be needed to fully evaluate this type of assistive control. Overall, we believe that our approach is a promising tool for high level exoskeleton control that can provide intuitive and safe assistance to the user for a variety of tasks.

Chapter 5

Effects of Simulated Microgravity and Hypergravity Conditions on Arm Movements in Normogravity

5.1 Introduction

Eye-hand coordination is necessary for many everyday tasks that involve grabbing or manipulating objects around us. High proficiency in eye-hand coordination is especially crucial for humans controlling vehicles or complex systems or performing piloting tasks [114]. However, human sensorimotor control has evolved in the Earth's environment where all movements are influenced by the gravitational force [115], [116]. Changes or the mere absence of this environmental force can drastically affect the performance of arm reaching movements especially in early exposure to the novel environmental dynamics as was observed in force field experiments [117], [118] or microgravity [119]. Adaptation and training for exposure to changing environmental conditions are critical especially in space flight exploration where astronauts must be prepared on how to operate and complete a multitude of tasks in periods of hypergravity as well as microgravity. Designing efficient training procedures or simulation environments requires good knowledge of how microgravity and hypergravity affect human sensorimotor control. Several studies have already explored the effect of these environmental conditions on arm reaching kinematics in space, during parabolic flights and in human centrifuges as well as the effects after returning to earth from space [120]. However, the results are not always consistent from study to study. In some cases, the authors found a reduction of movement duration in microgravity compared to normogravity [121]–[123] while in other cases, no significant changes were detected [124], [125]. In general, it has been shown that the new environmental conditions negatively affect the accuracy or pointing position of subjects as compared to normogravity [115], [126]. However, in studies where the subjects were trained cosmonauts, no changes in accuracy were found when comparing microgravity and normogravity conditions [122], [127]. These discrepancies in results could be just due to the limited number of subjects included in these studies or they might indicate that trained subjects are indeed able to perform better in such environments. One option for training astronauts before space missions is the use of parabolic flights. However, these are very expensive, the exposure time to microgravity is very limited, and the gravitational environment varies. The other, more established method to prepare astronauts for performing tasks in microgravity, is underwater training in neutral buoyancy [128]. Some studies explored the effects of neutral buoyancy on sensorimotor control and also compared the effect to those observed in microgravity [125]. However, training underwater does not affect the vestibular signals in the same way as

microgravity. Furthermore, faster movements generate additional viscous resistance forces that are not present in microgravity. An alternative for simulating microgravity would be the use of weight support systems to locally remove the effect of gravity on a limb of the individual. There has been some work exploring kinematic features with weight support systems, but mainly for rehabilitation purposes for stroke patients [129], [130]. In these studies, no significant differences were found for movement duration and movement symmetry. However, these studies did not investigate movements with or against gravity and therefore cannot be compared with other studies investigating movement kinematics in space or parabolic flights. In this study, we investigated whether simulation of hyper- and microgravity conditions locally on the arm could be a feasible approach for on-ground training of arm reaching movements in altered gravity conditions. To achieve this, we developed a low friction robotic device that was able to apply forces at the wrist in order to simulate micro- or hypergravity conditions for the arm while subjects performed pointing movements on a touch screen. We compared the results of various kinematic parameters using this system with data from a parabolic flight where the same subjects were fully exposed to micro- and hypergravity conditions.

5.2 Materials and Methods

The study was performed during the 142nd CNES parabolic flight campaign that included 3 flights over 3 days. The flights were composed of 31 parabolic maneuvers. Each maneuver consisted of 3 phases: 20 s of hypergravity (1.8 g, pull-up phase) followed by 22 s of microgravity (0 g) before a second period of 20 s of hypergravity (1.8 g, pull-out phase). A more technical and in-depth description of the parabolic flight maneuvers is presented by [131]. The second part of the study was performed on the ground, where we simulated micro- and hypergravity conditions for the arm of the subjects with a robotic system.

5.2.1 Subjects

Nine right-handed subjects (7 males, 2 females) participated in the study (age: 29.8 ± 7.4 years, height: 176.0 ± 10.8 cm; weight: 71.0 ± 15.7 kg). No subject reported any musculoskeletal disorders. To avoid motion sickness during the parabolic flight all subjects received a personalized dose of scopolamine prior to the flight. It has been previously shown that use of scopolamine does not interfere with sensorimotor control [132]. None of the subjects had prior microgravity or hypergravity experience. They were all naive with respect to the specific purpose of this experiment. All subjects gave their informed consent to participate in the study, stored by the Caen University Hospital. The experiment was conducted in accordance with the Declaration of Helsinki, procedures were approved by the French National Ethics committee (2018-A03379-46) and authorized by the ANSM (French National Agency for Biomedical Security).

5.2.2 Experimental setup

The subjects were seated in a chair (Figure 5.1A) positioned in front of a touch screen display (ProLite T2435MSC-B2, Iiyama, Hoofddorp, The Netherlands) oriented in portrait mode (display size 521 mm x 293 mm) as depicted in Figure 5.1B. The middle of the screen was positioned at a height of 750 mm so that subjects could comfortably reach the top and bottom of the screen. To prevent trunk displacement during the task, subjects were securely strapped to the chair using a four-point harness. The subject's legs were positioned on the outsides of the screen with the ankles strapped firmly in place. This was done in order to prevent involuntary leg movements during microgravity phases. During the

experiment, the subject's right wrist was strapped with a Velcro strap to a non-stretchable string (Dyneema® 1.5 mm, YSM and Partners, Dobra, Poland) which was connected to two motors (EMMS-AS-55-S-TM, Festo, Esslingen, Germany), positioned above and below the center of the screen. The distance between the motors was 1.5 m. To prevent string slack, a constant pretension force of 10 N was applied by both motors in the opposite direction. This allowed for unobstructed vertical movements of the arm while maintaining a constant connection of the wrist to the motors. In the trials performed on the ground, the motors were used to apply a force at the subject's wrist, mimicking the gravitational effects of microgravity or hypergravity conditions at the shoulder joint. To simulate microgravity, the motors applied a constant force in the upward direction, whereas to simulate hypergravity conditions, the force was applied in the downward direction. In simulated normogravity conditions, no additional force was applied to the wrist, only the pretension was used in order to prevent string slack. The force used was subject-specific and was measured beforehand (18.6 ± 4.8 N). The force controller to control the motors was running on a real-time computer at a rate of 1 kHz and in a closed loop. To monitor the kinematics of the subjects, a motion capture system consisting of 3 cameras was used (Vicon, Yarnton, United Kingdom). A marker was placed on the stylus used for performing the task. The acquisition frequency for the kinematics was 100 Hz. To collect data of muscle activity, EMG electrodes (SX230 sensor, Biometrics Ltd, New- port, UK) were placed on the skin following SENIAM recommendations [113] on the Anterior and Posterior Deltoid, Trapezius, and Pectoralis. Raw EMG signals were recorded at a frequency of 1000 Hz on a Sensoray Model 526 (Sensoray, Tigrad, USA).

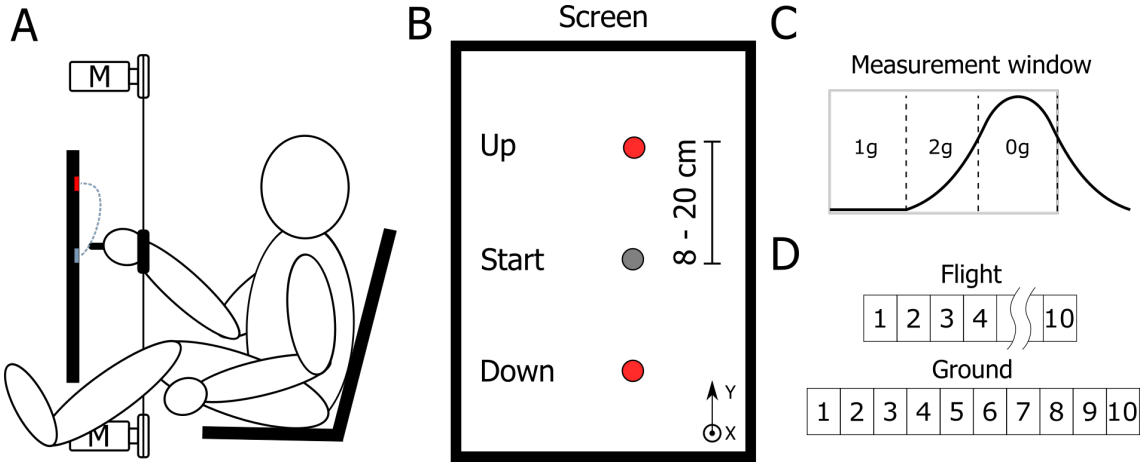

Figure 5.1: (A) Profile view of the experimental setup and (B) view of the screen indicating start (Grey) and end target (Red) locations. The orientation of the coordinate system is marked indicating the positive y coordinate pointing up and the x coordinate pointing out from the screen towards the subject. (C) The measurement window during each parabola consisted of 20 seconds of normogravity followed by 20 seconds of hypergravity and finally 22 seconds of microgravity. (D) Number of parabolas per subject. The parabolas from 5 to 9 during flight were part of another study.

5.2.3 Task

Subjects had to successfully point to a target presented on the screen in front of them. To perform the task, subjects used a tactile stylus held by the thumb, index, and middle finger. The starting position was indicated by a grey circle of a diameter of 60 mm and

was located approximately at the shoulder height. After a random delay of 0 - 500 ms, the end target (diameter of 20 mm) was presented to the subject. The seven possible end target positions were 8, 10, 12, 14, 16, 18, and 20 cm from the start target either vertically up or down. To prevent anticipation, the sequence of displayed targets was randomized. The subjects were instructed to perform the task as fast and as accurately as possible. On average subjects performed 20.8 $\pm$ 4.3 trials per each parabola.

5.2.4 Protocol

The whole experiment consisted of one in-flight session and one simulation session performed on the ground. In the in-flight session, each subject performed the experiment for 10 parabolas. This included 20 s before the parabola (normogravity), 20 s during hypergravity, and 22 s during microgravity. During other parts of the flight, the subjects were instructed to rest their arm on their right leg. In the simulation session (carried out one day after all the flight sessions), each subject performed the same task for the duration of 10 simulated parabolas. Each simulated parabola consisted of 20 s with the motors inactive (normogravity), followed by 20 s with the motors active and applying a downward force to the wrist simulating hypergravity and finally 22 s with the motors active and applying an upward force to the wrist, simulating microgravity. After each simulated parabola, the subjects rested their arm. In the simulation session, only 7 out of 9 subjects participated in the experiment. As indicated in Figure 5.1 D, only 5 parabolas during flight were used for the analysis in this study. The parabolas 5-9 were part of another study where the subjects received an assistive force at the wrist to compensate for the gravitational changes experienced during the parabolic flight and thus simulated constant normogravity conditions for the arm performing the experiment. For a concise representation of different conditions throughout this chapter, we will refer to the in-flight phases of normogravity, microgravity, and hypergravity with labels (1g, 0g, and 2g) respectively. For the trials performed on the ground, we will refer to them as simulated normogravity, microgravity, and hypergravity conditions with labels (1g S, 0g S, and 2g S). We use the term simulated normogravity, even though during these trials we did not simulate any additional forces. The colors used in the figures of results are coherent between actual or simulated conditions, where green denotes 1g/1g S conditions, blue denotes 0g/0g S conditions and red denotes 2g/2g S conditions.

5.2.4.1 Data processing and analysis

Data from the touch screen was used to calculate movement duration and accuracy. The trial started when the stylus moved away from the screen and ended when it touched the screen again. Movement duration was defined as the time from the start to the end of one trial. To assess accuracy, the pointing position relative to the target was calculated as the vertical distance between the center of the target and the position where the stylus touched the screen. We refer to these results as deviations from the targets, where a positive deviation represents a hit above the target location whereas a negative deviation represents a hit under the target location in the coordinate frame defined in Figure 5.1 B. Marker positions were interpolated for missing data and low pass filtered with 2nd order zero-phase lag Butterworth filter (10Hz cut-off frequency). Trials with excessive missing data or data with clear outliers were manually removed from the kinematic analysis. Position data were used to calculate displacement in the x direction, the velocity profiles, maximum velocity, and time-to-peak-velocity (TPV) as a measure of movement asymmetry. Motion trajectories were plotted with normalized positions in the vertical direction and averaged positions in the horizontal direction. EMG signals were band-pass filtered (zero phase

lag, 2nd order Butterworth filter with cut-off frequencies of 20 and 350 Hz) and full-wave rectified. The envelope of the signal was extracted with a moving average window of 100 samples. Finally, the signals were normalized to the mean of the 1g condition and integrated over time for each trial to express the magnitude of muscle activity (normalized iEMG). All data processing and generation of data figures were performed in Matlab (Mathworks, Natick, MA, USA).

5.2.5 Statistical analysis

To compare parameters across different conditions, we conducted a linear mixed models analysis with 3 gravitational conditions (1g, 0g, 2g) × 2 simulation conditions (real, simulated) × 7 targets statistical design where the subjects were included as random effects. The analysis was conducted in R [133] with the *nlme* [134] and *multcomp* [135] packages. We checked that the residuals of the fitted model were normally distributed. We performed all analyses separately for the upwards and downwards movements. We report only the main effects of gravity and simulation as well as the interaction effect of gravity × simulation. Post hoc tests (with Bonferroni correction for multiple comparisons) were conducted to determine significant differences between specific conditions. To specifically determine the effects of microgravity on task variables, we compared (1g – 0g and 1g S – 0g S) and also directly compared the parameters with simulated microgravity with actual microgravity on the plane (0g S – 0g). The same comparisons were conducted for changes of movement parameters in hypergravity (1g – 2g, 1g S – 2g S, 2g S – 2g). The final comparison included the two conditions of normogravity (1g S – 1g). The level of statistical significance was set at 0.05. We adopt conventional statistical significance labels: * $<$ .05, ** $<$ .01, *** $<$ .001.

5.3 Results

First, we present the results of the pointing accuracy which is the main task outcome. We then present movement kinematics. Starting with movement duration, velocity profiles, and maximum velocity, followed by the shape of the trajectories and time to peak velocity (TPV). Finally, we present the results of muscle activation during the different conditions. The results for each parameter are structured in the same form where the results for downward movements are presented first followed by results for upward movements. For each direction, we first report the effects of gravity, simulation, and the interaction of gravity × simulation. Then, individual differences and results of post hoc tests are first presented for microgravity conditions (0g), followed by hypergravity (2g) and finally, we report if there were any differences between normogravity conditions (1g) during flight versus the simulation trials. We do not report the effects of target positions, however as mentioned in subsection 2.5.1, the statistical analysis was performed taking into account the different target locations.

5.3.1 Task outcome: Accuracy

To evaluate the accuracy of pointing, we looked at the location of hits on the screen with respect to the displayed targets, which we refer to as deviations from the targets. The absolute deviations of hits for each gravitational and simulation condition, averaged for all parabolas and targets, are shown in Figure 5.2 A, D. Additionally, signed deviations of hits for each individual target are presented in Figure 5.2 B, E for microgravity and simulated microgravity and in Figure 5.2 C, F for hypergravity and simulated hypergravity conditions. Post hoc test results are presented in Table 5.1. For downward movements the

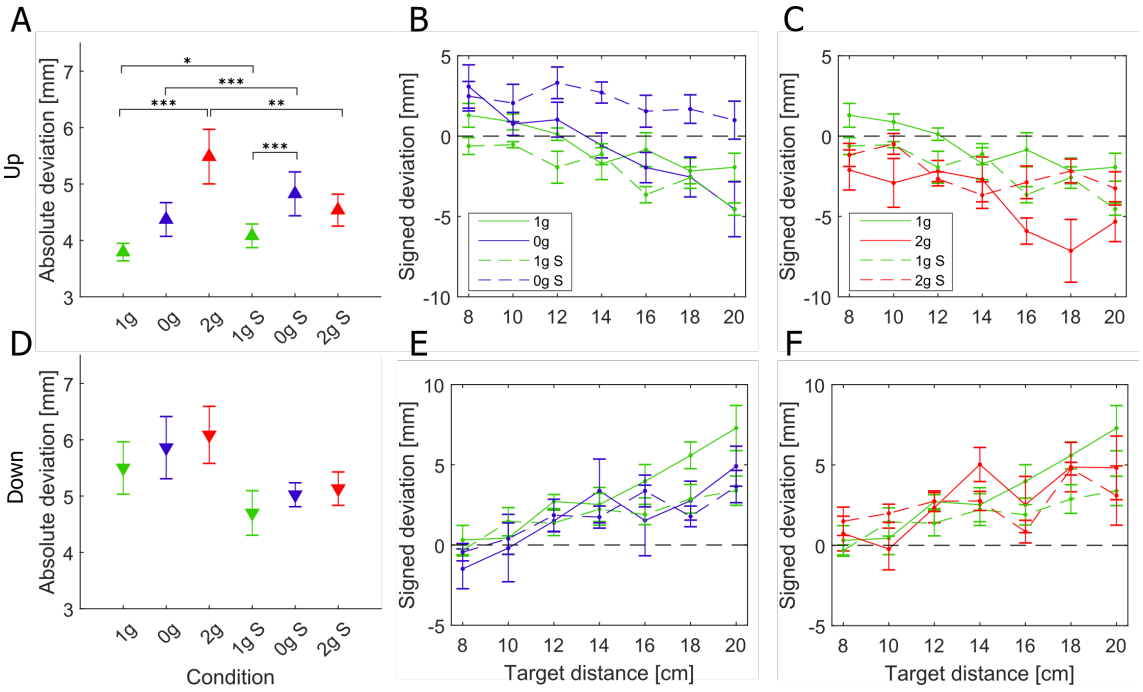

Figure 5.2: Absolute deviations of the pointing position averaged for all subjects and grouped per condition for upward movements (A) and downward movements (D). Signed deviations for every target in microgravity (B, E) and hypergravity (C, F) for upward and downward movements, respectively. Downward pointing triangles denote mean values for downward movements, upward pointing triangles denote mean values for upward movements, the whiskers denote the standard error of mean. Green represents normogravity, blue represents microgravity and red represents hypergravity conditions, (1g, 0g, 2g) denote in-flight gravitational conditions, (1g S, 0g S, 2g S) denote simulated gravitational conditions.* $p < 0.05$, ** $p < 0.01$, *** $p < 0.001$.

statistical analysis showed no significant effects of simulation ($F(1,278) = 3.52$, $p = 0.061$), gravity ($F(2,278) = 2.65$, $p = 0.071$) or the interaction of gravity × simulation ($F(2,278) = 1.40$, $p = .245$). For the microgravity conditions, no comparisons were significantly different. Despite that, a similar trend is visible where the absolute deviation of hits is slightly higher in microgravity compared to normogravity for both in-flight and simulated conditions. The same effects were observed in hypergravity and simulated hypergravity, where there was a slight increase in the absolute deviations, however this was not significant. The accuracy of downward movements in the simulated normogravity condition is better, however, this difference is not significant. For all gravitational conditions we observed a trend in the signed deviations of hits for each target, where the deviations increase with the increased target distance. For upward movements the statistical analysis showed a significant effect of gravity ($F(2,278) = 53.34$, $p < .001$), simulation ($F(1,278) = 11.21$, $p < .001$), and the interaction gravity × simulation ($F(2,278) = 18.49$, $p < .001$). Interestingly, for upward movements in microgravity, there was no significant difference in the deviations from normogravity conditions. There was, however, a significant increase in deviations in the simulated microgravity condition in comparison with normogravity or microgravity (0g S – 0g, 1g S – 0g S). Also, while we observed both positive and negative deviations of hits in normogravity and microgravity, the same was not true for the simulated microgravity where the subjects on average hit above all of the targets (only positive deviations). Concerning hypergravity conditions, the absolute deviations increased significantly compared

to normogravity (1g – 2g) whereas this was not the case for the simulated hypergravity, where there was only a small increase in the absolute deviations. We also noted marginally higher deviations in the simulated normogravity conditions compared to normogravity (1g S – 1g).

Table 5.1: Post hoc analysis for signed deviations of hits.

		Down			Up		
	Comparison	z	p	Comparison	z	p	
0 g	1g – 0g	2.436	0.104	1g – 0g	0.096	1.000	
	1g S – 0g S	0.122	1.000	1g S – 0g S	-7.757	<0.001	***
	0g S – 0g	0.297	1.000	0g S – 0g	-5.421	<0.001	***
2 g	1g – 2g	0.679	1.000	1g – 2g	6.976	<0.001	***
	1g S – 2g S	-1.058	1.000	1g S – 2g S	0.340	1.000	
	2g S – 2g	0.709	1.000	2g S – 2g	-3.452	0.004	**
1 g	1g S – 1g	2.470	0.095	1g S – 1g	2.733	0.044	*

5.3.2 Motion Kinematics

5.3.2.1 Duration of movements

The durations of movements for each gravitational and simulation condition averaged for all parabolas and targets are shown in Figure 5.3, whereas post hoc test results are presented in Table 5.2. For downward movements the statistical analysis showed a significant effect of gravity ($F(2,278) = 18.83$, $p < .001$), simulation ($F(1,278) = 19.15$, $p < .001$) and the interaction of gravity × simulation ($F(2,278) = 9.52$, $p = .001$). Concerning microgravity conditions, post hoc tests revealed that for downward movements there was a significant increase in movement duration compared to normogravity only in the simulated trials (1g S – 0g S). The movement durations during real and simulated microgravity (0g – 0g S) were not significantly different. Also for hypergravity conditions there was no significant difference between real and simulated conditions. However, a significant decrease in movement duration was observed during flight (1g – 2g) but not during the simulation. Interestingly, movement durations were significantly shorter in the simulated normogravity trials compared to those during flight (1g S – 1g). For upward movements the statistical analysis showed a significant effect of gravity ($F(2,278) = 109.28$, $p < .001$) and the interaction gravity × simulation ($F(2,278) = 3.71$, $p = .026$), but not simulation alone ($F(1,278) = 2.00$, $p = .158$). Post hoc test revealed that movement duration in microgravity increased significantly both during flight (1g – 0g) and in simulation (1g S – 0g S). Movement duration during real microgravity did not significantly differ from the simulated condition (0g S – 0g). Movement duration during hypergravity was significantly lower compared to normogravity only in the real condition (1g – 2g). No statistical difference was found when comparing both normogravity conditions (1g – 1g S).

5.3.2.2 Velocity profiles and maximum velocity

Figure 5.4 shows the mean velocity profiles for all gravitational and simulation conditions normalized for target distance in the y direction. Here we can see that the shape of velocity profiles remained constant throughout the various gravitational conditions, i.e. the peaks did not shift, which we already evaluated when analyzing the TPV parameter. However, we observed a change in the magnitude of the velocity profiles especially for the

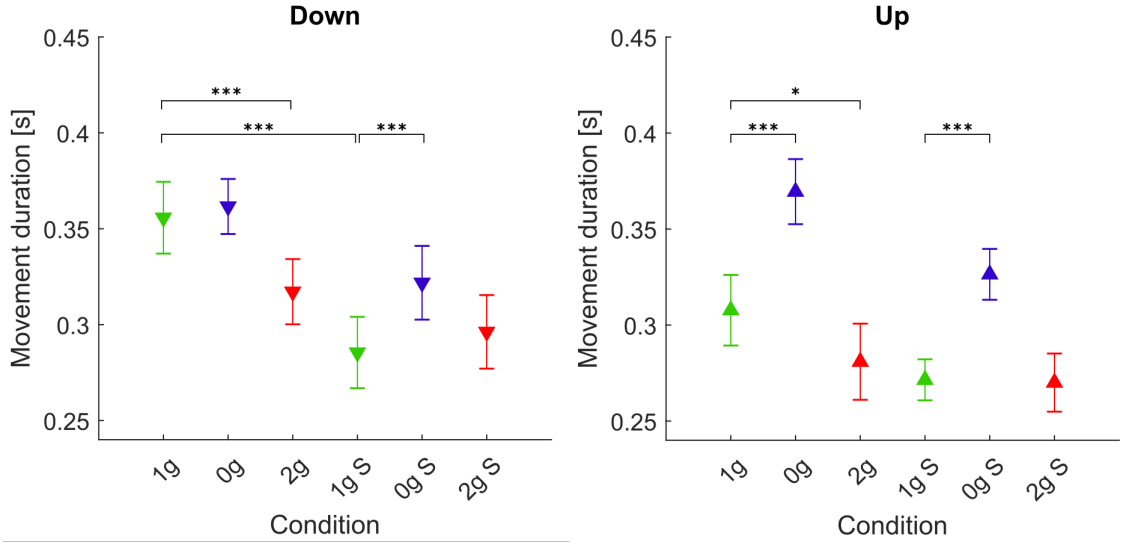

Figure 5.3: Movement durations in different gravitational and simulation conditions. Downward pointing triangles denote mean values for downward movements, upward pointing triangles denote mean values for upward movements, the whiskers denote the standard error of mean. Green represents normogravity, blue represents microgravity and red represents hypergravity conditions, (1g, 0g, 2g) denote in-flight gravitational conditions, (1g S, 0g S, 2g S) denote simulated gravitational conditions. * $p < 0.05$, ** $p < 0.01$, *** $p < 0.001$.

Table 5.2: Post hoc analysis for movement duration.

		Down			Up			
	Comparison	z	p		Comparison	z	p	
0 g	1g – 0g	-0.505	1.000		1g – 0g	-8.978	<.001	***
	1g S – 0g S	-4.173	<.001	***	1g S – 0g S	-7.069	<.001	***
	0g S – 0g	2.000	.318		0g S – 0g	2.437	.104	
2 g	1g – 2g	5.062	<.001	***	1g – 2g	3.148	.012	*
	1g S – 2g S	-1.238	1.000		1g S – 2g S	0.185	1.000	
	2g S – 2g	-0.130	1.000		2g S – 2g	-1.292	1.000	
1 g	1g S – 1g	5.881	<.001	***	1g S – 1g	1.455	1.000	

upward movements where the maximum velocities increased in hypergravity conditions. In order to more clearly illustrate these changes, we present the maximum velocities for each gravitational and simulation condition, averaged for all parabolas and targets in Figure 5.5. Post hoc test results are presented in Table 5.3. Statistical analysis for downward movements showed a significant main effect of simulation ($F(1,278) = 15.69$, $p < .001$) as well as the interaction of gravity × simulation ($F(2,278) = 6.68$, $p = .002$), whereas there was no significant main effect of gravity ($F(2,278) = 2.12$, $p = .122$). In microgravity conditions, the maximum velocity was significantly lower only in the simulated condition. However, there was no significant difference between the actual and simulated microgravity conditions (0g S – 0g). In contrast, the maximum velocity in simulated hypergravity was higher compared with the real hypergravity condition (2g S – 2g). Similarly, the maximum velocity in normogravity conditions was higher in the simulated trials compared to those

during flight (1g S – 1g). For upward movements, analyzing the maximum velocity revealed a significant main effect of gravity ($F(2,278) = 54.85$, $p < .001$). No significant effects of simulation ($F(1,278) = 0.54$, $p = .462$) or interaction of gravity × simulation ($F(2,278) = 1.24$, $p = .292$) were found. Concerning microgravity conditions, the maximum velocity was significantly lower than in normogravity both in flight and on the ground (1g – 0g, 1g S – 0g S). There was no significant difference between simulated and real microgravity conditions (0g S – 0g). For hypergravity conditions, the maximum velocity increased in both real and simulated conditions (1g – 2g, 1g S – 2g S) and there was no difference between the two hypergravity conditions (2g S – 2g). The maximum velocity in simulated normogravity was higher than in-flight, however, this difference was not statistically significant (1g S – 1g).

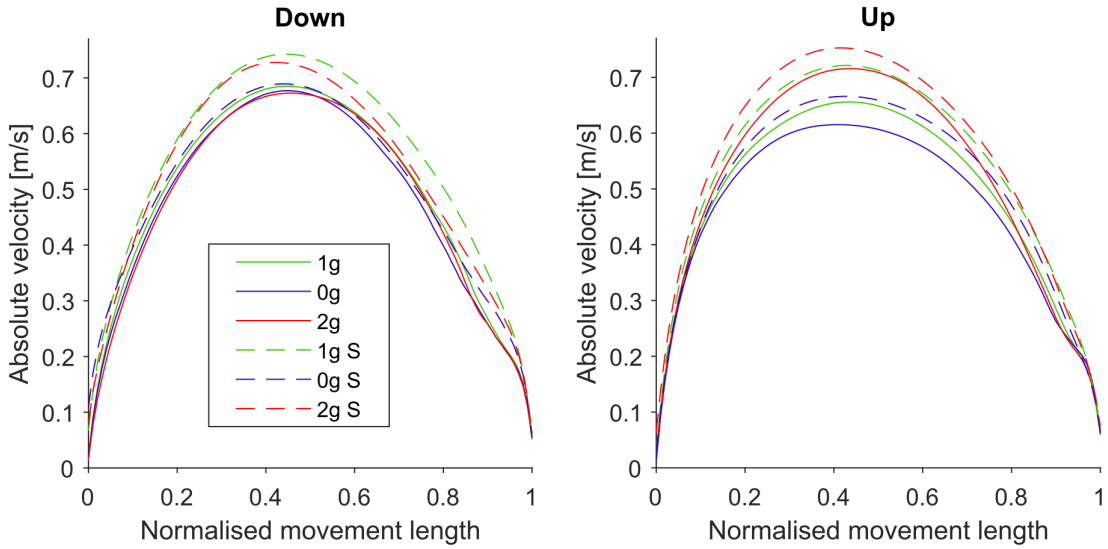

Figure 5.4: Mean velocity profiles for downward and upward movements in all conditions. Solid lines represent the conditions during flight (1g, 0g, 2g) whereas dashed lines represent the simulated conditions (1g S, 0g S, 2g S). Green represents normogravity, blue represents microgravity and red represents hypergravity conditions.

Table 5.3: Post hoc analysis for maximum velocity.

	Down				Up			
	Comparison	z	p		Comparison	z	p	
0 g	1g – 0g	-1.005	1.000		1g – 0g	3.260	.008	**
	1g S – 0g S	3.713	<.001	**	1g S – 0g S	4.323	<.001	***
	0g S – 0g	0.455	1.000		0g S – 0g	-0.079	1.000	
2 g	1g – 2g	-0.601	1.000		1g – 2g	-5.206	<.001	***
	1g S – 2g S	0.387	1.000		1g S – 2g S	-2.693	.050	*
	2g S – 2g	-3.346	.006	**	2g S – 2g	0.553	1.000	
1 g	1g S – 1g	4.334	<.001	***	1g S – 1g	-1.540	.865	

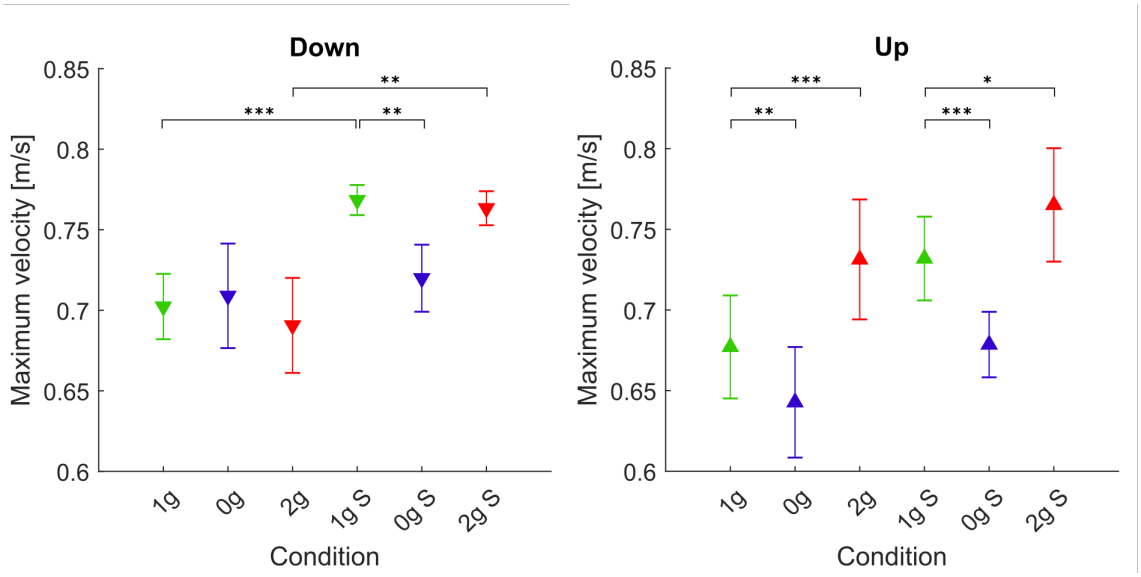

Figure 5.5: Maximum velocities. Downward pointing triangles denote mean values for downward movements, upward pointing triangles denote mean values for upward movements, the whiskers denote the standard error of mean. Green represents normogravity, blue represents microgravity and red represents hypergravity conditions, (1g, 0g, 2g) denote in-flight gravitational conditions, (1g S, 0g S, 2g S) denote simulated gravitational conditions. * $p < 0.05$, ** $p < 0.01$, *** $p < 0.001$.

5.3.2.3 Shape of trajectories

Figure 5.6 shows the mean trajectories for all gravitational and simulation conditions normalized for target distance in the y direction. Here we can observe an increased displacement in the x direction in microgravity for upward movements, whereas for the downward movements we can see a decreased displacement in the x direction both in microgravity and hypergravity. In order to more clearly compare the differences between conditions, we present the maximum normalized displacements in x direction for each gravitational and simulation condition, averaged for all parabolas and targets, in Figure 5.7. The post hoc tests results for the maximum displacements in x direction are presented in Table 5.4. For downward movements, the statistical analysis showed a significant effect of gravity ($F(2,278) = 64.02$, $p < .001$), simulation ($F(1,278) = 55.62$, $p < .001$) and the interaction of gravity × simulation ($F(2,278) = 4.95$, $p = .008$). In microgravity conditions, post hoc tests revealed that for downward movements there was a significant decrease in maximum x displacement for both the real and simulated trials (1g – 0g, 1g S – 0g S). The comparison of real and simulated microgravity conditions was not significantly different (0g S – 0g), albeit with a p value of 0.05. For hypergravity conditions, the maximum x displacement was lower than in normogravity for both real and simulated conditions (1g – 2g, 1g S– 2g S). At the same time, the displacement was significantly lower in the simulated hypergravity compared with the in-flight condition (2g S – 2g). Similarly, as with what we observed with the movement duration, the maximum x displacement in normogravity was lower in the simulated trials compared to those in-flight (1g S – 1g). For upward movements the statistical analysis showed a significant effect of gravity ($F(2,278) = 29.90$, $p < .001$), simulation ($F(1,278) = 90.97$, $p < .001$) and the interaction of gravity × simulation ($F(2,278) = 16.16$, $p < .001$). Post hoc test for microgravity conditions revealed that the maximum x displacement increased significantly only during flight (1g – 0g). The maximum x

displacement in the simulated microgravity appears to be unchanged from normogravity. This is also reflected in a significant difference between the real and simulated 0g condition (0g S – 0g). Maximum x displacement during hypergravity or simulated hypergravity was not significantly different compared to normogravity. However, a significant difference between real and simulated hypergravity (2g S – 2g) conditions was observed. No statistical difference was found when comparing both normogravity conditions for the upward movements.

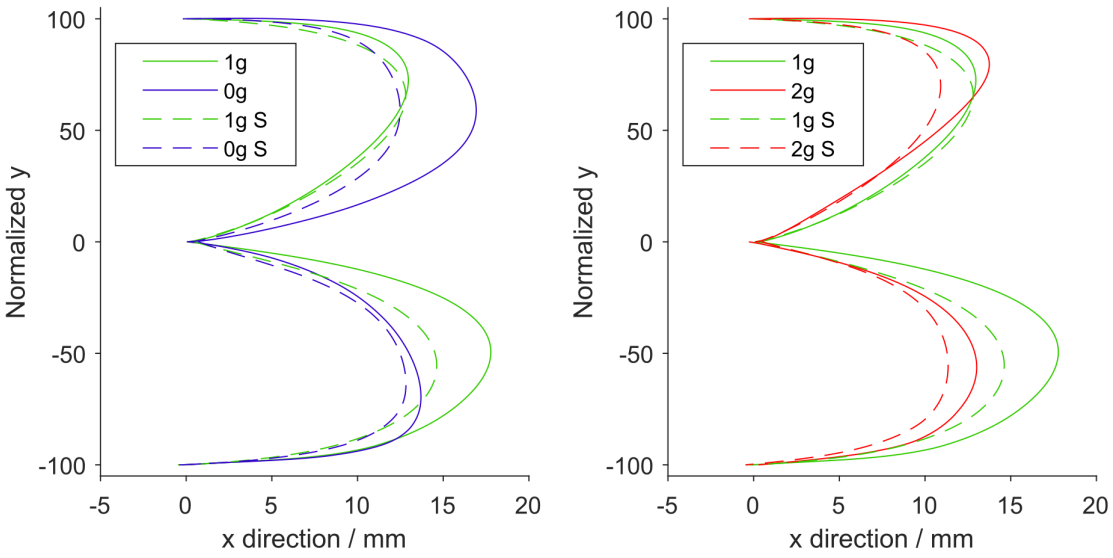

Figure 5.6: Mean trajectories normalized for target distance for different gravitational and simulation conditions. Left: normogravity and microgravity conditions, Right: normogravity and hypergravity conditions. All trajectories start at the coordinate (0,0) and end at either (0,100) for upward movements or (0,-100) for downward movements. Solid lines represent the conditions during flight (1g, 0g, 2g) whereas dashed lines represent the simulated conditions (1g S, 0g S, 2g S). Green represents normogravity, blue represents microgravity and red represents hypergravity conditions.

Table 5.4: Post hoc analysis for maximum displacement in the x direction.

	Down				Up			
	Comparison	z	p		Comparison	z	p	
0 g	1g – 0g	7.687	<.001	***	1g – 0g	-8.430	<.001	***
	1g S – 0g S	2.892	.027	*	1g S – 0g S	0.117	1.000	
	0g S – 0g	2.689	.050		0g S – 0g	9.707	<.001	***
2 g	1g – 2g	9.427	<.001	***	1g – 2g	-1.270	1.000	
	1g S – 2g S	5.459	<.001	***	1g S – 2g S	2.649	.057	
	2g S – 2g	3.715	.001	**	2g S – 2g	5.664	<.001	***
1 g	1g S – 1g	6.882	<.001	***	1g S – 1g	1.814	.488	

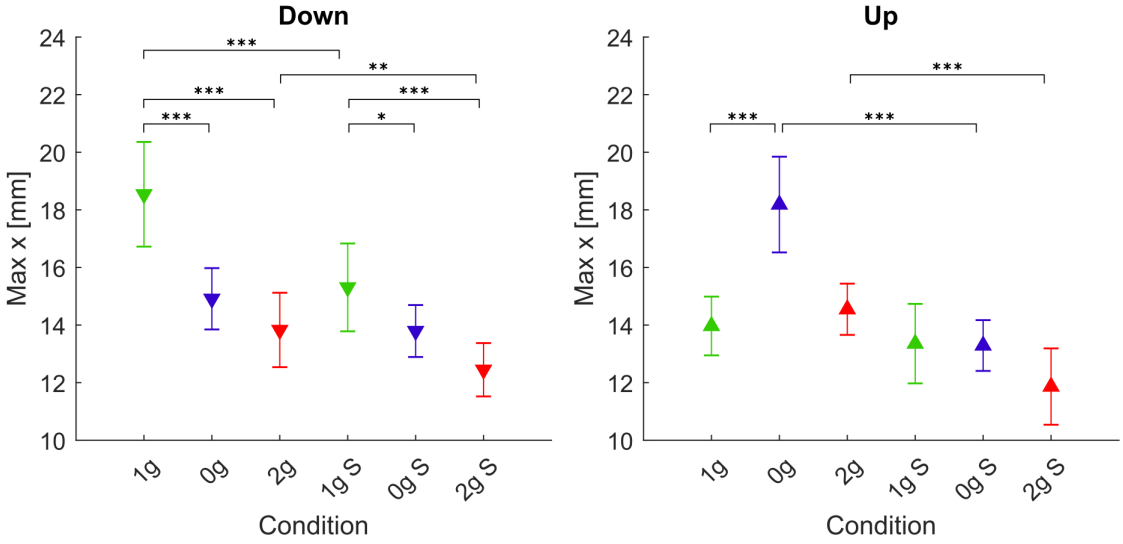

Figure 5.7: Maximum displacement in the x direction. Downward pointing triangles denote mean values for downward movements, upward pointing triangles denote mean values for upward movements, the whiskers denote the standard error of mean. Green represents normogravity, blue represents microgravity and red represents hypergravity conditions, (1g, 0g, 2g) denote in-flight gravitational conditions, (1g S, 0g S, 2g S) denote simulated gravitational conditions. * $p < 0.05$, ** $p < 0.01$, *** $p < 0.001$.

5.3.2.4 Movement asymmetry: time to peak velocity (TPV)

As a measure of the asymmetry of movement, we calculated the normalized TPV. The TPV for each gravitational and simulation condition averaged for all parabolas and targets, are shown in Figure 5.8, whereas post hoc tests results are presented in Table 5.5. For downward movements the statistical analysis showed a significant effect of simulation ($F(1,278) = 20.16$, $p < .001$), whereas the effect of gravity and the interaction of gravity × simulation were not significant ($F(2,278) = 2.30$, $p = .102$) and ($F(2,278) = 2.31$, $p = .101$) respectively. Concerning microgravity conditions, post hoc tests revealed no significant differences between conditions. For hypergravity conditions, TPV significantly decreased in the simulated condition (2g S – 2g). No changes were observed between normogravity conditions. For upward movements the statistical analysis showed no significant effects of gravity ($F(2,278) = 0.09$, $p = .912$) and simulation ($F(1,278) = 0.04$, $p = .839$), but it did reveal a significant interaction effect of gravity × simulation ($F(2,278) = 3.12$, $p = .046$) although the p value was nearly significant. The results of post hoc tests for the upward movements reflect the absence of significant effects.

5.3.3 Muscle activity

Due to a similar effect of conditions for both movement directions, we present the results of the muscle activity in a more concise form compared to the other parameters. The normalized iEMG of all muscles, for each gravitational and simulation condition, averaged for all parabolas and targets, are presented in Figure 5.9. The mean values for downward movements are denoted with downward pointing triangles and mean values of upward movements are denoted with upward pointing triangles. The ANOVA revealed a significant main effect of gravity for downward movements for the Trapezius ($F(2,246) = 152.99$, $p < .001$), Pectoralis ($F(2,246) = 12.60$, $p < .001$), Anterior Deltoid ($F(2,246) = 535.16$, $p <$

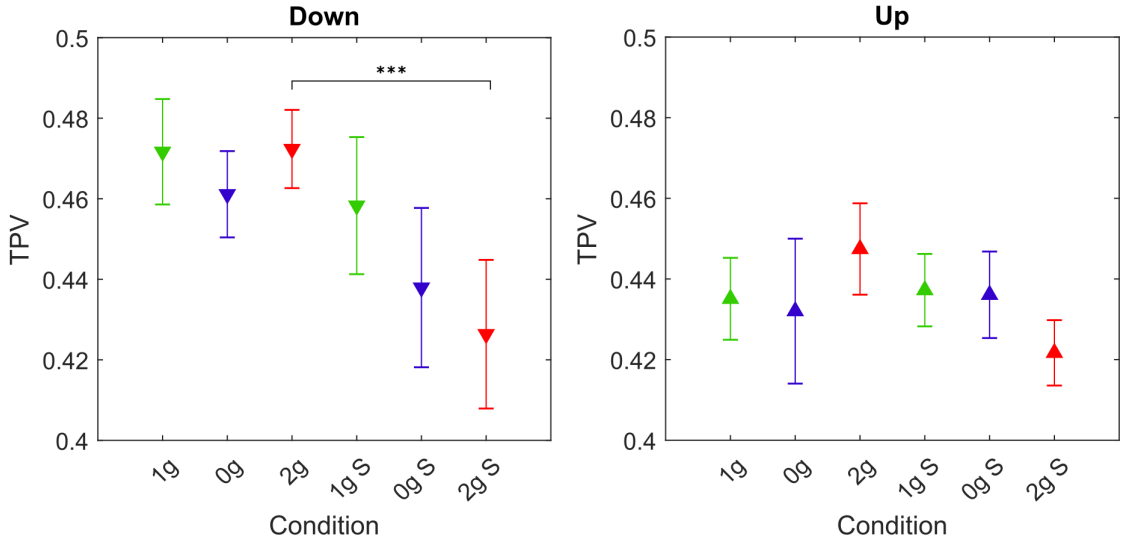

Figure 5.8: Values of the TPV parameter for different gravitational and simulation conditions. Downward pointing triangles denote mean values for downward movements, upward pointing triangles denote mean values for upward movements, the whiskers denote the standard error of mean. Green represents normogravity, blue represents microgravity and red represents hypergravity conditions, (1g, 0g, 2g) denote in-flight gravitational conditions, (1g S, 0g S, 2g S) denote simulated gravitational conditions. * $p < 0.05$, ** $p < 0.01$, *** $p < 0.001$.

Table 5.5: Post hoc analysis for TPV.

		Down			Up		
	Comparison	z	p		Comparison	z	p
0 g	1g – 0g	1.067	1.000		1g – 0g	0.395	1.000
	1g S – 0g S	1.708	.613		1g S – 0g S	0.115	1.000
	0g S – 0g	2.182	.204		0g S – 0g	-1.214	1.000
2 g	1g – 2g	-0.160	1.000		1g – 2g	-1.249	1.000
	1g S – 2g S	2.678	.052		1g S – 2g S	1.549	.850
	2g S – 2g	4.332	<.001	***	2g S – 2g	1.786	.519
1 g	1g S – 1g	1.430	1.000		1g S – 1g	-0.972	1.000

.001), and Posterior Deltoid ($F(2,246) = 185.83$, $p < .001$). A significant effect of simulation was found only for the Pectoralis ($F(1,246) = 43.33$, $p < .001$), Anterior Deltoid ($F(1,246) = 24.66$, $p < .001$) and Posterior Deltoid ($F(1,246) = 16.78$, $p < .001$) while there was no effect at the Trapezius muscle ($F(1,246) = 0.54$, $p = .461$). Most importantly, there was a significant interaction effect of gravity × simulation for the Trapezius ($F(2,246) = 4.55$, $p = .011$), Anterior Deltoid ($F(2,246) = 11.13$, $p < .001$) and Posterior Deltoid ($F(2,246) = 9.93$, $p < .001$), while there was no significant effect at the Pectoralis muscle ($F(2,246) = 0.31$, $p = .730$). Post hoc test results of the different conditions are presented in Table 5.6. For the upwards direction, the effects were exactly the same. We found a significant main effect of gravity for the Trapezius ($F(2,244) = 274.77$, $p < .001$), Pectoralis ($F(2,244) = 21.48$, $p < .001$) , Anterior Deltoid ($F(2,244) = 712.69$, $p < .001$) and Posterior Deltoid ($F(2,244) = 340.82$, $p < .001$). A significant effect of simulations was found for the Pectoralis ($F(1,244)$

= 44.55, p < .001), Anterior (F(1,244) = 38.41, p < .001) and Posterior Deltoid (F(1,244) = 17.35, p < .001), but not the Trapezius (F(1,244) = 0.03, p = .851). Analogous to the downward direction there was a significant interaction of gravity × simulation for the Trapezius (F(2,244) = 6.83, p = .001), Anterior Deltoid (F(2,244) = 20.02, p < .001) and Posterior Deltoid (F(2,244) = 11.87, p < .001), while there was no significant effect at the Pectoralis muscle (F(2,244) = 0.49, p = .609). Post hoc test results of the different conditions are presented in Table 5.6. For both directions and for all muscles we observed a decrease in muscle activity in both the real and simulated microgravity conditions compared to normogravity, whereas in the real and simulated hypergravity conditions we observed an increase in muscle activity compared to normogravity conditions.

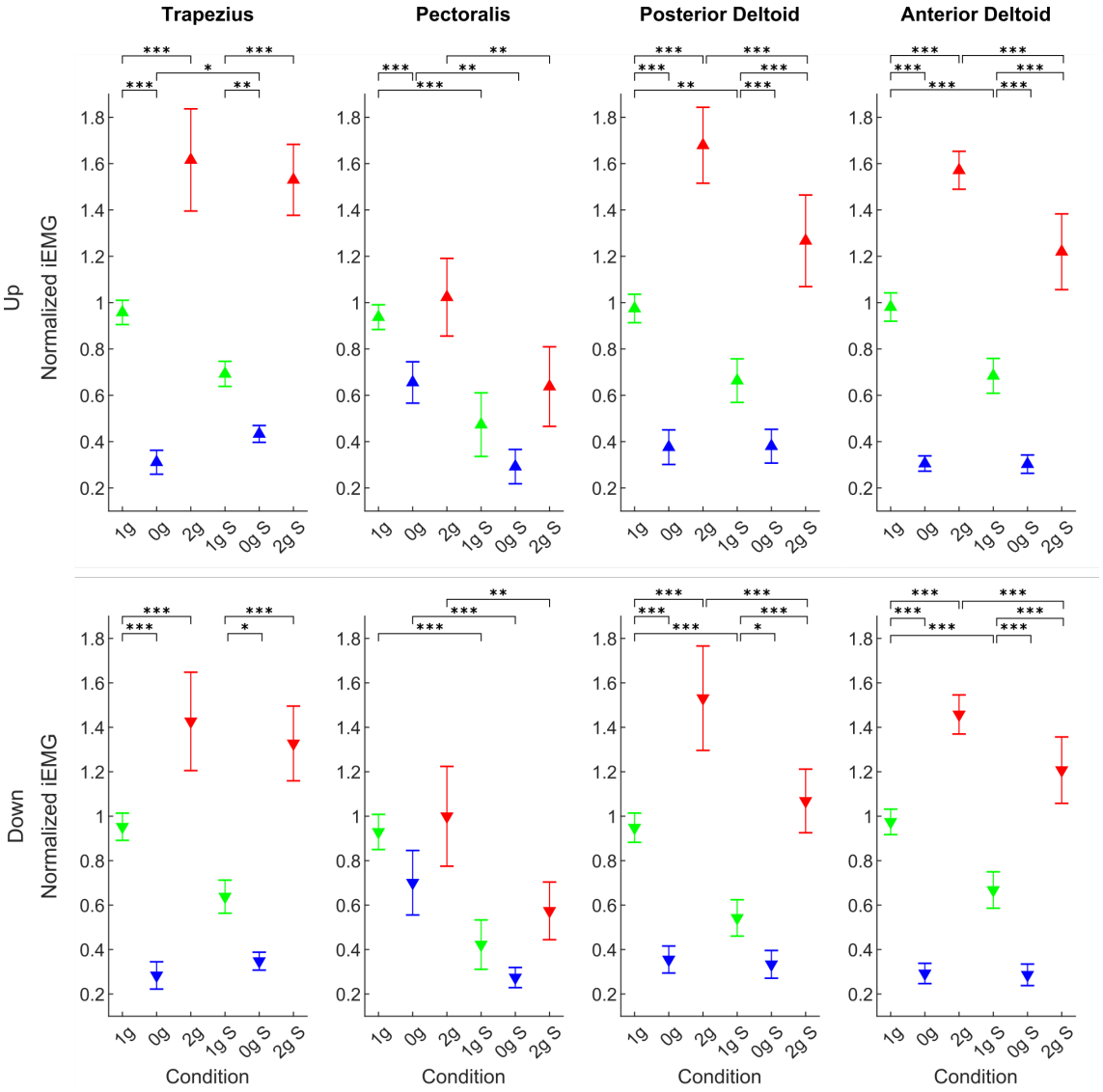

Figure 5.9: Normalized integrated EMG for the Trapezius, Pectoralis, Anterior Deltoid, and Posterior Deltoid for all conditions. Downward pointing triangles denote mean values for downward movements, upward pointing triangles denote mean values for upward movements, the whiskers denote the standard error of mean. Green represents normogravity, blue represents microgravity and red represents hypergravity conditions, (1g, 0g, 2g) denote in-flight gravitational conditions, (1g S, 0g S, 2g S) denote simulated gravitational conditions. * p < 0.05, ** p < 0.01, *** p < 0.001.

Table 5.6: Post hoc analysis for EMG.

		Down				Up			
		Comparison	z	p		Comparison	z	p	
Trapezius	0 g	1g – 0g	8.086	<.001	***	1g – 0g	9.387	<.001	***
		1g S – 0g S	3.188	.010	*	1g S – 0g S	3.365	.005	**
		0g S – 0g	-1.494	.946		0g S – 0g	-2.711	.047	*
	2g	1g – 2g	-5.789	<.001	***	1g – 2g	-9.345	<.001	***
		1g S – 2g S	-7.572	<.001	***	1g S – 2g S	-10.868	<.001	***
		2g S – 2g	0.135	1.000		2g S – 2g	-0.147	1.000	
	1 g	1g S – 1g	2.679	.052		1g S – 1g	2.465	.096	
Pectoralis	0 g	1g – 0g	2.665	.054		1g – 0g	3.877	<.001	***
		1g S – 0g S	1.719	.600		1g S – 0g S	2.192	.199	
		0g S – 0g	3.841	<.001	***	0g S – 0g	3.440	.004	**
	2g	1g – 2g	-0.780	1.000		1g – 2g	-1.051	1.000	
		1g S – 2g S	-1.760	.549		1g S – 2g S	-1.988	.328	
		2g S – 2g	3.417	.004	**	2g S – 2g	3.651	.002	**
	1 g	1g S – 1g	4.533	<.001	***	1g S – 1g	4.769	<.001	***
Posterior Deltoid	0 g	1g – 0g	8.512	<.001	***	1g – 0g	10.570	<.001	***
		1g S – 0g S	2.765	.040	*	1g S – 0g S	4.463	<.001	***
		0g S – 0g	-1.109	1.000		0g S – 0g	-1.386	1.000	
	2g	1g – 2g	-8.595	<.001	***	1g – 2g	-12.139	<.001	***
		1g S – 2g S	-6.967	<.001	***	1g S – 2g S	-9.512	<.001	***
		2g S – 2g	4.561	<.001	***	2g S – 2g	5.105	<.001	***
	1 g	1g S – 1g	3.893	<.001	***	1g S – 1g	3.745	.001	**
Anterior Deltoid	0 g	1g – 0g	15.632	<.001	***	1g – 0g	17.424	<.001	***
		1g S – 0g S	7.917	<.001	***	1g S – 0g S	8.717	<.001	***
		0g S – 0g	-0.776	1.000		0g S – 0g	-1.379	1.000	
	2g	1g – 2g	-11.278	<.001	***	1g – 2g	-14.970	<.001	***
		1g S – 2g S	-11.190	<.001	***	1g S – 2g S	-12.246	<.001	***
		2g S – 2g	4.213	<.001	***	2g S – 2g	6.808	<.001	***
	1 g	1g S – 1g	5.464	<.001	***	1g S – 1g	5.671	<.001	***

5.4 Discussion

During the parabolic flights, the subjects experienced changes in gravitational conditions that affected their whole body including the vestibular system. The forces exerted on the limbs of the individuals were continuous and acted on the entirety of the limb. Additionally, the stylus that the subjects were manipulating in order to perform the task was also subjected to these gravitational changes. On the other hand, in the trials on the ground, the subjects experienced only a locally applied force on the wrist that simulated the same torque in the shoulder joint the subjects experienced during microgravity and hypergravity during flight. Comparing these two conditions, we aimed to answer our main question.

Can we elicit the same changes in movement parameters only with simulating local gravity conditions on the arm compared to full body micro- and hypergravity conditions?

Effects on the task outcome

Looking at the task outcome, we noted a trend of increased hit deviations (reduced accuracy) in microgravity and hypergravity for upward and downward movements both in-flight and in simulation. This is in line with other studies which observed a decreased accuracy in these conditions [115], [124], [126]. However, these changes in deviations were only significant for the upward movements. We could not mimic the changes in hypergravity with our simulation, the subjects seemed to be better able to compensate for the force exerted on the wrist than when dealing with full-body hypergravity conditions. At first glance, we saw an increase in the absolute hit deviations in the simulated microgravity which coincided with the increased deviations observed in microgravity. However, the inspection of the signed deviations per target (Figure 5.2 B) revealed that the simulated microgravity condition affected the accuracy of subjects in a different way. Namely, in the 0g S condition, subjects overshot all of the targets whereas in microgravity as well as both normogravity conditions, the targets further away from the starting position (4-7) were mostly undershot. This shows that the subjects were better able to adapt to microgravity conditions during flight than in our simulation setup. Since the setup could not provide an adequate representation of microgravity conditions, namely the vestibular system and manipulated object were unaffected, it is probable that this resulted in some sort of sensory conflict that prevented the subjects from completing the task in the same way as in normogravity.

Effects on movement kinematics

Our analysis of the movement kinematics parameters showed that (compared to normogravity) the duration of movements increased in microgravity (0g and 0g S) for both upward and downward movements. The only exception being the downward movements in-flight (0g) where the increase in movement duration was not significant. On the other hand, the movement durations were lower in hypergravity in-flight for both directions of movement, but there was no change in movement duration in the simulation trials. These results are mostly consistent with other studies, where they also noted an increase of movement duration in microgravity and a decrease in hypergravity [119], [126], [136]. Interestingly, movement durations for downward movements were shorter in the simulated normogravity trials compared to those during flight (1g S versus 1g). Regarding the shape of the trajectories, we found an increased displacement in the x direction only in microgravity for the upward movements in-flight while there was no change during simulation. This could be explained by the fact that during flight the whole environment was isotropous which meant that subjects had to more actively refrain from moving sideways. In contrast, for the downward movements, we observed a decrease in displacement in the x direction in both microgravity and hypergravity in-flight and in the simulated trials. Compared to the upward movements, the task stability may have improved when performing downward movements which decreased the displacement in the x direction.

Changes in velocity profiles

The shape of the velocity profiles did not vary across different gravitational or simulation conditions which we showed with the analysis of the TPV parameter. However, we did note some changes in the maximum velocities. Namely, the maximum velocity was lower

in microgravity and higher in hypergravity for the upward movements both in-flight and in simulation. For the downward movements, however, there were no differences in flight, but in simulation, the maximum velocity was lower for the 0g S condition. Additionally, we observed that the TPV parameter remained largely unaffected by the different gravitational conditions both in-flight and in simulation. However, we noted a lower TPV in the simulated hypergravity compared to the in-flight hypergravity (2g S versus 2g).

Changes in muscle activity

The analysis of muscle activity showed that the Pectoralis muscle was the least affected by gravitational conditions both in flight and during simulation. This is probably because it acts primarily perpendicular to the gravitational vector. However, we still noted a significant decrease of activity in microgravity in-flight (0g). For all other muscles we observed the same results, where for both directions, the muscle activity was significantly increased in real and simulated hypergravity conditions and lowered in the microgravity conditions. This is comparable with other studies with pointing tasks performed on parabolic flights [137], where EMG activity increased in hypergravity and decreased in microgravity. Our results therefore show that the simulations of gravitational environments with our system were quite good from an action point of view.

Could on-ground training with simulated gravitational conditions be beneficial?

Apart from the trajectory shape, the locally simulated microgravity and hypergravity conditions of the limb appear to have a similar effect on the kinematic parameters analyzed. That is, increased movement durations in microgravity, decreased maximum velocities in microgravity and increased in hypergravity as well as an unaffected asymmetry of movement. Additionally, the muscle activity was lower in microgravity and higher in hypergravity conditions. This indicates that training in normogravity conditions with only locally simulated microgravity or hypergravity could be beneficial for training arm reaching movements in microgravity and hypergravity [138]. The discrepancy between the changes in the maximal x displacement and movement durations could potentially stem from the fact that our active support system had contact only at the wrist. Such a simulation of microgravity did not have the full effect as during the parabolic flight, it did however elicit similar responses when looking at the duration of movements. This also demonstrates that proprioceptive feedback provides a lot of relevant information to control kinematics. Perhaps analyzing the impact of an exoskeleton device with a distributed whole limb gravity compensation would be interesting. A distributed unloading of the arm could potentially provide better feedback to the subjects and hence provide a better environment for training movements in microgravity and hypergravity. In [124] they observed reduced accuracy of subjects in both microgravity and hypergravity conditions. In microgravity, their accuracy was restored to normal when they applied a gravity-like torque before and during the movements performed. Their results suggest that arm motor planning and control are tuned with respect to gravitational information issued from joint torque. Similar conclusions were found by [139], where they showed that information coming from the initial state of the sensorimotor system is determinant to planning movements in the gravity field. However, in these studies, the subjects were not manipulating any object with their hand as was the case in our experiment. During the microgravity condition, the subjects did not feel any weight at the stylus while maintaining the position at the starting position. The motor system is likely to interpret this as the absence of mass and resultantly reduces the motor command for the movements. However, the motor command to accelerate the stylus should remain unchanged because the mass is not changed, slowing the movement and increasing

the movement duration. In our simulated microgravity conditions, the object manipulated was still affected by gravity thereby creating a sensory conflict in the estimation of the arm and object dynamics. While we still observed similar changes in 0g and 0g S (e.g. increased movement duration), the analysis of the deviations of target hits revealed that the subjects consistently overshot the targets, which resulted in a worse performance in the simulated microgravity (0g S) compared to the microgravity (0g) condition. Notably, our observed changes in movement duration and maximum velocity in the simulated microgravity conditions are in contrast with some other studies that analyzed changes in kinematic features of arm movements in normogravity with weight support systems [129], [130], where such changes were not present. However, in these studies, movements were not limited to vertical arm movements which might be the cause of the differences in the observed results. Similarly, in a parabolic flight study where subjects performed pointing movements predominantly in the horizontal direction no significant differences between gravitational conditions were observed for movement duration and accuracy of pointing [140]. Overall, we showed that locally simulated gravity alterations can elicit similar changes in movement characteristics for arm reaching movements and could potentially be used as a means of training individuals prior to undertaking tasks in changed gravitational conditions.

Chapter 6

Conclusions

The major contributions of this thesis are summarised in the following four points.

First, we expanded the field of exoskeleton control by developing a control architecture based on probabilistic approaches for use in quasi-passive or quasi-active exoskeleton devices [141]. With a successful implementation of the proposed approach we confirmed our first hypothesis. This is an important contribution as such types of exoskeletons are being increasingly developed in recent years while at the same time there is a lack of suitable control algorithms that are developed and tested on such devices.

Second, we explored the capabilities of using probabilistic approaches for predicting gait kinematic parameters for the purpose of using these predictions as control inputs for lower limb exoskeletal devices. The results confirmed our second hypothesis since we were able to accurately predict user step lengths. Such an approach can be used in combination with other environmental sensing modalities in order to predict possible collisions of the user's limbs with obstacles [142] and use this information to execute preventive countermeasures with the exoskeleton the user is wearing.

Third, we expanded the use cases of state-of-the-art path guidance algorithms used in rehabilitation with robotic devices. This was achieved through the integration of these guiding algorithms with probabilistic methods for user movement trajectory prediction [99]. We successfully confirmed hypothesis H3-H5 by accurately predicting user movement intention even for new target locations which enabled a seamless human-robot interaction and assistance for all end targets. Overall, this approach enhances the field of exoskeleton control as well as control of end effector based types of rehabilitation devices where there is currently a lack of user movement prediction and the approaches used are rather static, and apart from use with chronic stroke patients, are still not as effective as conventional physical therapy.

Fourth, we showed that locally simulated gravity alterations can elicit similar changes in movement characteristics for arm reaching movements thereby confirming our sixth and final hypothesis. We concluded that such an approach can potentially be used as a means of training individuals prior to undertaking tasks in changed gravitational conditions with the use of robotic devices such as exoskeletons [143].

As with all research, for every question we answered we opened up many new ones. We will attempt to address as many of them as possible in our future work. Hopefully however, this thesis and the work published in the scope of it will serve as inspiration also for other researchers in the field of exoskeleton control and human-robot interaction and contribute to a collective expansion of the state of the art for these fields of robotics.

References

[1] T. McFarland and S. Fischer, "Considerations for Industrial Use: A Systematic Review of the Impact of Active and Passive Upper Limb Exoskeletons on Physical Exposures," *IISE Transactions on Occupational Ergonomics and Human Factors*, vol. 7, no. 3-4, pp. 322–347, Oct. 2019, ISSN: 2472-5838. DOI: 10.1080/24725838.2019.1684399.

[2] D. Shi, W. Zhang, W. Zhang, and X. Ding, "A Review on Lower Limb Rehabilitation Exoskeleton Robots," *Chinese Journal of Mechanical Engineering (English Edition)*, vol. 32, no. 1, 2019, ISSN: 21928258. DOI: 10.1186/s10033-019-0389-8.

[3] A. Wall, J. Borg, and S. Palmcrantz, "Clinical application of the Hybrid Assistive Limb (HAL) for gait training a systematic review," *Frontiers in Systems Neuroscience*, vol. 9, no. March, Mar. 2015, ISSN: 1662-5137. DOI: 10.3389/fnsys.2015.00048.

[4] G. Bao, L. Pan, H. Fang, *et al.*, "Academic Review and Perspectives on Robotic Exoskeletons," *IEEE Transactions on Neural Systems and Rehabilitation Engineering*, vol. 27, no. 11, pp. 2294–2304, 2019, ISSN: 15580210. DOI: 10.1109/TNSRE.2019.2944655.

[5] S. Toxiri, A. Calanca, J. Ortiz, P. Fiorini, and D. G. Caldwell, "A Parallel-Elastic Actuator for a Torque-Controlled Back-Support Exoskeleton," *IEEE Robotics and Automation Letters*, vol. 3, no. 1, pp. 492–499, Jan. 2018, ISSN: 2377-3766. DOI: 10.1109/LRA.2017.2768120.

[6] H. Hara and Y. Sankai, "Development of HAL for lumbar support," in *SCIS and ISIS 2010 - Joint 5th International Conference on Soft Computing and Intelligent Systems and 11th International Symposium on Advanced Intelligent Systems*, Okayama, Japan: Japan Society for Fuzzy Theory and Intelligent Informatics, 2010, pp. 416–421. DOI: 10.14864/softscis.2010.0.416.0.

[7] T. Noda, T. Teramae, B. Ugurlu, and J. Morimoto, "Development of an upper limb exoskeleton powered via pneumatic electric hybrid actuators with bowden cable," *IEEE International Conference on Intelligent Robots and Systems*, no. Iros, pp. 3573–3578, 2014, ISSN: 21530866. DOI: 10.1109/IROS.2014.6943062.

[8] P. Maurice, S. Ivaldi, J. Babic, *et al.*, "Objective and Subjective Effects of a Passive Exoskeleton on Overhead Work," *IEEE Transactions on Neural Systems and Rehabilitation Engineering*, vol. 28, no. 1, pp. 152–164, 2019, ISSN: 1534-4320. DOI: 10.1109/tnsre.2019.2945368.

[9] E. Rashedi, S. Kim, M. A. Nussbaum, and M. J. Agnew, "Ergonomic evaluation of a wearable assistive device for overhead work," *Ergonomics*, vol. 57, no. 12, pp. 1864–1874, 2014. DOI: 10.1080/00140139.2014.952682.

[10] S. J. Baltrusch, J. H. van Dieën, S. M. Bruijn, A. S. Koopman, C. A. M. van Bennekom, and H. Houdijk, "The effect of a passive trunk exoskeleton on metabolic costs during lifting and walking," *Ergonomics*, vol. 62, no. 7, pp. 903–916, 2019. DOI: 10.1080/00140139.2019.1602288.

[11] S. J. Baltrusch, J. H. van Dieën, A. S. Koopman, *et al.*, "SPEXOR passive spinal exoskeleton decreases metabolic cost during symmetric repetitive lifting," *European Journal of Applied Physiology*, vol. 120, no. 2, pp. 401–412, 2020, ISSN: 14396327. DOI: 10.1007/s00421-019-04284-6.

[12] M. Dežman, J. Babič, and A. Gams, "Qualitative assessment of a clutch-actuated ankle exoskeleton," in *Mechanisms and Machine Science*, vol. 49, Springer Netherlands, 2018, pp. 778–786, ISBN: 9783319612751. DOI: 10.1007/978-3-319-61276-8_82.

[13] M. Grimmer, M. Eslamy, S. Gliech, and A. Seyfarth, "A comparison of parallel- and series elastic elements in an actuator for mimicking human ankle joint in walking and running," in *Proceedings - IEEE International Conference on Robotics and Automation*, Institute of Electrical and Electronics Engineers Inc., 2012, pp. 2463–2470, ISBN: 9781467314039. DOI: 10.1109/ICRA.2012.6224967.

[14] M. Dežman and A. Gams, "Rotatable cam-based variable-ratio lever compliant actuator for wearable devices," *Mechanism and Machine Theory*, vol. 130, pp. 508–522, Dec. 2018, ISSN: 0094114X. DOI: 10.1016/j.mechmachtheory.2018.09.006.

[15] H. A. Varol, F. Sup, and M. Goldfarb, "Multiclass real-time intent recognition of a powered lower limb prosthesis," *IEEE Transactions on Biomedical Engineering*, vol. 57, no. 3, pp. 542–551, Mar. 2010, ISSN: 00189294. DOI: 10.1109/TBME.2009.2034734.

[16] M. R. Tucker, J. Olivier, A. Pagel, *et al.*, "Control strategies for active lower extremity prosthetics and orthotics: a review," *Journal of NeuroEngineering and Rehabilitation*, vol. 12, no. 1, p. 1, 2015, ISSN: 1743-0003. DOI: 10.1186/1743-0003-12-1.

[17] M. A. Gull, S. Bai, and T. Bak, "A review on design of upper limb exoskeletons," *Robotics*, vol. 9, no. 1, pp. 1–35, 2020, ISSN: 22186581. DOI: 10.3390/robotics9010016.

[18] D. Baiden and O. Ivlev, "Human-robot-interaction control for orthoses with pneumatic soft-actuators - Concept and initial trails," in *IEEE International Conference on Rehabilitation Robotics*, 2013, ISBN: 9781467360241. DOI: 10.1109/ICORR.2013.6650353.

[19] O. Dermy, A. Paraschos, M. Ewerton, J. Peters, F. Charpillet, and S. Ivaldi, "Prediction of intention during interaction with iCub with probabilistic movement primitives," *Frontiers Robotics AI*, vol. 4, no. OCT, pp. 1–27, 2017, ISSN: 22969144. DOI: 10.3389/frobt.2017.00045.

[20] M. Goldfarb, B. E. Lawson, and A. H. Shultz, "Realizing the promise of robotic leg prostheses," *Science Translational Medicine*, vol. 5, no. 210, 2013, ISSN: 19466234. DOI: 10.1126/scitranslmed.3007312.

[21] A. J. Young and D. P. Ferris, "State of the Art and Future Directions for Lower Limb Robotic Exoskeletons.," *IEEE transactions on neural systems and rehabilitation engineering : a publication of the IEEE Engineering in Medicine and Biology Society*, vol. 25, no. 2, pp. 171–182, 2017, ISSN: 1558-0210 (Electronic). DOI: 10.1109/TNSRE.2016.2521160.

[22] F. Sup, H. A. Varol, and M. Goldfarb, "Upslope walking with a powered knee and ankle prosthesis: Initial results with an amputee subject," *IEEE Transactions on Neural Systems and Rehabilitation Engineering*, vol. 19, no. 1, pp. 71–78, Feb. 2011, ISSN: 15344320. DOI: 10.1109/TNSRE.2010.2087360.

[23] B. Chen, L. Grazi, F. Lanotte, N. Vitiello, and S. Crea, "A real-time lift detection strategy for a hip exoskeleton," *Frontiers in Neurorobotics*, vol. 12, no. APR, Apr. 2018, ISSN: 16625218. DOI: 10.3389/fnbot.2018.00017.

[24] F. Attal, S. Mohammed, M. Dedabrishvili, F. Chamroukhi, L. Oukhellou, and Y. Amirat, "Physical Human Activity Recognition Using Wearable Sensors," *Sensors 2015, Vol. 15, Pages 31314-31338*, vol. 15, no. 12, pp. 31 314–31 338, Dec. 2015. DOI: 10.3390/s151229858.

[25] S. J. Preece, J. Y. Goulermas, L. P. J. Kenney, D. Howard, K. Meijer, and R. Crompton, "Activity identification using body-mounted sensors—a review of classification techniques," *Physiological Measurement*, vol. 30, no. 4, R1–R33, Apr. 2009, ISSN: 0967-3334. DOI: 10.1088/0967-3334/30/4/R01.

[26] D. Novak and R. Riener, "A survey of sensor fusion methods in wearable robotics," *Robotics and Autonomous Systems*, vol. 73, pp. 155–170, 2015, ISSN: 09218890. DOI: 10.1016/j.robot.2014.08.012.

[27] B. Chen, F. Lanotte, L. Grazi, N. Vitiello, and S. Crea, "Classification of Lifting Techniques for Application of A Robotic Hip Exoskeleton," *Sensors*, vol. 19, no. 4, p. 963, Feb. 2019, ISSN: 1424-8220. DOI: 10.3390/s19040963.

[28] M. Roerdink, B. Coolen, B. Clairbois, C. J. Lamoth, and P. J. Beek, "Online gait event detection using a large force platform embedded in a treadmill," *Journal of Biomechanics*, vol. 41, no. 12, pp. 2628–2632, Aug. 2008, ISSN: 00219290. DOI: 10.1016/j.jbiomech.2008.06.023.

[29] M. Pijnappels, M. F. Bobbert, and J. H. van Dieën, "Changes in walking pattern caused by the possibility of a tripping reaction," *Gait & Posture*, vol. 14, no. 1, pp. 11–18, Jul. 2001, ISSN: 09666362. DOI: 10.1016/S0966-6362(01)00110-2.

[30] M. Roerdink, C. J. Lamoth, G. Kwakkel, P. C. van Wieringen, and P. J. Beek, "Gait Coordination After Stroke: Benefits of Acoustically Paced Treadmill Walking," *Physical Therapy*, vol. 87, no. 8, pp. 1009–1022, Aug. 2007, ISSN: 0031-9023. DOI: 10.2522/ptj.20050394.

[31] L. Hak, H. Houdijk, F. Steenbrink, *et al.*, "Stepping strategies for regulating gait adaptability and stability," *Journal of Biomechanics*, vol. 46, no. 5, pp. 905–911, Mar. 2013, ISSN: 00219290. DOI: 10.1016/j.jbiomech.2012.12.017.

[32] A. Martínez, B. Lawson, and M. Goldfarb, "A Controller for Guiding Leg Movement during Overground Walking with a Lower Limb Exoskeleton," *IEEE Transactions on Robotics*, vol. 34, no. 1, pp. 183–193, 2018, ISSN: 15523098. DOI: 10.1109/TRO.2017.2768035.

[33] B. Chen, L. Grazi, F. Lanotte, N. Vitiello, and S. Crea, "Lift movement detection with a QDA classifier for an active hip exoskeleton," in *Biosystems and Biorobotics*, vol. 22, Springer International Publishing, 2019, pp. 224–228, ISBN: 9783030018870. DOI: 10.1007/978-3-030-01887-0_43.

[34] T. Poliero, M. Lazzaroni, S. Toxiri, C. Di Natali, D. G. Caldwell, and J. Ortiz, "Applicability of an Active Back-Support Exoskeleton to Carrying Activities," *Frontiers in Robotics and AI*, vol. 7, p. 579 963, Dec. 2020, ISSN: 22969144. DOI: 10.3389/frobt.2020.579963.

[35] T. Yan, M. Cempini, C. M. Oddo, and N. Vitiello, "Review of assistive strategies in powered lower-limb orthoses and exoskeletons," *Robotics and Autonomous Systems*, vol. 64, pp. 120–136, Feb. 2015, ISSN: 09218890. DOI: 10.1016/j.robot.2014.09.032.

[36] H. Vallery, J. Veneman, E. van Asseldonk, R. Ekkelenkamp, M. Buss, and H. van Der Kooij, "Compliant actuation of rehabilitation robots," *IEEE Robotics and Automation Magazine*, vol. 15, no. 3, pp. 60–69, 2008, ISSN: 10709932. DOI: 10.1109/MRA.2008.927689.

[37] D. Aoyagi, W. E. Ichinose, S. J. Harkema, D. J. Reinkensmeyer, and J. E. Bobrow, "A robot and control algorithm that can synchronously assist in naturalistic motion during body-weight-supported gait training following neurologic injury," *IEEE Transactions on Neural Systems and Rehabilitation Engineering*, vol. 15, no. 3, pp. 387–400, Sep. 2007, ISSN: 15344320. DOI: 10.1109/TNSRE.2007.903922.

[38] A. Martinez, B. Lawson, C. Durrough, and M. Goldfarb, "A Velocity-Field-Based Controller for Assisting Leg Movement during Walking with a Bilateral Hip and Knee Lower Limb Exoskeleton," *IEEE Transactions on Robotics*, vol. 35, no. 2, pp. 307–316, 2019, ISSN: 15523098. DOI: 10.1109/TRO.2018.2883819.

[39] S. K. Banala, S. H. Kim, S. K. Agrawal, and J. P. Scholz, "Robot assisted gait training with active leg exoskeleton (ALEX)," *Proceedings of the 2nd Biennial IEEE/RAS-EMBS International Conference on Biomedical Robotics and Biomechatronics, BioRob 2008*, vol. 17, no. 1, pp. 653–658, 2008. DOI: 10.1109/BIOROB.2008.4762885.

[40] A. Duschau-Wicke, J. von Zitzewitz, A. Caprez, L. Lunenburger, and R. Riener, "Path Control: A Method for Patient-Cooperative Robot-Aided Gait Rehabilitation," *IEEE Transactions on Neural Systems and Rehabilitation Engineering*, vol. 18, no. 1, pp. 38–48, Feb. 2010, ISSN: 1534-4320. DOI: 10.1109/TNSRE.2009.2033061.

[41] A. Ijspeert, J. Nakanishi, and S. Schaal, "Movement imitation with nonlinear dynamical systems in humanoid robots," in *Proceedings 2002 IEEE International Conference on Robotics and Automation (Cat. No.02CH37292)*, vol. 2, IEEE, 2002, pp. 1398–1403, ISBN: 0-7803-7272-7. DOI: 10.1109/ROBOT.2002.1014739.

[42] A. J. Ijspeert, J. Nakanishi, H. Hoffmann, P. Pastor, and S. Schaal, "Dynamical Movement Primitives: Learning Attractor Models for Motor Behaviors," *Neural Computation*, vol. 25, no. 2, pp. 328–373, Feb. 2013, ISSN: 0899-7667. DOI: 10.1162/NECO_a_00393.

[43] E. Ugur and H. Girgin, "Compliant parametric dynamic movement primitives," *Robotica*, vol. 38, no. 3, pp. 457–474, 2020, ISSN: 14698668. DOI: 10.1017/S02635747.1900078X.

[44] S. Calinon, F. D'halluin, E. Sauser, D. Caldwell, and A. Billard, "Learning and Reproduction of Gestures by Imitation," *IEEE Robotics & Automation Magazine*, vol. 17, no. 2, pp. 44–54, Jun. 2010, ISSN: 1070-9932. DOI: 10.1109/MRA.2010.936947.

[45] A. Paraschos, G. Neumann, and J. Peters, "A probabilistic approach to robot trajectory generation," in *IEEE-RAS International Conference on Humanoid Robots*, vol. 2015-Febru, IEEE Computer Society, Feb. 2015, pp. 477–483, ISBN: 9781479926176. DOI: 10.1109/HUMANOIDS.2013.7030017.

[46] D. Vogt, S. Stepputtis, S. Grehl, B. Jung, and H. Ben Amor, "A system for learning continuous human-robot interactions from human-human demonstrations," in *Proceedings - IEEE International Conference on Robotics and Automation*, Institute of Electrical and Electronics Engineers Inc., Jul. 2017, pp. 2882–2889, ISBN: 9781509046331. DOI: 10.1109/ICRA.2017.7989334.

[47] T. Osa, K. Harada, N. Sugita, and M. Mitsuishi, "Trajectory planning under different initial conditions for surgical task automation by learning from demonstration," in *Proceedings - IEEE International Conference on Robotics and Automation*, Institute of Electrical and Electronics Engineers Inc., Sep. 2014, pp. 6507–6513. DOI: 10.1109/ICRA.2014.6907819.

[48] C. Perez-D'Arpino and J. A. Shah, "Fast target prediction of human reaching motion for cooperative human-robot manipulation tasks using time series classification," in *Proceedings - IEEE International Conference on Robotics and Automation*, vol. 2015-June, Institute of Electrical and Electronics Engineers Inc., Jun. 2015, pp. 6175–6182. DOI: 10.1109/ICRA.2015.7140066.

[49] M. Wu, B. Taetz, E. D. Saraiva, G. Bleser, and S. Liu, "On-line Motion Prediction and Adaptive Control in Human-Robot Handover Tasks," in *Proceedings of IEEE Workshop on Advanced Robotics and its Social Impacts, ARSO*, vol. 2019-Octob, IEEE Computer Society, Oct. 2019, pp. 1–6, ISBN: 9781728131764. DOI: 10.1109/ARSO46408.2019.8948750.

[50] Q. Li, Z. Zhang, Y. You, Y. Mu, and C. Feng, "Data Driven Models for Human Motion Prediction in Human-Robot Collaboration," *IEEE Access*, 2020, ISSN: 21693536. DOI: 10.1109/ACCESS.2020.3045994.

[51] M. Ewerton, G. Maeda, J. Peters, and G. Neumann, "Learning motor skills from partially observed movements executed at different speeds," *IEEE International Conference on Intelligent Robots and Systems*, vol. 2015-Decem, pp. 456–463, 2015, ISSN: 21530866. DOI: 10.1109/IROS.2015.7353412.

[52] G. Maeda, M. Ewerton, G. Neumann, R. Lioutikov, and J. Peters, "Phase estimation for fast action recognition and trajectory generation in human–robot collaboration," *International Journal of Robotics Research*, vol. 36, no. 13-14, pp. 1579–1594, 2017, ISSN: 17413176. DOI: 10.1177/0278364917693927.

[53] E. Rueckert, J. Čamernik, J. Peters, and J. Babič, "Probabilistic Movement Models Show that Postural Control Precedes and Predicts Volitional Motor Control," *Scientific Reports*, vol. 6, no. 1, p. 28 455, Sep. 2016, ISSN: 2045-2322. DOI: 10.1038/srep28455.

[54] C. Nguiadem, M. Raison, and S. Achiche, *Motion planning of upper-limb exoskeleton robots: A review*, Nov. 2020. DOI: 10.3390/app10217626.

[55] L. Peternel, N. Tsagarakis, D. Caldwell, and A. Ajoudani, "Robot adaptation to human physical fatigue in human–robot co-manipulation," *Autonomous Robots*, vol. 42, no. 5, pp. 1011–1021, Jun. 2018, ISSN: 15737527. DOI: 10.1007/s10514-017-9678-1.

[56] L. Peternel, T. Petrič, and J. Babič, "Robotic assembly solution by human-in-the-loop teaching method based on real-time stiffness modulation," *Autonomous Robots*, vol. 42, no. 1, pp. 1–17, Jan. 2018, ISSN: 15737527. DOI: 10.1007/s10514-017-9635-z.

[57] L. Peternel, T. Noda, T. Petrič, A. Ude, J. Morimoto, and J. Babič, "Adaptive control of exoskeleton robots for periodic assistive behaviours based on EMG feedback minimisation," *PLoS ONE*, vol. 11, no. 2, pp. 1–26, 2016, ISSN: 19326203. DOI: 10.1371/journal.pone.0148942.

[58] H. I. Krebs, J. J. Palazzolo, L. Dipietro, *et al.*, "Rehabilitation Robotics: Performance-Based Progressive Robot-Assisted Therapy," *Autonomous Robots 2003 15:1*, vol. 15, no. 1, pp. 7–20, Jul. 2003, ISSN: 1573-7527. DOI: 10.1023/A:1024494031121.

[59] R. Riener, L. Lünenburger, S. Jezernik, M. Anderschitz, G. Colombo, and V. Dietz, "Patient-cooperative strategies for robot-aided treadmill training: First experimental results," *IEEE Transactions on Neural Systems and Rehabilitation Engineering*, vol. 13, no. 3, pp. 380–394, Sep. 2005, ISSN: 15344320. DOI: 10.1109/TNSRE.2005.848628.

[60] W. Kim, L. Peternel, M. Lorenzini, J. Babič, and A. Ajoudani, "A Human-Robot Collaboration Framework for Improving Ergonomics During Dexterous Operation of Power Tools," *Robotics and Computer-Integrated Manufacturing*, vol. 68, Apr. 2021, ISSN: 07365845. DOI: 10.1016/j.rcim.2020.102084.

[61] E. B. Weston, M. Alizadeh, G. G. Knapik, X. Wang, and W. S. Marras, "Biomechanical evaluation of exoskeleton use on loading of the lumbar spine," *Applied Ergonomics*, vol. 68, pp. 101–108, Apr. 2018, ISSN: 18729126. DOI: 10.1016/j.apergo.2017.11.006.

[62] J. Theurel, K. Desbrosses, T. Roux, and A. Savescu, "Physiological consequences of using an upper limb exoskeleton during manual handling tasks," *Applied Ergonomics*, vol. 67, pp. 211–217, Feb. 2018, ISSN: 18729126. DOI: 10.1016/j.apergo.2017.10.008.

[63] L. Van Engelhoven, N. Poon, H. Kazerooni, A. Barr, D. Rempel, and C. Harris-Adamson, "Evaluation of an adjustable support shoulder exoskeleton on static and dynamic overhead tasks," *Proceedings of the Human Factors and Ergonomics Society Annual Meeting*, vol. 62, no. 1, pp. 804–808, Sep. 2018, ISSN: 2169-5067. DOI: 10.1177/1541931218621184.

[64] S. Kim, M. A. Nussbaum, M. I. Mokhlespour Esfahani, M. M. Alemi, S. Alabdulkarim, and E. Rashedi, "Assessing the influence of a passive, upper extremity exoskeletal vest for tasks requiring arm elevation: Part I - Expected effects on discomfort, shoulder muscle activity, and work task performance," *Applied Ergonomics*, vol. 70, no. September 2017, pp. 315–322, 2018, ISSN: 18729126. DOI: 10.1016/j.apergo.2018.02.025.

[65] N. Sylla, V. Bonnet, F. Colledani, and P. Fraisse, "Ergonomic contribution of ABLE exoskeleton in automotive industry," *International Journal of Industrial Ergonomics*, vol. 44, no. 4, pp. 475–481, Jul. 2014, ISSN: 18728219. DOI: 10.1016/j.ergon.2014.03.008.

[66] M. P. de Looze, T. Bosch, F. Krause, K. S. Stadler, and L. W. O'Sullivan, "Exoskeletons for industrial application and their potential effects on physical work load," *Ergonomics*, vol. 59, no. 5, pp. 671–681, 2016, ISSN: 13665847. DOI: 10.1080/00140139.2015.1081988.

[67] S. Alabdulkarim and M. A. Nussbaum, "Influences of different exoskeleton designs and tool mass on physical demands and performance in a simulated overhead drilling task," *Applied Ergonomics*, vol. 74, no. February 2018, pp. 55–66, 2019, ISSN: 18729126. DOI: 10.1016/j.apergo.2018.08.004.

[68] S. Toxiri, M. B. Näf, M. Lazzaroni, *et al.*, "Back-Support Exoskeletons for Occupational Use: An Overview of Technological Advances and Trends," *IISE Transactions on Occupational Ergonomics and Human Factors*, vol. 7, no. 3-4, pp. 237–249, Oct. 2019, ISSN: 2472-5838. DOI: 10.1080/24725838.2019.1626303.

[69] X. Jin, Y. Cai, A. Prado, and S. K. Agrawal, "Effects of exoskeleton weight and inertia on human walking," *Proceedings - IEEE International Conference on Robotics and Automation*, pp. 1772–1777, 2017, ISSN: 10504729. DOI: 10.1109/ICRA.2017.7989210.

[70] S. J. Baltrusch, J. H. van Dieën, C. A. van Bennekom, and H. Houdijk, "The effect of a passive trunk exoskeleton on functional performance in healthy individuals," *Applied Ergonomics*, vol. 72, no. July 2017, pp. 94–106, 2018, ISSN: 18729126. DOI: 10.1016/j.apergo.2018.04.007.

[71] M. Plooij, W. Wolfslag, and M. Wisse, "Clutched elastic actuators," *IEEE/ASME Transactions on Mechatronics*, vol. 22, no. 2, pp. 739–750, 2017, ISSN: 10834435. DOI: 10.1109/TMECH.2017.2657224.

[72] D. F. B. Haeufle, M. D. Taylor, S. Schmitt, and H. Geyer, "A clutched parallel elastic actuator concept: Towards energy efficient powered legs in prosthetics and robotics," in *2012 4th IEEE RAS & EMBS International Conference on Biomedical Robotics and Biomechatronics (BioRob)*, IEEE, Jun. 2012, pp. 1614–1619, ISBN: 978-1-4577-1200-5. DOI: 10.1109/BioRob.2012.6290722.

[73] K. Endo, D. Paluska, and H. Herr, "A quasi-passive model of human leg function in level-ground walking," *IEEE International Conference on Intelligent Robots and Systems*, pp. 4935–4939, 2006. DOI: 10.1109/IROS.2006.282454.

[74] K. Anam and A. A. Al-Jumaily, "Active exoskeleton control systems: State of the art," *Procedia Engineering*, vol. 41, no. Iris, pp. 988–994, 2012, ISSN: 18777058. DOI: 10.1016/j.proeng.2012.07.273.

[75] M. D. C. Sanchez-Villamañan, J. Gonzalez-Vargas, D. Torricelli, J. C. Moreno, and J. L. Pons, "Compliant lower limb exoskeletons: A comprehensive review on mechanical design principles," *Journal of NeuroEngineering and Rehabilitation*, vol. 16, no. 1, pp. 1–16, 2019, ISSN: 17430003. DOI: 10.1186/s12984-019-0517-9.

[76] P. K. Artemiadis and K. J. Kyriakopoulos, "EMG-Based Position and Force Estimates in Coupled Human-Robot Systems: Towards EMG-Controlled Exoskeletons," in *Springer Tracts in Advanced Robotics*, vol. 54, Springer, Berlin, Heidelberg, 2009, pp. 241–250, ISBN: 9783642001956. DOI: 10.1007/978-3-642-00196-3_29.

[77] A. Kilicarslan, S. Prasad, R. G. Grossman, and J. L. Contreras-Vidal, "High accuracy decoding of user intentions using EEG to control a lower-body exoskeleton," in *2013 35th Annual International Conference of the IEEE Engineering in Medicine and Biology Society (EMBC)*, IEEE, Jul. 2013, pp. 5606–5609, ISBN: 978-1-4577-0216-7. DOI: 10.1109/EMBC.2013.6610821.

[78] H. Siu, J. Shah, and L. Stirling, "Classification of Anticipatory Signals for Grasp and Release from Surface Electromyography," *Sensors*, vol. 16, no. 11, p. 1782, Oct. 2016, ISSN: 1424-8220. DOI: 10.3390/s16111782.

[79] F. R. Allen, E. Ambikairajah, N. H. Lovell, and B. G. Celler, "Classification of a known sequence of motions and postures from accelerometry data using adapted Gaussian mixture models," *Physiological Measurement*, vol. 27, no. 10, pp. 935–951, Oct. 2006, ISSN: 0967-3334. DOI: 10.1088/0967-3334/27/10/001.

[80] H. A. Varol, F. Sup, and M. Goldfarb, "Powered sit-to-stand and assistive stand-to-sit framework for a powered transfemoral prosthesis," *2009 IEEE International Conference on Rehabilitation Robotics, ICORR 2009*, pp. 645–651, 2009. DOI: 10.1109/ICORR.2009.5209582.

[81] M. B. Näf, A. S. Koopman, S. Baltrusch, C. Rodriguez-Guerrero, B. Vanderborght, and D. Lefeber, "Passive Back Support Exoskeleton Improves Range of Motion Using Flexible Beams," *Frontiers in Robotics and AI*, vol. 5, no. June, pp. 1–16, 2018. DOI: 10.3389/frobt.2018.00072.

[82] C. Fraley and A. E. Raftery, "Model-Based Clustering, Discriminant Analysis, and Density Estimation," *Journal of the American Statistical Association*, vol. 97, no. 458, pp. 611–631, Jun. 2002, ISSN: 0162-1459. DOI: 10.1198/016214502760047131.

[83] W. Kim, J. Lee, L. Peternel, N. Tsagarakis, and A. Ajoudani, "Anticipatory Robot Assistance for the Prevention of Human Static Joint Overloading in Human-Robot Collaboration," *IEEE Robotics and Automation Letters*, vol. 3, no. 1, pp. 68–75, Jan. 2018, ISSN: 2377-3766. DOI: 10.1109/LRA.2017.2729666.

[84] S. Toxiri, A. S. Koopman, M. Lazzaroni, *et al.*, "Rationale, Implementation and Evaluation of Assistive Strategies for an Active Back-Support Exoskeleton," *Frontiers in Robotics and AI*, vol. 5, no. MAY, pp. 1–14, May 2018, ISSN: 2296-9144. DOI: 10.3389/frobt.2018.00053.

[85] T. Bosch, J. van Eck, K. Knitel, and M. de Looze, "The effects of a passive exoskeleton on muscle activity, discomfort and endurance time in forward bending work," *Applied Ergonomics*, vol. 54, pp. 212–217, May 2016, ISSN: 00036870. DOI: 10.1016/j.apergo.2015.12.003.

[86] W. P. Berg, H. M. Alessio, E. M. Mills, and C. Tong, "Circumstances and consequences of falls in independent community-dwelling older adults," *Age and Ageing*, vol. 26, no. 4, pp. 261–268, 1997, ISSN: 00020729. DOI: 10.1093/ageing/26.4.261.

[87] United Nations Population Fund (UNFPA) and and HelpAge Internationa, *Ageing in the Twenty-First Century: A Celebration and A Challenge*. 2012, pp. 20, 192, ISBN: 9780897149815. DOI: 978-0-89714-981-5.

[88] G. Shi, C. S. Chan, W. J. Li, K.-S. Leung, Y. Zou, and Y. Jin, "Mobile Human Airbag System for Fall Protection Using MEMS Sensors and Embedded SVM Classifier," *IEEE Sensors Journal*, vol. 9, no. 5, pp. 495–503, May 2009, ISSN: 1530-437X. DOI: 10.1109/JSEN.2008.2012212.

[89] J. Babič, M. Laffranchi, F. Tessari, *et al.*, "Challenges and solutions for application and wider adoption of wearable robots," *Wearable Technologies*, vol. 2, e14, Nov. 2021, ISSN: 2631-7176. DOI: 10.1017/wtc.2021.13.

[90] D. Kobsar, J. M. Charlton, C. T. Tse, *et al.*, *Validity and reliability of wearable inertial sensors in healthy adult walking: A systematic review and meta-analysis*, May 2020. DOI: 10.1186/s12984-020-00685-3.

[91] C. A. Rusu, C. Constantinescu, and S. C. Marinescu, "A generic hybrid Human Exoskeleton Digital Model towards Digital Transformation of Exoskeletons-integrated workplaces," in *Procedia CIRP*, vol. 104, Elsevier B.V., Jan. 2021, pp. 1787–1790. DOI: 10.1016/j.procir.2021.11.301.

[92] S. M. Bruijn and J. H. Van Dieën, "Control of human gait stability through foot placement," *Journal of the Royal Society Interface*, vol. 15, no. 143, 2018, ISSN: 17425662. DOI: 10.1098/rsif.2017.0816.

[93] S. Kajita, F. Kanehiro, K. Kaneko, K. Yokoi, and H. Hirukawa, "The 3D linear inverted pendulum mode: A simple modeling for a biped walking pattern generation," *IEEE International Conference on Intelligent Robots and Systems*, vol. 1, pp. 239–240, 2001. DOI: 10.1109/IROS.2001.973365.

[94] M. A. Townsend, "Biped gait stabilization via foot placement," *Journal of Biomechanics*, vol. 18, no. 1, pp. 21–38, Jan. 1985, ISSN: 00219290. DOI: 10.1016/0021-9290(85)90042-9.

[95] J. Pratt, J. Carff, S. Drakunov, and A. Goswami, "Capture point: A step toward humanoid push recovery," in *Proceedings of the 2006 6th IEEE-RAS International Conference on Humanoid Robots, HUMANOIDS*, 2006, pp. 200–207, ISBN: 142440200X. DOI: 10.1109/ICHR.2006.321385.

[96] K. Zhang, H. Liu, Z. Fan, *et al.*, "Foot Placement Prediction for Assistive Walking by Fusing Sequential 3D Gaze and Environmental Context," *IEEE Robotics and Automation Letters*, vol. 6, no. 2, pp. 2509–2516, Apr. 2021, ISSN: 23773766. DOI: 10.1109/LRA.2021.3062003.

[97] X. Chen, Z. Liu, J. Zhu, K. Zhang, Y. Leng, and C. Fu, "Comparison of machine learning regression algorithms for foot placement prediction," *2021 27th International Conference on Mechatronics and Machine Vision in Practice, M2VIP 2021*, pp. 169–174, 2021. DOI: 10.1109/M2VIP49856.2021.9665043.

[98] N. Thatte, N. Srinivasan, and H. Geyer, "Real-Time Reactive Trip Avoidance for Powered Transfemoral Prostheses," 2019. DOI: 10.15607/rss.2019.xv.034.

[99] M. Jamsek, T. Kunavar, U. Bobek, E. Rueckert, and J. Babic, "Predictive Exoskeleton Control for Arm-Motion Augmentation Based on Probabilistic Movement Primitives Combined with a Flow Controller," *IEEE Robotics and Automation Letters*, vol. 6, no. 3, pp. 4417–4424, Jul. 2021, ISSN: 23773766. DOI: 10.1109/LRA.2021.3068892.

[100] J. Padulo, K. Chamari, and L. P. Ardigò, *Walking and running on treadmill: The standard criteria for kinematics studies*, 2014. DOI: 10.11138/mltj/2014.4.2.159.

[101] G. Wu, S. Siegler, P. Allard, *et al.*, *ISB recommendation on definitions of joint coordinate system of various joints for the reporting of human joint motion - Part I: Ankle, hip, and spine*, Apr. 2002. DOI: 10.1016/S0021-9290(01)00222-6.

[102] J. T. Zhang, A. C. Novak, B. Brouwer, and Q. Li, "Concurrent validation of Xsens MVN measurement of lower limb joint angular kinematics," *Physiological Measurement*, vol. 34, no. 8, pp. 63–69, Aug. 2013, ISSN: 09673334. DOI: 10.1088/0967-3334/34/8/N63.

[103] X. Chen, Z. Liu, J. Zhu, K. Zhang, Y. Leng, and C. Fu, "Comparison of machine learning regression algorithms for foot placement prediction," *2021 27th International Conference on Mechatronics and Machine Vision in Practice, M2VIP 2021*, pp. 169–174, 2021. DOI: 10.1109/M2VIP49856.2021.9665043.

[104] M. Ewerton, G. Maeda, G. Neumann, *et al.*, "Movement primitives with multiple phase parameters," in *2016 IEEE International Conference on Robotics and Automation (ICRA)*, vol. 2016-June, IEEE, May 2016, pp. 201–206, ISBN: 978-1-4673-8026-3. DOI: 10.1109/ICRA.2016.7487134.

[105] S. Scataglini, S. Verwulgen, E. Roosens, R. Haelterman, and D. Van Tiggelen, "Measuring Spatiotemporal Parameters on Treadmill Walking Using Wearable Inertial System," *Sensors*, vol. 21, no. 13, p. 4441, Jun. 2021, ISSN: 1424-8220. DOI: 10.3390/s21134441.

[106] M. Al-Amri, K. Nicholas, K. Button, V. Sparkes, L. Sheeran, and J. Davies, "Inertial Measurement Units for Clinical Movement Analysis: Reliability and Concurrent Validity," *Sensors*, vol. 18, no. 3, p. 719, Feb. 2018, ISSN: 1424-8220. DOI: 10.3390/s18030719.

[107] T. Proietti and V. Crocher, "Upper-Limb Robotic Exoskeletons for Neurorehabilitation : A Review on Control Strategies," vol. 9, pp. 4–14, 2016.

[108] H. Lee, W. Kim, J. Han, and C. Han, "The technical trend of the exoskeleton robot system for human power assistance," *International Journal of Precision Engineering and Manufacturing*, vol. 13, no. 8, pp. 1491–1497, Aug. 2012, ISSN: 12298557. DOI: 10.1007/s12541-012-0197-x.

[109] S. Calinon, D. Florent, E. L. Sauser, D. G. Caldwell, and A. G. Billard, "An approach based on Hidden Markov Model and Gaussian Mixture Regression," *IEEE Robotics and Automation Magazine*, vol. 17, no. June, pp. 44–45, 2010.

[110] A. Paraschos, E. Rueckert, J. Peters, and G. Neumann, "Model-free Probabilistic Movement Primitives for physical interaction," in *IEEE International Conference on Intelligent Robots and Systems*, vol. 2015-Decem, Institute of Electrical and Electronics Engineers Inc., Dec. 2015, pp. 2860–2866, ISBN: 9781479999941. DOI: 10.1109/IROS.2015.7353771.

[111] A. Paraschos, C. Daniel, J. Peters, and G. Neumann, "Using probabilistic movement primitives in robotics," *Autonomous Robots*, vol. 42, no. 3, pp. 529–551, 2018, ISSN: 15737527. DOI: 10.1007/s10514-017-9648-7.

[112] S. G. Hart and L. E. Staveland, "Development of NASA-TLX (Task Load Index): Results of Empirical and Theoretical Research," in *Power Technology and Engineering*, 5, vol. 43, Sep. 1988, pp. 139–183. DOI: 10.1016/S0166-4115(08)62386-9.

[113] H. J. Hermens, B. Freriks, C. Disselhorst-Klug, and G. Rau, "Development of recommendations for SEMG sensors and sensor placement procedures," *Journal of Electromyography and Kinesiology*, vol. 10, no. 5, pp. 361–374, Oct. 2000, ISSN: 10506411. DOI: 10.1016/S1050-6411(00)00027-4.

[114] W. H. Paloski, C. M. Oman, J. J. Bloomberg, *et al.*, "Risk of sensory-motor performance failures affecting vehicle control during space missions: a review of the evidence," *Journal of Grav. Phisiology*, vol. 15, no. 2, pp. 1–29, 2008.

[115] J. Fisk, J. R. Lackner, and P. DiZio, "Gravitoinertial force level influences arm movement control," *Journal of Neurophysiology*, vol. 69, no. 2, pp. 504–511, 1993, ISSN: 00223077. DOI: 10.1152/jn.1993.69.2.504.

[116] B. N. Smetanin and K. E. Popov, "Effect of Body Orientation with Respect to Gravity on Directional Accuracy of Human Pointing Movements," *European Journal of Neuroscience*, vol. 9, no. 1, pp. 7–11, Jan. 1997, ISSN: 0953816X. DOI: 10.1111/j.1460-9568.1997.tb01347.x.

[117] J. R. Lackner and P. Dizio, "Rapid adaptation to Coriolis force perturbations of arm trajectory," *Journal of Neurophysiology*, vol. 72, no. 1, pp. 299–313, 1994, ISSN: 00223077. DOI: 10.1152/jn.1994.72.1.299.

[118] R. Shadmehr and Z. M. Moussavi, "Spatial generalization from learning dynamics of reaching movements," *Journal of Neuroscience*, vol. 20, no. 20, pp. 7807–7815, Oct. 2000, ISSN: 02706474. DOI: 10.1523/jneurosci.20-20-07807.2000.

[119] C. Papaxanthis, T. Pozzo, and J. McIntyre, "Kinematic and dynamic processes for the control of pointing movements in humans revealed by short-term exposure to microgravity," *Neuroscience*, vol. 135, no. 2, pp. 371–383, Jan. 2005, ISSN: 03064522. DOI: 10.1016/j.neuroscience.2005.06.063.

[120] L. N. Kornilova, D. O. Glukhikh, E. V. Habarova, I. A. Naumov, G. A. Ekimovskiy, and A. S. Pavlova, "Visual–manual tracking after long spaceflights," *Human Physiology*, vol. 42, no. 3, pp. 301–311, May 2016, ISSN: 16083164. DOI: 10.1134/S0362119716030105.

[121] F. Crevecoeur, J. McIntyre, J.-L. Thonnard, and P. Lefèvre, "Movement Stability Under Uncertain Internal Models of Dynamics," *Journal of Neurophysiology*, vol. 104, no. 3, pp. 1301–1313, Sep. 2010, ISSN: 0022-3077. DOI: 10.1152/jn.00315.2010.

[122] S. Mechtcheriakov, M. Berger, E. Molokanova, *et al.*, "Slowing of human arm movements during weightlessness: The role of vision," *European Journal of Applied Physiology*, vol. 87, no. 6, pp. 576–583, Oct. 2002, ISSN: 14396319. DOI: 10.1007/s00421-002-0684-3.

[123] O. White, Y. Bleyenheuft, R. Ronsse, A. M. Smith, J. L. Thonnard, and P. Lefèvre, "Altered gravity highlights central pattern generator mechanisms," *Journal of Neurophysiology*, vol. 100, no. 5, pp. 2819–2824, 2008, ISSN: 00223077. DOI: 10.1152/jn.90436.2008.

[124] L. Bringoux, J. Blouin, T. Coyle, H. Ruget, and L. Mouchnino, "Effect of gravity-like torque on goal-directed arm movements in microgravity," *Journal of Neurophysiology*, vol. 107, no. 9, pp. 2541–2548, 2012, ISSN: 00223077. DOI: 10.1152/jn.00364.2011.

[125] T. Macaluso, C. Bourdin, F. Buloup, *et al.*, "Sensorimotor Reorganizations of Arm Kinematics and Postural Strategy for Functional Whole-Body Reaching Movements in Microgravity," *Frontiers in Physiology*, vol. 8, no. OCT, p. 821, Oct. 2017, ISSN: 1664-042X. DOI: 10.3389/fphys.2017.00821.

[126] O. Bock, I. P. Howard, K. E. Money, and K. E. Arnold, "Accuracy of aimed arm movements in changed gravity.," *Aviation, space, and environmental medicine*, vol. 63, no. 11, pp. 994–8, Nov. 1992, ISSN: 0095-6562.

[127] M. Berger, S. Mescheriakov, E. Molokanova, S. Lechner-Steinleitner, N. Seguer, and I. Kozlovskaya, "Pointing arm movements in short- and long-term spaceflights.," *Aviation, space, and environmental medicine*, vol. 68, no. 9, pp. 781–7, Sep. 1997, ISSN: 0095-6562. DOI: 10.1007/s00421-002-0684-3.

[128] H. Bolender, H. Stevenin, L. Bessone, and A. Torres, "Preparing for space," *European Space Agency Bulletin*, no. 128, pp. 32–40, 2006, ISSN: 03764265.

[129] M. Coscia, V. C. Cheung, P. Tropea, *et al.*, "The effect of arm weight support on upper limb muscle synergies during reaching movements," *Journal of Neuro-Engineering and Rehabilitation*, vol. 11, no. 1, p. 22, 2014, ISSN: 17430003. DOI: 10.1186/1743-0003-11-22.

[130] G. B. Prange, L. A. Kallenberg, M. J. Jannink, *et al.*, "Influence of gravity compensation on muscle activity during reach and retrieval in healthy elderly," *Journal of Electromyography and Kinesiology*, vol. 19, no. 2, e40–e49, Apr. 2009, ISSN: 10506411. DOI: 10.1016/j.jelekin.2007.08.001.

[131] V. Pletser, S. Rouquette, U. Friedrich, *et al.*, "The First European Parabolic Flight Campaign with the Airbus A310 ZERO-G," *Microgravity Science and Technology*, vol. 28, no. 6, pp. 587–601, Dec. 2016, ISSN: 18750494. DOI: 10.1007/s12217-016-9515-8.

[132] R. Ritzmann, K. Freyler, A. Krause, and A. Gollhofer, "No Neuromuscular Side-Effects of Scopolamine in Sensorimotor Control and Force-Generating Capacity Among Parabolic Fliers," *Microgravity Science and Technology*, vol. 28, no. 5, pp. 477–490, Oct. 2016, ISSN: 18750494. DOI: 10.1007/s12217-016-9504-y.

[133] R Core Team, *R: A Language and Environment for Statistical Computing*, R Foundation for Statistical Computing, Vienna, Austria, 2020.

[134] J. Pinheiro, D. Bates, S. DebRoy, D. Sarkar, and R Core Team, *{nlme}: Linear and Nonlinear Mixed Effects Models*, 2020.

[135] T. Hothorn, F. Bretz, and P. Westfall, "Simultaneous Inference in General Parametric Models," *Biometrical Journal*, vol. 50, no. 3, pp. 346–363, 2008.

[136] T. Macaluso, C. Bourdin, F. Buloup, *et al.*, "Kinematic features of whole-body reaching movements underwater: Neutral buoyancy effects," *Neuroscience*, vol. 327, pp. 125–135, Jul. 2016, ISSN: 18737544. DOI: 10.1016/j.neuroscience.2016.04.014.

[137] Y. Chen, S. Mori, K. Koga, Y. Ohta, Y. Wada, and M. Tanaka, "Shift in Arm-pointing Movements During Gravity Changes Produced by Aircraft Parabolic Flight.," *Biological Sciences in Space*, vol. 13, no. 2, pp. 77–81, 1999, ISSN: 0914-9201. DOI: 10.2187/bss.13.77.

[138] C. Papaxanthis, T. Pozzo, K. E. Popov, and J. McIntyre, "Hand trajectories of vertical arm movements in one- G and zero- G environments," *Experimental Brain Research*, vol. 120, no. 4, pp. 496–502, May 1998, ISSN: 0014-4819. DOI: 10.1007/s002210050423.

[139] C. Rousseau, C. Papaxanthis, J. Gaveau, T. Pozzo, and O. White, "Initial information prior to movement onset influences kinematics of upward arm pointing movements," *J Neurophysiol*, vol. 116, pp. 1673–1683, 2016. DOI: 10.1152/jn.00616.2015.-To.

[140] A. D. Artiles, D. Schor, and G. Clément, "Effects of inverted vision on hand-pointing performance in altered gravity during parabolic flight," in *IEEE Aerospace Conference Proceedings*, vol. 2018-March, IEEE Computer Society, Jun. 2018, pp. 1–9, ISBN: 9781538620144. DOI: 10.1109/AERO.2018.8396370.

[141] M. Jamšek, T. Petrič, and J. Babič, "Gaussian Mixture Models for Control of Quasi-Passive Spinal Exoskeletons," *Sensors*, vol. 20, no. 9, p. 2705, May 2020, ISSN: 1424-8220. DOI: 10.3390/s20092705.

[142] U. Bobek, E. Rueckert, M. Jamšek, S. Barišić, and J. Babič, "Combining Foot Placement Prediction with Obstacle Detection to Detect Tripping," *Proceedings of the Twenty-eighth Electrotechnical and Computer Science Conference ERK 2019*, pp. 110–113, 2019.

[143] M. Jamšek, T. Kunavar, G. Blohm, *et al.*, "Effects of Simulated Microgravity and Hypergravity Conditions on Arm Movements in Normogravity," *Frontiers in Neural Circuits*, vol. 15, p. 150, Dec. 2021, ISSN: 1662-5110. DOI: 10.3389/fncir.2021.750176.

[144] M. Jamšek and J. Babič, "Design and preliminary testing of a pneumatic exoskeleton for walking assistance," in *27th International Electrotechnical and Computer Science Conference ERK 2018*, 2018, pp. 159–162.

[145] M. Jamšek and J. Babič, "Human Trunk Stabilization with Hip Exoskeleton for Enhanced Postural Control," in *Wearable Robotics: Challenges and Trends*, Springer International Publishing, 2019, pp. 450–454, ISBN: 978-3-030-01887-0. DOI: 10.1007/978-3-030-01887-0_87.

[146] M. Cevzar, T. Petrič, M. Jamšek, and J. Babič, "Real-time control of quasi-active hip exoskeleton based on gaussian mixture model approach," in *Biosystems and Biorobotics*, ser. Biosystems & Biorobotics 687662, M. C. Carrozza, S. Micera, and J. L. Pons, Eds., vol. 22, Cham: Springer International Publishing, 2019, pp. 244–248, ISBN: 978-3-030-01886-3. DOI: 10.1007/978-3-030-01887-0_47.

[147] T. Petrič, M. Jamšek, and J. Babič, "Exoskeleton Control Based on Network of Stable Heteroclinic Channels (SHC) Combined with Gaussian Mixture Models (GMM)," in Springer, Cham, Dec. 2021, pp. 341–348. DOI: 10.1007/978-3-030-50975-0_42.

Bibliography

Publications Related to the Thesis

Journal Articles

M. Jamšek, T. Petrič, and J. Babič, "Gaussian Mixture Models for Control of Quasi-Passive Spinal Exoskeletons," *Sensors*, vol. 20, no. 9, p. 2705, May 2020, ISSN: 1424-8220. DOI: 10.3390/s20092705.

M. Jamsek, T. Kunavar, U. Bobek, E. Rueckert, and J. Babic, "Predictive Exoskeleton Control for Arm-Motion Augmentation Based on Probabilistic Movement Primitives Combined with a Flow Controller," *IEEE Robotics and Automation Letters*, vol. 6, no. 3, pp. 4417–4424, Jul. 2021, ISSN: 23773766. DOI: 10.1109/LRA.2021.3068892.

M. Jamšek, T. Kunavar, G. Blohm, *et al.*, "Effects of Simulated Microgravity and Hypergravity Conditions on Arm Movements in Normogravity," *Frontiers in Neural Circuits*, vol. 15, p. 150, Dec. 2021, ISSN: 1662-5110. DOI: 10.3389/fncir.2021.750176.

Conference Papers

U. Bobek, E. Rueckert, M. Jamšek, S. Barišić, and J. Babič, "Combining Foot Placement Prediction with Obstacle Detection to Detect Tripping," *Proceedings of the Twenty-eighth Electrotechnical and Computer Science Conference ERK 2019*, pp. 110–113, 2019.

M. Jamšek and J. Babič, "Design and preliminary testing of a pneumatic exoskeleton for walking assistance," in *27th International Electrotechnical and Computer Science Conference ERK 2018*, 2018, pp. 159–162.

M. Jamšek and J. Babič, "Human Trunk Stabilization with Hip Exoskeleton for Enhanced Postural Control," in *Wearable Robotics: Challenges and Trends*, Springer International Publishing, 2019, pp. 450–454, ISBN: 978-3-030-01887-0. DOI: 10.1007/978-3-030-01887-0_87.

T. Petrič, M. Jamšek, and J. Babič, "Exoskeleton Control Based on Network of Stable Heteroclinic Channels (SHC) Combined with Gaussian Mixture Models (GMM)," in Springer, Cham, Dec. 2021, pp. 341–348. DOI: 10.1007/978-3-030-50975-0_42.

M. Cevzar, T. Petrič, M. Jamšek, and J. Babič, "Real-time control of quasi-active hip exoskeleton based on gaussian mixture model approach," in *Biosystems and Biorobotics*, ser. Biosystems & Biorobotics 687662, M. C. Carrozza, S. Micera, and J. L. Pons, Eds., vol. 22, Cham: Springer International Publishing, 2019, pp. 244–248, ISBN: 978-3-030-01886-3. DOI: 10.1007/978-3-030-01887-0_47.

Other Publications

Journal Articles

T. Kunavar, M. Jamšek, M. Barbiero, *et al.*, "Effects of Local Gravity Compensation on Motor Control During Altered Environmental Gravity," *Frontiers in Neural Circuits*, vol. 15, p. 121, Oct. 2021, ISSN: 16625110. DOI: 10.3389/FNCIR.2021.750267.

Biography

Marko Jamšek mag.inž.str., is a PhD Student at Jožef Stefan International Postgraduate School working in the Laboratory for Neuromechanics and Biorobotics at Jožef Stefan Institute. He was awarded the degrees of BSc in 2014 and MSc in 2017 both at the University of Ljubljana, Faculty of Mechanical Engineering. For his master's thesis of "Development of controller for parallel robotic platform" he was awarded the Faculty's Prešeren Award in 2017. His current research is primarily focused on assistive exoskeletons, human robot interactions, ergonomics, control of real-time systems and probabilistic modelling of human movements. He was actively involved in two larger European projects H2020 Spexor and H2020 AnDy. In the scope of his research he published three original scientific articles [99], [141], [143] and several scientific conference contributions [142], [144]–[147].